Stark Zeeman Effect of the $2p\ ^2P_{\frac{3}{2}}$ Hyperfine Levels of $^6\mathsf{Li}$ and $^7\mathsf{Li}$ for Perpendicular Fields

Diploma Thesis

Ewald Rößl

Supervisor: Univ.-Prof.Dr.phil.B.Schnizer

Institute for Theoretical Physics
Technical University Graz

7 April 1999

Dedicated to my parents

Abstract

The Stark Zeeman effect of the $2p\ ^2P_{\frac{3}{2}}$ hyperfine levels of ^{6}Li (nuclear spin $I = 1$) and ^{7}Li (nuclear spin $I = \frac{3}{2}$) is investigated for perpendicular fields. This is done by diagonalizing the perturbation matrices comprising the hyperfine interaction and the interactions with the external magnetic (B) and electric (E) fields for each pair of field values. The energy surfaces $\epsilon_n(B, E)$ describe the behavior of all the energy levels including the case of adiabatically varying fields.

For each isotope the total $2p\ ^2P_{\frac{3}{2}}$ level splits into two noninteracting subsystems: the odd subsystem (with M_F odd) and the even subsystem for ^{7}Li ($I = \frac{3}{2}$ and $J = \frac{3}{2}$); the positive subsystem ($M_F = \frac{5}{2}, \frac{1}{2}, -\frac{3}{2}$) and the negative subsystem ($M_F = \frac{3}{2}, -\frac{1}{2}, -\frac{5}{2}$) for ^{6}Li ($I = 1$ and $J = \frac{3}{2}$). In each subsystem the energy surfaces meet in discrete points of degeneracy. Adiabatic field cycles may induce level transfers.

Within the ranges $0 \leq B \leq 1\mathrm{mT}$ and $0 \leq E \leq 300\,\mathrm{keV/cm}$, the odd subsystem comprises the crossing points **Bon** ($n = 1..4$; with $E = 0$), **Eon** ($n = 1, 2$; with $B = 0$) and the point **BEo** ($E \neq 0, B \neq 0$), the even subsystem comprises the points **Ben** ($n = 1, 2, 3$; with $E = 0$) and the point **BEe** ($E \neq 0, B \neq 0$).

For the ranges $0 \leq |B| \leq 1\mathrm{mT}$ and $0 \leq E \leq 300\,\mathrm{keV/cm}$, the positive subsystem has 5 magnetic crossing points **Bpn** ($n = 1..5$; with $E = 0$), 1 electric crossing point **Ep1** (with $B = 0$) and one **BEp** point ($E \neq 0, B \neq 0$). The crossing points of the negative subsystem appear at the same field values as the corresponding points of the positive subsystem, but with opposite signs for the magnetic field B. For some field cycles surrounding crossing points a geometric phase (Berry phase) occurs.

Contents

Chapter 1

Introduction

This diploma thesis is based on theoretical considerations by Musso and Windholz [1], [2] concerning adiabatic hyperfine structure level transfer and on an experiment performed by Windholz et.al. in 1994 [3] at the Institute of Experimental Physics of the Technical University in Graz. While the subject of the theoretical investigations were Na atoms traversing a region of space filled by static, perpendicular, inhomogeneous electric and magnetic fields, in the experiment an atomic beam of Ga has been used, since the lifetime of the excited state $3p\ ^2P_{\frac{3}{2}}$ of Na is too small to perform the experiment. A first detailed theoretical explanation of the effects observed has been given by Heubrandtner [4].

1.1 Adiabatic Hyperfine Level Transfer in ^{23}Na, ^{69}Ga, ^{71}Ga and ^{7}Li

While passing through the static, inhomogeneous electromagnetic fields of the experimental device, the Ga atoms experience time-dependent electric and magnetic fields in their comoving proper frames of reference. Assuming for simplicity a constant velocity of the Ga atoms and linear variations of the fields (in space), the time dependence of the former (as experienced by the atomic beam) can be identified approximately with the one given in Fig. 1.1 below the energy splitting diagram of ^{7}Li. For an adiabatic process, the time variations of the fields have to be slow (as compared to the atomic periods) which corresponds to small velocities and small values for the field gradients. The reason for presenting the treatment of the adiabatic hyperfine level transfer of the corresponding levels $np\ ^2P_{\frac{3}{2}}$ of Na, Ga and ^{7}Li within one

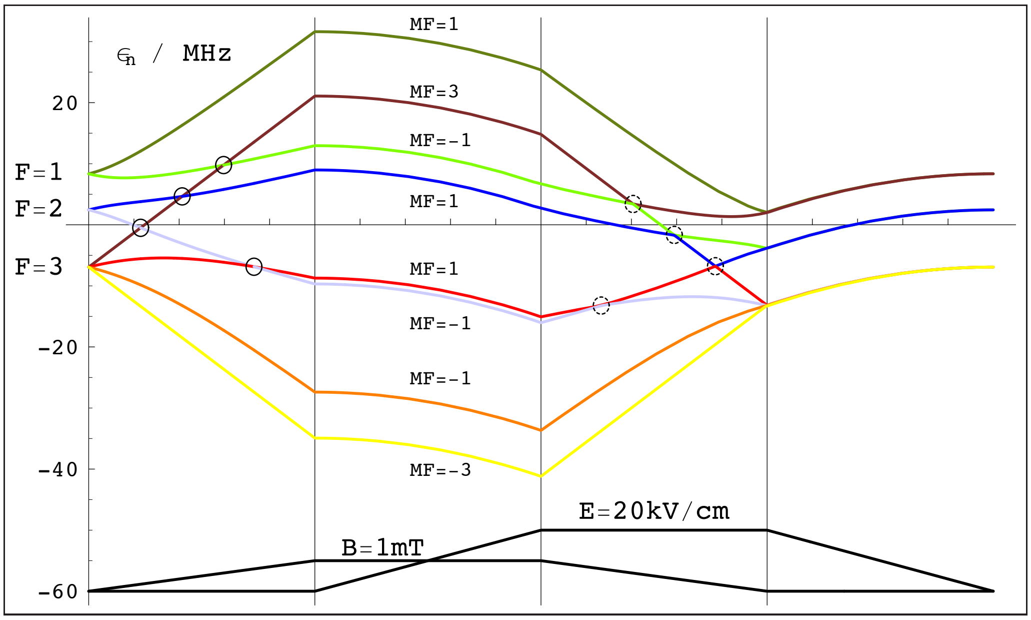

Figure 1.1: Special field cycle of the electromagnetic field with the corresponding splitting of the $2p\ ^2P_{\frac{3}{2}}$ hyperfine levels of ^{7}Li in the odd subsystem (M_F = odd).

section is that all these atoms possess the same nuclear spin, characterized by the quantum number $I = \frac{3}{2}$. Therefore, the degrees of degeneracy of the levels mentioned above are the same.

According to the behavior of the field variations there exist four different regions:

Region 1: *linearly increasing magnetic field - zero electric field*

Region 2: *linearly increasing electric field - constant magnetic field*

Region 3: *linearly decreasing magnetic field - constant electric field*

Region 4: *linearly decreasing electric field - zero magnetic field*

By the combined influence of the time-dependent magnetic and electric fields, the degeneracies of the hyperfine structure energy levels are removed (totally in the case of the magnetic interaction and partially in the case of the electric interaction) and the corresponding energy eigenvalues show a splitting similar to the one given in Fig. 1.1 for ^{7}Li. This diagram for ^{7}Li is somehow different from those of Na and Ga since the hyperfine structure of ^{7}Li is inverted, i.e. the energy levels characterized by higher values of the quantum number of the total atomic angular momentum F have lower energies (in the absence of external fields) than those characterized by lower F values. Corresponding diagrams for Na are given in [2] and [4].

The field cycle starts with zero field values. The ^{7}Li atom is assumed to be in a quantum state characterized by the quantum numbers $F = 3$ and $M_F = 3$ (brown line in Fig. 1.1). The labels of the M_F quantum numbers shown in Fig. 1.1 should have been drawn in region 1 of the diagram. For a lack of space, however, the labels are sketched in region 2. The influence of the magnetic field leads to crossings (points of accidental degeneracy) of the energy levels marked by bold black circles. Following the eigenvectors beyond these crossing points suggests the coloring of the lines in that region of the diagram. In region 3, however, the additional electric field leads to anticrossings marked by dashed black circles. In the case of adiabatic field variations, the energy splitting diagram may be interpreted as a diagram showing the evolution of the eigenstates and the energy eigenvalues of the total Hamiltonian. The sequence of crossings and anticrossings is responsible for a final state characterized by the quantum numbers $F' = 1$ and $M_F' = -1$ differing from the quantum numbers of the initial state. In the course of a field cycle that induces a hyperfine structure level transfer, the atoms energy and angular momentum are changed.

It was one of the goals of this diploma thesis to find out, whether adiabatic hyperfine structure level transfer should also be observable in the case of Li. Since there are two isotopes of lithium on earth, ^{6}Li and ^{7}Li, the investigations have to be performed separately for the two isotopes. For both, ^{6}Li and ^{7}Li, right as in the cases of Na and Ga, the characteristic combinations of pairs of crossing and anticrossing points appear (see Fig. 1.1 for ^{7}Li).

The theoretical treatment of the $2p\ ^2P_{\frac{3}{2}}$ level of ^{7}Li is identical to the treatment of the corresponding $3p\ ^2P_{\frac{3}{2}}$ level of Na (performed by Musso [1]) except for some slight modifications.

In lithium the fine structure level $2p\ ^2P_{\frac{1}{2}}$ is much closer to the $2p\ ^2P_{\frac{3}{2}}$ level under study than the corresponding $np\ ^2P_{\frac{1}{2}}$ to the $np\ ^2P_{\frac{3}{2}}$ levels in Na and Ga. In a first approximation, this influence is neglected, so that the matrices representing the perturbation operators of the hyperfine structure, the Zeeman effect and the Stark effect have dimension 16. By symmetry considerations, Heubrandtner showed that the state space under study can be subdivided into two noninteracting subspaces characterized by odd and even values of the magnetic quantum number of the total angular momentum M_F, respectively (see the number of energy eigenvalues in Fig. 1.1). By diagonalizing the matrices representing the perturbation in the two subsystems, the energy corrections belonging to arbitrary values of the external fields can be evaluated.

In order to discuss the influence of the nearby $2p\,^2P_{\frac{1}{2}}$ level in ^{7}Li on the splitting, it is necessary to extend the theoretical treatment. Some new analytic calculations were done to obtain the matrix elements of the perturbation operators involving states belonging to the $2p\,^2P_{\frac{1}{2}}$ fine structure level. The dimension of the state space ($2p\,^2P_{\frac{1}{2}}$ plus $2p\,^2P_{\frac{3}{2}}$) increases to 24. The same symmetry considerations as above, however, again permit the separation into two subsystems of dimension 12. Summarizing, the influence of the $2p\,^2P_{\frac{1}{2}}$ fine structure level on the splitting behavior of the $2p\,^2P_{\frac{3}{2}}$ hyperfine structure levels in ^{7}Li caused by the perturbation operators (hyperfine structure, Zeeman and Stark operators) consists merely in a slight shift of the energy eigenvalues and field values of the crossing points. This result supports the possibility of the approximation of neglecting this influence.

1.2 Adiabatic Hyperfine Level Transfer in ^{6}Li

The fact that the ^{6}Li nucleus has nuclear spin $I = 1$ has far reaching consequences. First of all, the quantum numbers of the total angular momentum F and the corresponding magnetic quantum number M_F are both half odd integers. Furthermore, the degeneracy of the fine structure level $2p\,^2P_{\frac{3}{2}}$ is 12, less than that of ^{7}Li. Even though the relation that permits the separation into two subsystems

$$\Delta M_F = \text{even} \tag{1.1}$$

is still valid, the use of the terms "odd" and "even" subsystems (as in the cases of Na, Ga and ^{7}Li) is no longer appropriate. Here a different nomenclature is introduced. The selection rule (1.1) separates the system of ^{6}Li levels into two noninteracting subsystems. State vectors characterized by the magnetic quantum numbers

$$M_F = \left\{\frac{5}{2}, \quad \frac{1}{2}, \quad -\frac{3}{2}\right\} \tag{1.2}$$

belong to the *positive* subsystem, states characterized by

$$M_F = \left\{\frac{3}{2}, \quad -\frac{1}{2}, \quad -\frac{5}{2}\right\} \tag{1.3}$$

belong to the *negative* subsystem. The magnetic quantum numbers M_F of the first subsystem are just the negative of the second subsystem. This entails above all that the Zeeman diagrams of the two subsystems are no longer symmetric with respect to a magnetic field reversal as in the cases of ^{7}Li, Na or Ga. Furthermore, the Stark diagrams of the two subsystems in ^{6}Li are identical, which again is a consequence of the particular division into subsystems given in eqs. (1.2) and (1.3).

The symmetry $C_{\infty v}$ prevailing in a Hamiltonian comprising the hyperfine interaction and the interaction with a constant electric field entails that there remains a degeneracy of the energy levels. As a consequence, the energy eigenvalues depend only on the absolute value of the magnetic quantum number $|M_F|$, if the quantization axis (which is also the vertical axis for $C_{\infty v}$) coincides with the electric field direction. However, this presupposition does not apply in the case treated here, where the z-axis is the quantization axis (even if there is no magnetic field present) while the electric field is aligned with the x-axis. The degeneracy is still present, but it is not expressible in such a simple way. This is discussed in more detail in section 3.4, Figs. 3.7 and 3.8 (cf. section 4.4, Figs. 4.9 and 4.10).

Despite all these differences, the theory predicts adiabatic hyperfine structure level transfer also in ^{6}Li. The combination of pairs of crossing and anticrossing points, a characteristic feature of the appearance of the level transfer, is found in both subsystems.

Since the hyperfine levels belonging to the $2p\ ^2P_{\frac{3}{2}}$ fine structure level in ^{6}Li are less separated than those of ^{7}Li and since the energy difference between the levels $2p\ ^2P_{\frac{1}{2}}$ and $2p\ ^2P_{\frac{3}{2}}$ is nearly independent of the isotope considered, a separate investigation on the influence of the nearby $2p\ ^2P_{\frac{1}{2}}$ fine structure level for ^{6}Li was deemed to be unnecessary.

Chapter 2

Theoretical Introduction

This chapter serves as a brief presentation of the theoretical foundations as far as they are necessary for the comprehension of this work. At the beginning all relevant properties of lithium are discussed, thereafter the evaluation of energy eigenvalues in the framework of time-independent perturbation theory of nonrelativistic quantum mechanics is presented. For a more detailed treatment, see e.g. [1].

2.1 General Considerations on the Lithium Atom

Natural lithium exists in two stable isotopes on earth: $^6\mathsf{Li}$ and $^7\mathsf{Li}$. The ground state of the $^6\mathsf{Li}$ nucleus is characterized by a nuclear spin $I = 1$, the ground state of the $^7\mathsf{Li}$ nucleus by $I = \frac{3}{2}$. The abundance of $^6\mathsf{Li}$ is only about 6%.

For low excitation energies the properties of the electron shells of the alkalines are completely determined by their unpaired outer valence electrons. In the case of lithium this is a $2s^1$-electron with the corresponding ground state configuration $1s^2\ 2s^1$. Therefore, the name of the ground state is $2s\ ^2S_{\frac{1}{2}}$. By taking the interaction between the orbital angular momentum and the spin of the valence electron into account, the first excited state in lithium splits into two fine structure levels $2p\ ^2P_{\frac{1}{2}}$ and $2p\ ^2P_{\frac{3}{2}}$. The corresponding energy difference is 10.050 GHz for $^6\mathsf{Li}$ and 10.056 GHz for $^7\mathsf{Li}$ [5] and therefore shows hardly any dependence on the nuclear mass. Besides, this is the smallest value amongst all the alkalines. The corresponding energy splitting due to the fine structure interaction amounts to 516 GHz in sodium, and even to about 1730 GHz in potassium.

2.2 Treatment of Interactions by Perturbation Theory

A nonrelativistic treatment of the lithium atom starts with an attempt to obtain approximate solutions of the time independent Schrödinger equation; in this case the wavefunctions depend at least on the orbital degrees of freedom of the three electrons. As already mentioned, however, especially for lithium (or other alkalines), the Schrödinger equation can approximately be reduced to a one particle wave equation by neglecting non-central forces between the electrons. The valence electron is then considered to be exposed to the Coulomb potential of the nucleus, screened by the two core electrons (*central field approximation*). This examination leads to the energy eigenvalues and the corresponding eigenvectors of the Hamiltonian with definite orbital angular momentum. The inclusion of the spin-orbit interaction is responsible for the fine structure splitting of the levels.

The point of main effort of the investigations in this diploma thesis is the perturbation-theoretical treatment of simultaneous Stark and Zeeman effects (for perpendicular fields) of the hyperfine levels belonging to the fine structure level $2p\ {}^2P_{\frac{3}{2}}$ of lithium. For this purpose the three perturbation operators (hyperfine structure operator, Zeeman operator and Stark operator) have to be represented within a certain basis by square matrices, each of which has a dimension that corresponds to the degree of degeneracy of the $2p\ {}^2P_{\frac{3}{2}}$ level under study. The latter depends on the isotope considered because of the different values for the quantum number of the nuclear spin I.

By means of the general quantum mechanical rules for the addition of two angular momenta, the total angular momentum of the atom $\hat{\vec{F}}$ is obtained by the coupling between the nuclear spin $\hat{\vec{I}}$ and the total angular momentum of the electrons $\hat{\vec{J}}$. In the absence of external fields the $2p\ {}^2P_{\frac{3}{2}}$ $(J = \frac{3}{2})$ level of $^7\mathsf{Li}$ $(I = \frac{3}{2})$ splits into four hyperfine levels characterized by the quantum numbers $F = 3, 2, 1, 0$ (eigenvalues of the operator $\hat{\vec{F}}^2$ of the form $F(F+1)$; all angular momentum operators discussed in this work are dimensionless). The degeneracy is removed up to the natural degeneracy. In the case of $^6\mathsf{Li}$ $(I = 1)$ the same $2p\ {}^2P_{\frac{3}{2}}$ level splits into three hyperfine levels characterized by the quantum numbers $F = \frac{5}{2}, \frac{3}{2}, \frac{1}{2}$. Since the natural degeneracy of a hyperfine level characterized by the quantum number F is $2F+1$ the total degrees of degeneracy of the $2p\ {}^2P_{\frac{3}{2}}$ level are

$$\begin{array}{lcccc} {}^7\mathsf{Li} & : & 16 & = & 7+5+3+1 \\ {}^6\mathsf{Li} & : & 12 & = & 6+4+2. \end{array} \tag{2.1}$$

2.2.1 The Hyperfine Structure Interaction

Multipole Expansion of the Interaction Energy

The electric potential of any given distribution of charges can be decomposed into a sum of terms involving the various electric multipole moments. Analogously, it is possible to represent the Hamiltonian of the hyperfine structure (operator of the interaction between the two charge distributions of the electrons and the nucleus) by a multipole expansion as a sum of scalar products of spherical tensor operators:

$$\hat{H}_{\text{hyp}} = \sum_{k>0} \left(\hat{\mathbf{T}}^{(k)} \cdot \hat{\mathbf{M}}^{(k)} \right) = \sum_{k>0} \sum_{q=-k}^{k} (-1)^q \, \hat{T}_q^{(k)} \hat{M}_{-q}^{(k)} \tag{2.2}$$

The operators $\hat{\mathbf{T}}^{(k)}$ contain the electronic degrees of freedom of the interaction, the operators $\hat{\mathbf{M}}^{(k)}$ the nuclear degrees of freedom. The latter operators, $\hat{\mathbf{M}}^{(k)}$, can be identified with the generalized nuclear moments. The exclusion of the term with $k=0$ in the upper expansion is based on the fact that it describes the interaction between the valence electron and the spherical part of the electric nuclear charge distribution. This influence, however, is already taken into account by the unperturbed Hamiltonian via the central field potential.

In general it can be stated that for reasons of parity, terms corresponding to odd k-values describe the magnetic, terms corresponding to even k-values the electric interaction.

The term with $k=1$ takes into account the interaction between the nuclear magnetic moment

$$\hat{\mathbf{M}}^{(1)} = g_I \mu_N \hat{\vec{I}} = \hat{g}_I \mu_B \hat{\vec{I}} \tag{2.3}$$

and the magnetic field at the position of the nucleus, induced by the orbital angular momenta and spin angular momenta of the outer electrons

$$\hat{\mathbf{T}}^{(1)} = \frac{\mu_0 \mu_B}{4\pi} \left\{ \frac{2g_L}{\hat{r}^3} \hat{\vec{L}} - \frac{g_S}{\hat{r}^3} [\hat{\vec{S}} - 3 \frac{\hat{\vec{S}} \hat{\vec{r}}}{\hat{r}^2} \hat{\vec{r}}] + \frac{2}{3} g_S \frac{\delta(\hat{r})}{\hat{r}^2} \hat{\vec{S}} \right\}, \tag{2.4}$$

where $\mu_B > 0$ is the Bohr magneton and $\mu_N > 0$ the nuclear magneton. Furthermore,

$$\hat{g}_I = g_I \frac{m_e}{m_p} \tag{2.5}$$

is the so-called *g-factor of the nucleus* in units of the Bohr magneton.

The magnetic field induced at the position of the nucleus is composed of three different parts: the *orbital term*, containing the orbital angular momentum $\hat{\vec{L}}$, is determined, classically speaking, by the periodic movement of the valence electron around the nucleus. The *spin-dipole term* describes the interaction between the spin $\hat{\vec{S}}$ of the valence electron and the nuclear spin $\hat{\vec{I}}$. The *contact term* finally, takes the polarization of the nucleus by the electrons into account. Such a polarization is possible only because of the small but finite spatial extent of the nucleus. Since only the wavefunctions of s-electrons are nonvanishing at the position of the nucleus, only these electrons contribute to the contact term.

The term corresponding to $k = 2$ contains the interaction between the electric quadrupole moment of the nucleus, represented by

$$\hat{\mathbf{M}}^{(2)} = \frac{e}{2} \frac{\sqrt{6}\, Q}{I(2I-1)} \left(\hat{\vec{\mathbf{I}}} \cdot \hat{\vec{\mathbf{I}}} \right)^{(2)} \tag{2.6}$$

and the gradient of the electric field at the position of the nucleus generated by the valence electron

$$\hat{\mathbf{T}}^{(2)} = -\frac{e}{4\pi\epsilon_0} \frac{1}{\hat{r}^3} \hat{\mathbf{C}}^{(2)}. \tag{2.7}$$

Q is called the *quadrupole moment* of the nucleus, whereas $\hat{\mathbf{C}}^{(2)}$ represent the renormalized spherical harmonics of the order 2. In general

$$C_q^{(k)} := \sqrt{\frac{4\pi}{2k+1}} Y_q^{(k)} \tag{2.8}$$

holds.

The terms corresponding to $k = 3, 4$ describe the magnetic octupole interaction and the electric hexadecapole interaction, respectively, whose contributions to the total interaction energy are assumed to be negligible with respect to the other terms.

Representation of the Hyperfine Structure Operator in the "Coupled" Basis $|\gamma_I \gamma_J I J F M_F\rangle$

It makes sense to adapt the basis vectors in the space $2p\,^2P_{\frac{3}{2}}$ to the particular problem to be solved. In the case of zero or small external field strengths, the coupling between $\hat{\vec{I}}$ and $\hat{\vec{J}}$ to $\hat{\vec{F}}$ is (approximately) maintained and the quantum numbers F and M_F remain *good quantum numbers.* Therefore, it is reasonable to represent the perturbation operators in the basis of common eigenvectors of the operator $\hat{\vec{I}}^2$, $\hat{\vec{J}}^2$, $\hat{\vec{F}}^2$ and $\hat{F}_z$. These vectors are denoted by $|\gamma_I \gamma_J I J F M_F\rangle$ in the following. γ_I and γ_J represent the eigenvalues of all the other operators which together with the aforementioned form a complete set of commuting observables of the state space. For the matrix elements of the operator $\hat{H}_{\text{hyp}}$ one now obtains in the considered basis:

$$\begin{aligned} &\langle \gamma_I \gamma_J I J F M_F | \hat{H}_{\text{hyp}} | \gamma_I' \gamma_J' I' J' F' M_F' \rangle = \\ &\sum_{k>0} \delta_{M_F, M_F'} \delta_{F,F'} (-1)^{I'+J+F} \begin{Bmatrix} J' & I' & F' \\ I & J & k \end{Bmatrix} \cdot \\ &\cdot \langle \gamma_J J \| \hat{\mathbf{T}}^{(k)} \| \gamma_J' J' \rangle \langle \gamma_I I \| \hat{\mathbf{M}}^{(k)} \| \gamma_I' I' \rangle . \end{aligned} \tag{2.9}$$

The symbols resembling matrix elements and containing the double bars

$$\begin{gathered} \langle \gamma_J J \| \hat{\mathbf{T}}^{(k)} \| \gamma_J' J' \rangle \\ \langle \gamma_I I \| \hat{\mathbf{M}}^{(k)} \| \gamma_I' I' \rangle \end{gathered} \tag{2.10}$$

are the so-called *reduced matrix elements* which are independent of all magnetic quantum numbers M_I, M_I', M_J, M_J' as well as on a particular choice of the number q representing one of the $2k+1$ spherical tensor operators $\hat{T}_q^{(k)}$. The symbol

$$\begin{Bmatrix} j_1 & j_2 & j_3 \\ j_4 & j_5 & j_6 \end{Bmatrix} \tag{2.11}$$

is called a *Wigner 6j symbol.* A detailed discussion of its properties and those of the reduced matrix elements is given e.g. in [6] or [7].

The expressions for the matrix elements can appreciably be simplified by the following considerations. First of all the matrix elements nondiagonal in the quantum numbers γ_I and I given in eq. (2.9) can be neglected to a very good approximation since the energy differences corresponding to different energy levels of the nucleus clearly exceed the energy differences corresponding to different electronic states. For this reason, in nearly all problems of the electron shells, the nucleus can be assumed to remain in its ground state.

Secondly, in a variety of cases neglecting the interaction between states corresponding to different γ_J values is still an excellent approximation (always assuming that the field strengths remain appropriately small). Such a simplification is possible because the terms corresponding to different γ_J values are energetically far apart from each other as compared to the energy corrections caused by the perturbation.

Finally, the restriction to small external field strengths guarantees that the matrix elements nondiagonal in the quantum number J can be ignored in a first approximation. Once more this is justified by the negligibly small hyperfine splitting in comparison with the effects of fine structure ($\sim$ 10 GHz for lithium between the levels $2p\ ^2P_{\frac{3}{2}}$ and $2p\ ^2P_{\frac{1}{2}}$).

Before giving explicit expressions for the matrix representation of the hyperfine structure operator, the so-called *diagonal hyperfine structure constants* are defined via

$$\begin{aligned} A_k &= \langle \gamma_J J J | \hat{T}_0^k | \gamma_J J J \rangle \langle \gamma_I I I | \hat{M}_0^k | \gamma_I I I \rangle = \\ &= \begin{pmatrix} J & k & J \\ -J & 0 & J \end{pmatrix} \begin{pmatrix} I & k & I \\ -I & 0 & I \end{pmatrix} \langle \gamma_J J \| \hat{\mathbf{T}}^{(k)} \| \gamma_J J \rangle \langle \gamma_I I \| \hat{\mathbf{M}}^{(k)} \| \gamma_I I \rangle . \end{aligned} \tag{2.12}$$

The symbols of the form

$$\begin{pmatrix} j_1 & j_2 & j_3 \\ m_1 & m_2 & m_3 \end{pmatrix} \tag{2.13}$$

are the so-called *Wigner 3j symbols* whose definition involves *Clebsch-Gordan-coefficients*. However, they possess a larger variety of symmetry operations with respect to the interchange of quantum numbers than the Clebsch-Gordan-coefficients. For a detailed treatment of their properties, see again [6] or [7].

One finally obtains for the matrix elements of the hyperfine structure operator

$$\begin{aligned} &\langle \gamma_I \gamma_J I J F M_F | \hat{H}_{\text{hyp}} | \gamma_I \gamma_J I J F' M_F' \rangle = \\ &= \sum_{k>0} (-1)^{I+J+F} \begin{Bmatrix} J & I & F \\ I & J & k \end{Bmatrix} \frac{h A_k \, \delta_{M_F, M_F'} \delta_{F,F'}}{\begin{pmatrix} J & k & J \\ -J & 0 & J \end{pmatrix} \begin{pmatrix} I & k & I \\ -I & 0 & I \end{pmatrix}} . \end{aligned} \tag{2.14}$$

By the very definition of the diagonal hyperfine structure constants A_k, the matrix elements no longer depend explicitly on the radial wavefunctions via the reduced matrix elements. So the lack of knowledge concerning the radial wavefunctions can be compensated by the inclusion of hyperfine structure constants found either from experiment or from *ab-initio* calculations. The traditionally used hyperfine structure constants a,b,... are related to the diagonal hyperfine structure constants in the following way:

$$\begin{aligned} A_1(J) &= IJa(J) \\ A_2(J) &= \tfrac{1}{4}b(J). \end{aligned} \tag{2.15}$$

Representation of the Hyperfine Structure Operator in the "Decoupled" Basis $|\gamma_I \gamma_J I J M_I M_J\rangle$

If external fields are present, it may be advantageous to use the basis of common eigenvectors of the operators $\hat{\vec{I}}^2$, $\hat{I}_z$, $\hat{\vec{J}}^2$ and $\hat{J}_z$, since in this case the coupling between $\hat{\vec{I}}$ and $\hat{\vec{J}}$ to $\hat{\vec{F}}$ is weakened (or even removed). Because of the aforementioned reasons, only matrix elements diagonal in the quantum numbers γ_I, γ_J, I and J are given:

$$\begin{aligned} &\langle \gamma_I \gamma_J I J M_I M_J | \hat{H}_{\text{hyp}} | \gamma_I \gamma_J I J M_I' M_J' \rangle = \\ &= ha(J)(-1)^{M_J - M_J'}(-1)^{J+I-M_J-M_I}\sqrt{(2J+1)(J+1)J(2I+1)(I+1)I}\cdot \\ &\cdot \begin{pmatrix} J & 1 & J \\ -M_J & M_J - M_J' & M_J' \end{pmatrix} \begin{pmatrix} I & 1 & I \\ -M_I & M_J' - M_J & M_I' \end{pmatrix} + \\ &+ hb(J)(-1)^{M_J - M_J'}(-1)^{J+I-M_J-M_I}\frac{\sqrt{(2J+3)(J+1)(2J+1)J(2J-1)(2I+3)(I+1)(2I+1)I(2I-1)}}{4IJ(2I-1)(2J-1)}\cdot \\ &\cdot \begin{pmatrix} J & 2 & J \\ -M_J & M_J - M_J' & M_J' \end{pmatrix} \begin{pmatrix} I & 2 & I \\ -M_I & M_J' - M_J & M_I' \end{pmatrix}. \end{aligned} \tag{2.16}$$

The equation above can immediately be obtained by using the *Wigner-Eckart Theorem* twice and consecutive evaluation of the 3j symbols appearing in the definition of the diagonal hyperfine structure constants.

2.2.2 The Interaction with the External Magnetic Field

The investigations performed are limited to a range of the magnetic field strength in such a way that the interaction between the atom and the external magnetic field is based on paramagnetic effects only. The corresponding perturbation operator is linear in the magnetic field strength and describes the potential energy of a magnetic dipole of magnetic moment $\vec{\mu}$ in the field:

$$\hat{H}_{\text{mag}} = -\hat{\vec{\mu}} \cdot \hat{\vec{B}}. \tag{2.17}$$

The total magnetic interaction energy is obtained from eq. (2.17) by combining in $\hat{\vec{\mu}}$ the sum of the magnetic moments of the valence electron and the nucleus:

$$\begin{aligned} \hat{\vec{\mu}}_J &= -\mu_B g_J \hat{\vec{J}}, && (\mu_B > 0); \\ \hat{\vec{\mu}}_I &= \mu_N g_I \hat{\vec{I}} = \mu_B \hat{g}_I \hat{\vec{I}}, && (\mu_N > 0). \end{aligned} \tag{2.18}$$

Here it is assumed that the perturbation does not remove the spin-orbit coupling, so that J remains a good quantum number. If the magnetic field is chosen to be directed along the z-axis of the coordinate system, the magnetic perturbation operator can be rewritten in the form:

$$\hat{H}_{\text{mag}} = -\left(\hat{\vec{\mu}}_J + \hat{\vec{\mu}}_I\right)\hat{\vec{B}} = \left(g_J \hat{J}_z - \hat{g}_I \hat{I}_z\right)\mu_B B_z. \tag{2.19}$$

Representation of the Magnetic Perturbation Operator

By making use of eq. (2.19) it is straightforward to find the matrix representation of the Zeeman operator within the two bases $|\gamma_I \gamma_J I J F M_F\rangle$ and $|\gamma_I \gamma_J I J M_I M_J\rangle$. Once more only those matrix elements between basis vectors are given which belong to the same eigenvalues of the operator $\hat{\vec{J}}^2$.

In the representation of the basis vectors $|\gamma_I \gamma_J I J F M_F\rangle$ one obtains:

$$\begin{aligned} &\langle \gamma_I \gamma_J I J F M_F | \hat{H}_{\text{mag}} | \gamma_I \gamma_J I J F' M_F' \rangle = \\ &= \mu_B B_z (-1)^{F-M_F} \begin{pmatrix} F & 1 & F' \\ -M_F & 0 & M_F' \end{pmatrix} \sqrt{(2F+1)(2F'+1)} \;\cdot \\ &\cdot \Bigg[g_J (-1)^{I+J+1+F} \sqrt{(2J+1)(J+1)J} \begin{Bmatrix} J & F & I \\ F' & J & 1 \end{Bmatrix} - \\ &- \hat{g}_I (-1)^{I+J+1+F'} \sqrt{(2I+1)(I+1)I} \begin{Bmatrix} I & F & J \\ F' & I & 1 \end{Bmatrix} \Bigg]. \end{aligned} \tag{2.20}$$

A 3j symbols is zero if the sum of the elements of the second line differs from zero. Therefore, the matrix elements given above are diagonal with respect to the magnetic quantum number M_F.

Since the basis vectors $|\gamma_I \gamma_J I J M_I M_J\rangle$ are simultaneous eigenvectors of the operators in eq. (2.19), the matrix elements of $\hat{H}_{\text{mag}}$ in that basis are simply:

$$\begin{aligned} &\langle \gamma_I \gamma_J I J M_I M_J | \hat{H}_{\text{mag}} | \gamma_I \gamma_J I J M_I' M_J' \rangle = \\ &= \delta_{M_I, M_{I'}} \delta_{M_J, M_{J'}} \left(g_J M_J - \hat{g}_I M_I\right) \mu_B B_z. \end{aligned} \tag{2.21}$$

They are diagonal in the quantum number M_I as well as in the quantum number M_J and consequently in $M_F = M_I + M_J$.

2.2.3 The Interaction with the External Electric Field

Similar to the case of the magnetic interaction, the electric interaction energy can be written as the potential energy of a dipole:

$$\hat{H}_{\text{el}} = -\hat{\vec{p}} \cdot \hat{\vec{E}}; \tag{2.22}$$

$\hat{\vec{p}}$ is the operator of the dipole moment of the electron shell

$$\hat{\vec{p}} = -e \sum_{i=1}^{N} \hat{\vec{r}}_i \tag{2.23}$$

and $\hat{\vec{r}}_i$ is the position operator of the i-th electron.

Amongst all atoms only hydrogen shows a linear Stark effect. This is due to the fact that both, the dipole operator and, therefore, the operator $\hat{H}_{\text{el}}$ have odd parity. Since in general the electronic wavefunctions of the atoms have well-defined parity, all matrix elements of the kind

$$\langle a|\hat{H}_{\text{el}}|a\rangle \tag{2.24}$$

are zero. By using perturbation theory in second order for a (nondegenerate) state $|a\rangle$, the energy corrections are given by

$$\Delta W_a = \sum_{b \neq a} \frac{\langle a| - \hat{\vec{p}} \cdot \hat{\vec{E}}|b\rangle\langle b| - \hat{\vec{p}} \cdot \hat{\vec{E}}|a\rangle}{W_a - W_b}. \tag{2.25}$$

Following a method developed by Schmieder [8], [9] it is possible to calculate the energy corrections caused by the electric field by the introduction of an effective electric operator

$$\hat{H}_{\text{el,eff}} = \hat{\vec{p}}\hat{\vec{E}}\,\hat{\lambda}\,\hat{\vec{p}}\hat{\vec{E}} \tag{2.26}$$

with

$$\hat{\lambda} = \sum_{b \neq a} \frac{|b\rangle\langle b|}{W_a - W_b}. \tag{2.27}$$

The sum in $\hat{\lambda}$ extends over all quantum states differing from the state $|a\rangle$ itself. According to Schmieder, the energy corrections are simply the eigenvalues of the matrix representing the operator $\hat{H}_{\text{el,eff}}$. This corresponds to a transition to first order perturbation theory, however, with a modified effective electric operator $\hat{H}_{\text{el,eff}}$.

$\hat{H}_{\text{el,eff}}$ neither acts on the electron spin nor on the nuclear spin, so it is diagonal in the quantum numbers S and I. Right as in the case of the hyperfine structure interaction and the magnetic interaction, it is again assumed that the energy corrections caused by the external electric field remain significantly smaller than the energy differences of the fine structure, which corresponds to neglecting nondiagonal matrix elements in the quantum number J.

It is convenient to write also $\hat{H}_{\text{el,eff}}$ as a sum of scalar products of spherical tensor operators

$$\hat{H}_{\text{el,eff}} = \sum_k a_k \left(\hat{\mathbf{Y}}^{(k)}\Big(\frac{\vec{E}}{E}\Big) \cdot \hat{\mathbf{Y}}^{(k)}\Big(\frac{\vec{J}}{\sqrt{J(J+1)}}\Big) \right) \tag{2.28}$$

since this notation has the advantage of having separated the dependencies of $\hat{H}_{\text{el,eff}}$ on the modulus and the direction of the electric field strength. The coefficients a_k depend only on the modulus of the electric field, the scalar products of the tensor operators only on the direction of the electric field. In addition, the summation index k is subjected to the following restrictions:

$$k \leq 2, \qquad k \text{ ... even.} \tag{2.29}$$

The latter follows for reasons of parity. $\hat{H}_{\text{el,eff}}$ takes on the form:

$$\hat{H}_{\text{el,eff}} = a_0 \hat{\mathbf{Y}}^{(0)}\Big(\frac{\vec{E}}{E}\Big) \cdot \hat{\mathbf{Y}}^{(0)}\Big(\frac{\vec{J}}{\sqrt{J(J+1)}}\Big) + a_2 \hat{\mathbf{Y}}^{(2)}\Big(\frac{\vec{E}}{E}\Big) \cdot \hat{\mathbf{Y}}^{(2)}\Big(\frac{\vec{J}}{\sqrt{J(J+1)}}\Big). \tag{2.30}$$

Comparison with the classical notation

$$\hat{H}_{\text{el,eff}} = -\frac{1}{2}\hat{\hat{\boldsymbol{\alpha}}} E^2 \tag{2.31}$$

leads to

$$\hat{\hat{\boldsymbol{\alpha}}} = \alpha_0 \hat{\mathbb{1}} + \alpha_2 \hat{\mathbf{Q}}, \tag{2.32}$$

where $\hat{\mathbf{Q}}$ is an operator proportional to

$$\hat{\mathbf{Y}}^{(2)}\Big(\frac{\vec{E}}{E}\Big) \cdot \hat{\mathbf{Y}}^{(2)}\Big(\frac{\vec{J}}{\sqrt{J(J+1)}}\Big). \tag{2.33}$$

α_0 and α_2 represent the scalar and tensorial polarizabilities which can be incorporated into the theory as determined from experiment or as calculated by means of *ab-initio* theories. (See. App. B for the numerical values of α_0 and α_2 in the case of ^{6}Li and ^{7}Li.)

Representation of the Effective Electric Perturbation Operator

By choosing the basis vectors of the "coupled" basis $|\gamma_I\gamma_J IJFM_F\rangle$, one obtains

$$\begin{aligned}\langle\gamma_I\gamma_J IJFM_F|\hat{H}_{\text{el,eff}}|\gamma_I\gamma_J IJF'M_F'\rangle &= \\ = -\tfrac{1}{2}\alpha_0 E^2\delta_{FF'}\delta_{M_F M_F'} - \tfrac{1}{2}\alpha_2 E^2 Q_{FM_F,F'M_F'}\end{aligned} \tag{2.34}$$

with

$$\begin{aligned}Q_{FM_F,F'M_F'} &= \sqrt{\frac{15}{2}}\sqrt{\frac{(J+1)(2J+1)(2J+3)}{J(2J-1)}}\sqrt{(2F+1)(2F'+1)}\cdot \\ &\left\{\begin{array}{ccc} F & 2 & F' \\ J & I & J\end{array}\right\}\sum_{q=-2}^{2}\sum_{\mu=-1}^{1}\sum_{\mu'=-1}^{1}\left(\begin{array}{ccc} 1 & 2 & 1 \\ \mu & -q & \mu'\end{array}\right)\cdot \\ &(-1)^{I+J-F'+F-M_F}\left(\begin{array}{ccc} F & 2 & F' \\ M_F & q & -M_F'\end{array}\right)n_\mu n_{\mu'}\end{aligned} \tag{2.35}$$

and

$$n_\mu = \frac{E_\mu}{E} \quad \mu = -1,0,1 \quad E_\mu = \left(\begin{array}{c} E_1 \\ E_0 \\ E_{-1}\end{array}\right) = \left(\begin{array}{c} -(E_x + \imath E_y)/\sqrt{2} \\ E_z \\ (E_x - \imath E_y)/\sqrt{2}\end{array}\right). \tag{2.36}$$

In the "decoupled" basis $|\gamma_I\gamma_J IJM_IM_J\rangle$, however, the matrix elements of $\hat{H}_{\text{el,eff}}$ are

$$\begin{aligned}\langle\gamma_I\gamma_J IJM_IM_J|\hat{H}_{\text{el,eff}}|\gamma_I\gamma_J IJM_I'M_J'\rangle &= \\ = -\tfrac{1}{2}\alpha_0 E^2\delta_{M_I M_I'}\delta_{M_J M_J'} - \tfrac{1}{2}\alpha_2 E^2 Q_{M_IM_J,M_I'M_J'}\end{aligned} \tag{2.37}$$

with

$$\begin{aligned}Q_{M_IM_J,M_I'M_J'} &= \\ &= \sqrt{\frac{15}{2}}\sqrt{\frac{(J+1)(2J+1)(2J+3)}{J(2J-1)}}\delta_{M_IM_I'}(-1)^{J-M_J}\cdot \\ &\cdot\sum_{q=-2}^{2}\left(\begin{array}{ccc} J & 2 & J \\ -M_J & q & M_J'\end{array}\right)\sum_{\mu=-1}^{1}\sum_{\mu'=-1}^{1}\left(\begin{array}{ccc} 1 & 2 & 1 \\ \mu & q & \mu'\end{array}\right)n_\mu n_{\mu'}.\end{aligned} \tag{2.38}$$

Even though the expressions above contain the general case of arbitrary electric field direction, in this work the latter is always assumed to be directed along the x-axis, which guarantees perpendicularly crossed magnetic and electric fields.

2.3 Reduction of the State Space into two Noninteracting Subspaces of Identical Dimension

In order to compute the energy corrections of the hyperfine structure levels belonging to the $2p\ ^2P_{\frac{3}{2}}$ fine structure level in the presence of external fields, one has to perform a diagonalization of the three perturbation operators introduced in the last subsection. In the case of $^7\mathsf{Li}$ this is a 16x16 square matrix, in the case of $^6\mathsf{Li}$ a 12x12 square matrix. The remaining symmetries of the system, however, can be used very advantageously to gain a great simplification of the numerical calculations.

First of all it is easy to recognize that the operator $\hat{H}_{\text{hyp}}$ commutes with both, the operator of the z-component $\hat{F}_z$ and the operator $\hat{\vec{F}}^2$ of the square of the total angular momentum of the atom:

$$[\hat{H}_{\text{hyp}}, \hat{F}_z] \; = \; 0 \tag{2.39}$$

$$[\hat{H}_{\text{hyp}}, \hat{\vec{F}}^2] \; = \; 0. \tag{2.40}$$

This result can be deduced from the fact that those three operators already have diagonal form in the basis $|\gamma_I \gamma_J I J F M_F\rangle$. The operator $\hat{H}_{\text{hyp}}$, therefore, only connects states corresponding to the same quantum numbers F and M_F, a property, that can be seen directly from the formulae for the matrix elements as well.

The operator of the magnetic interaction $\hat{H}_{\text{mag}}$ contains the angular momentum operators $\hat{I}_z$ and $\hat{J}_z$, which on their own commute with $\hat{F}_z$ and so one obtains:

$$[\hat{H}_{\text{mag}}, \hat{F}_z] = 0. \tag{2.41}$$

The magnetic perturbation operator, therefore, only connects states belonging to the same value of the quantum number M_F. Again, this property manifests itself in the formula for the matrix elements, in particular in the 3j symbol (see eq. (2.20)).

Even in the case of the electric field and for perpendicularly crossed fields ($\vec{E}$ in xy-plane, $\vec{B} \parallel$ z-axis) it is possible to find a selection rule for nonvanishing matrix elements by making use of symmetry considerations. The independence with respect to an electric field reversal of the energy corrections caused by $\hat{H}_{\text{el,eff}}$ correspond to the symmetry operation of rotation around the z-axis by 180°. Such a rotation, however, is related to the selection rule

$$M_F - M_F' = \text{even} \tag{2.42}$$

as shown in [4].

By combining the different selection rules of the three perturbation operators, one finally obtains the selection rule of the total perturbation operator (sum of $\hat{H}_{\rm hyp}$, $\hat{H}_{\rm mag}$ and $\hat{H}_{\rm el,eff}$), which is of greatest importance:

$$\begin{aligned} &\langle \gamma_I \gamma_J I J F M_F | \hat{H}_{\rm tot} | \gamma_I \gamma_J I J F' M_F' \rangle = \\ &= \left\{ \begin{array}{rcrcl} 0 & ... & M_F - M_F' & = & \text{odd} \\ \neq 0 & ... & M_F - M_F' & = & \text{even} \end{array} \right. . \end{aligned} \tag{2.43}$$

Any basis vector $|\gamma_I \gamma_J I J F M_F\rangle$ can now be assigned unambiguously to one of the two subspaces, corresponding to the particular value of the quantum number M_F. For this reason, the representation reduces to two blocks arranged along the main diagonal. This procedure reduces the problem of diagonalizing the total matrix to the problem of diagonalizing instead two submatrices with half dimension. A more detailed discussion of the symmetry considerations presented in this section can be found in [4] and [10].

Subsequently to this rather general separation into two subsystems, the same process shall now be examined in particular for ^{7}Li and ^{6}Li, respectively. Both, the similarities and the differences are emphasized. A summary of the most important results of this separation is given in Tab. 6.1 in section 6.1.2. The basis vectors $|\gamma_I \gamma_J I J F M_F\rangle$ are abbreviated by $|F M_F\rangle$. A first observation is that the possible values of the quantum numbers F and M_F are integers in the case of ^{7}Li whereas they are half odd integers in the case of ^{6}Li.

The selection rule $\Delta M_F =$ even, therefore, divides the set of natural numbers into the sets of the even and odd ones, just as for ^{23}Na ($I = 3/2$). Heubrandtner was led by this fact to denote the two subsystems by the odd subsystem and the even subsystem. For ^{7}Li this notation can be adapted analogously.

For ^{6}Li, the relation $\Delta M_F =$ even, too, devides the set of half odd integers into two disjoint subsets but the naming of these has to be chosen in a different way. The subsystem containing the basis states $|\gamma_I \gamma_J I J F M_F\rangle$ with

$$M_F = \left\{ \frac{5}{2}, \quad \frac{1}{2}, \quad -\frac{3}{2} \right\} \tag{2.44}$$

is called the *positive* subsystem, whereas the subsystem with the basis states corresponding to the M_F values

$$M_F = \left\{ \frac{3}{2}, \quad -\frac{1}{2}, \quad -\frac{5}{2} \right\} \tag{2.45}$$

is called the *negative* subsystem, since a division modulo 4 of the numerators of the quantum numbers M_F gives +1 in the first case and -1 in the second case, respectively.

Another significant difference should already be pointed out: the two state vectors $|F M_F\rangle$ and $|F - M_F\rangle$ can always be found in different subsystems for ^{6}Li whereas for ^{7}Li they always belong to the same subsystem. For this pair of state vectors one obtains

$$\Delta M_F = 2\, M_F = \begin{cases} \text{odd} & \text{...} \quad {}^6\mathrm{Li} \\ \text{even} & \text{...} \quad {}^7\mathrm{Li}, \end{cases} \tag{2.46}$$

a fact that will be of great importance for the interpretation of different symmetries between the subsystems of ^{6}Li and ^{7}Li with respect to a magnetic field reversal.

Chapter 3

^{7}Li

This chapter serves in the main as a presentation of the results obtained for ^{7}Li. Starting with the discussion of the structure of the perturbation matrix elements especially for ^{7}Li and a brief overall view of the use of the relation between colors and quantum numbers, the next issues are the pure Zeeman and Stark effects. Thereafter follows the presentation of splitting diagrams obtained by implementing a specific field cycle of the external field parameters. Finally these investigations are to be completed by the calculations of the energy surfaces. By the term "energy surface" is meant the surface obtained by displaying the energy corrections above the BE-plane of the external field parameters.

Heubrandtner showed [4], that in each subsystem degeneracies appear only at single isolated points within the BE-plane. The energy surfaces of one subsystem do not intersect along extended lines, as may be expected, even though the energy surfaces belonging to different subsystems do intersect along lines.

In the course of the investigations concerning the hyperfine structure level transfer, however, these lines are of secondary interest, since for the adiabatic transfer of hyperfine levels the most important factor is the combination of crossing points and anticrossing points. The name "crossing point" is used in the following as a synonym for "point of accidental degeneracy". All observed points of accidental degeneracy are shown together in the so-called crossing diagram (comp. section 3.7).

In the section concluding this chapter it is demonstrated, that wavefunctions may assume in addition to the ordinary dynamical change in phase

$$\zeta_{\text{dyn}}(t_1) = e^{-\frac{i}{\hbar}\int_{t_0}^{t_1} \epsilon(\tau)d\tau} \tag{3.1}$$

a geometric change in phase, equal to

$$\zeta_{\text{geo}} = e^{+\imath\pi} = -1 \tag{3.2}$$

when the external field parameters B and E vary adiabatically along closed cunrves around certain crossing points in the BE-plane. These geometric changes in phase are often refered to as *Berry phases*.

3.1 Matrix Elements of the Perturbation Operators

Evaluating the expressions for the matrix elements of the three perturbation operators presented in the preceding chapter leads in the case of ^{7}Li to the

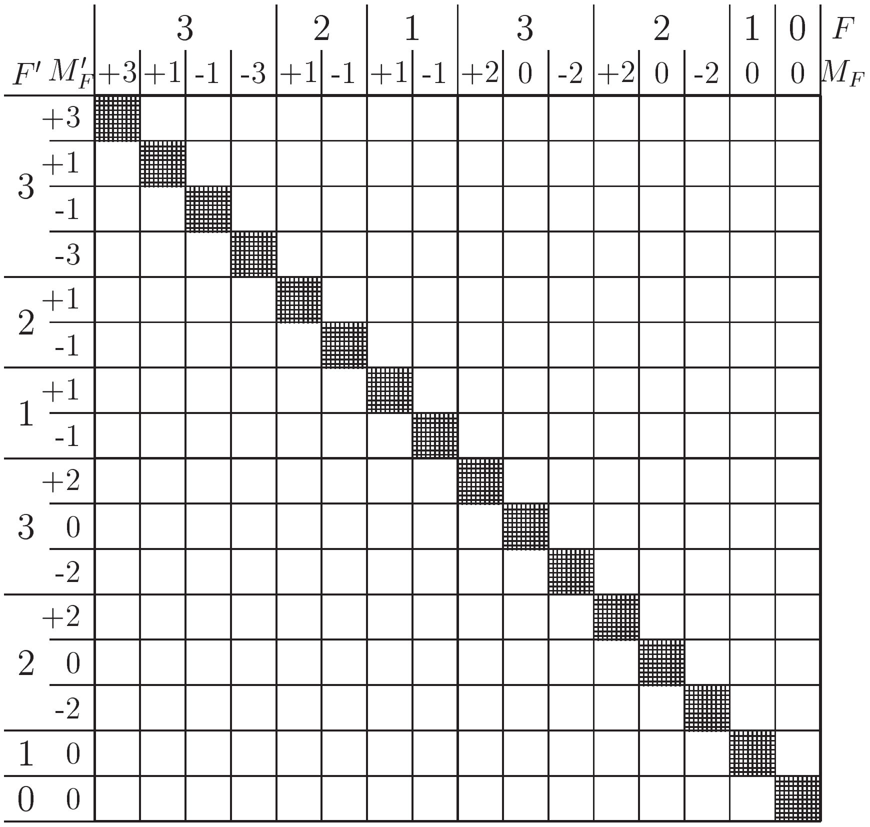

Figure 3.1: Hyperfine matrix elements $\langle \gamma_I \gamma_J I J F M_F | \hat{H}_{\text{hyp}} | \gamma_I \gamma_J I J F' M'_F \rangle$ of the $2p\,^2P_{\frac{3}{2}}$ level of ^{7}Li as given in eq. (2.14). F...total atomic angular momentum; M_F...corresponding magnetic quantum number $-F \leq M_F \leq +F$

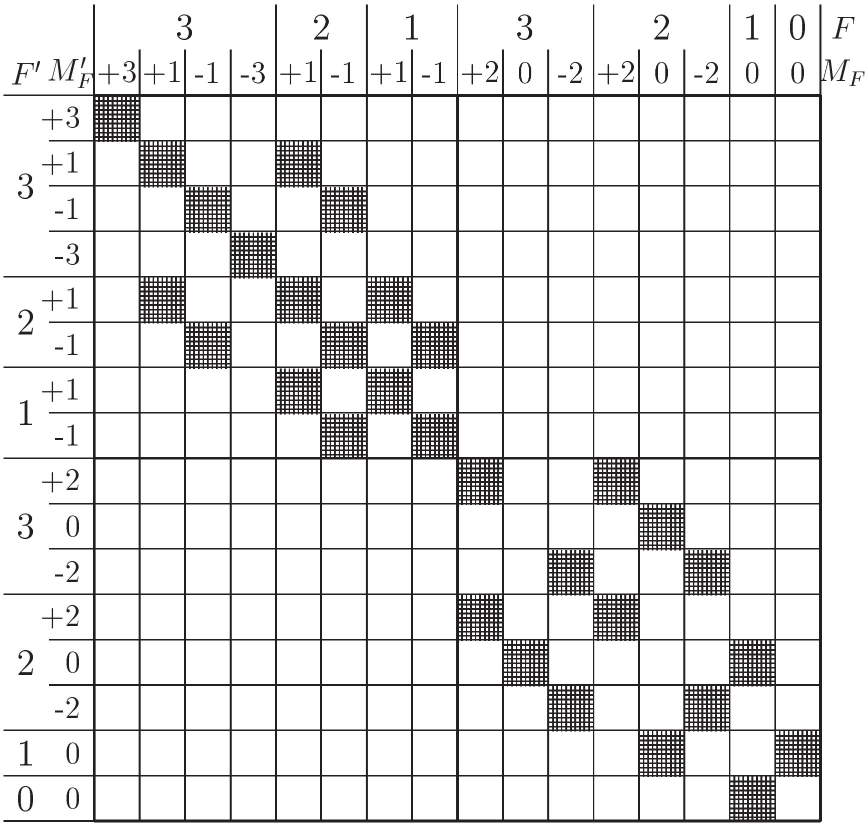

Figure 3.2: Zeeman matrix elements $\langle \gamma_I \gamma_J I J F M_F | \hat{H}_{\mathrm{mag}} | \gamma_I \gamma_J I J F' M'_F \rangle$ of the $2p\ ^2P_{\frac{3}{2}}$ level of $^7\mathsf{Li}$ as given in eq. (2.20). F...total atomic angular momentum; M_F...corresponding magnetic quantum number $-F \leq M_F \leq +F$

structure of the matrices, given in Figs. (3.1), (3.2) and (3.3). Even though some calculations are also performed in the representation with the basis vectors $|\gamma_I \gamma_J I J M_I M_J\rangle$, the corresponding structure of the matrix elements is not given explicitly. The diagrams show representations of the perturbation operators in the basis $|\gamma_I \gamma_J I J F M_F\rangle$, where a special ordering of the basis states is used: the vectors of the odd subsystem are followed by those of the even subsystem. Nonzero matrix elements are shown hatched, elements equal to zero remain white.

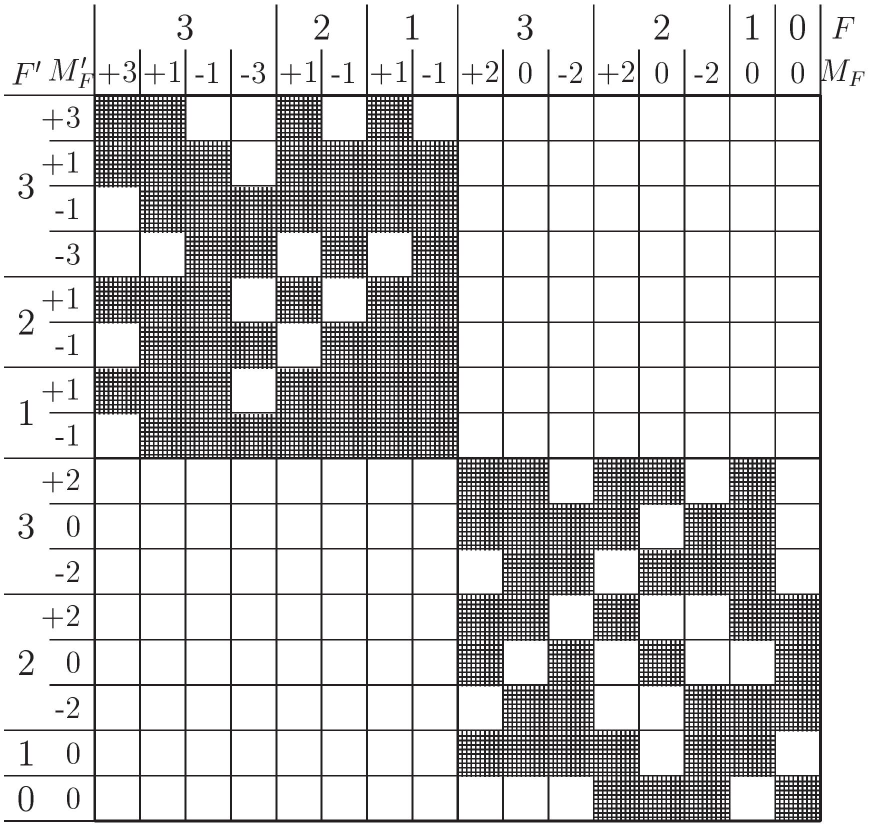

Figure 3.3: Stark matrix elements $\langle \gamma_I \gamma_J I J F M_F | \hat{H}_{\mathrm{el,eff}} | \gamma_I \gamma_J I J F' M'_F \rangle$ of the $2p\ ^2P_{\frac{3}{2}}$ level of ^{7}Li as given in eqs. (2.34) and (2.35). F...total atomic angular momentum; M_F...corresponding magnetic quantum number $-F \leq M_F \leq +F$

3.2 Relation between Quantum Numbers and Colors for ^{7}Li

Before starting the discussion of the crossing points, the color code used in this work, determining the relation between quantum numbers and colors should be presented. The inverted hyperfine structure is a characteristic of lithium among all the alkalines. This simply means, that levels characterized by higher values of the quantum number F have lower energies than those levels characterized by lower F values. This particular feature of lithium manifest itself in negative values of the hyperfine structure constants which is true for ^{7}Li as well as for ^{6}Li and implies among other certain disadvantages in the color code used until now.

In contrast to the arbitrary old color code (used in [4]), the new code is based on the convention to use different shades of one color for the hyperfine structure levels characterized by one and the same value of the quantum number F. Darker shades are consistently used for higher values of the quantum number M_F. The details for ^{7}Li are shown in Tab. 3.1.

Even Subsystem			**Odd Subsystem**		
F	M_F	**Color**	F	M_F	**Color**
0	0		1	1	
1	0		1	-1	
2	2		2	1	
2	0		2	-1	
2	-2		3	3	
3	2		3	1	
3	0		3	-1	
3	-2		3	-3	

Table 3.1: Color code used for the even and the odd subsystems of the energy levels in ^{7}Li.

3.3 Zeeman Effect of the $2p\ ^2P_{\frac{3}{2}}$ Level of ^{7}Li

In order to obtain Zeeman diagrams (energy corrections versus magnetic field strength) one has to diagonalize the sum of the operators $\hat{H}_{\text{hyp}}$ and $\hat{H}_{\text{mag}}$, a task that can be performed separately for the odd and the even subsystem. The results are given in Figs. 3.4 and 3.5. Since the Zeeman diagrams corresponding to negative magnetic field values are symmetrical with respect to the ordinate of the diagrams shown, these parts of the diagrams are omitted. The last observation is true in the case of ^{7}Li for both, the total level and for the two sublevels separately but in the case of ^{6}Li it is only valid for the total set of $2p\ ^2P_{\frac{3}{2}}$ levels. More profound investigations on the origin of this difference are carried out in chapter 6.

It can be seen directly from the diagrams, that in the odd subsystem there exist 4 points of accidental degeneracy for field values up to 1 mT, whereas in the even subsystem there exist only three such points. These points are simply refered to as magnetic crossing points and are denoted by **Bon** and **Ben**. The letters **o** and **e** represent the words "odd" and "even", **n** numbers the points according to increasing magnetic field strength. A listing of the most important data relating to the crossing points, including field values,

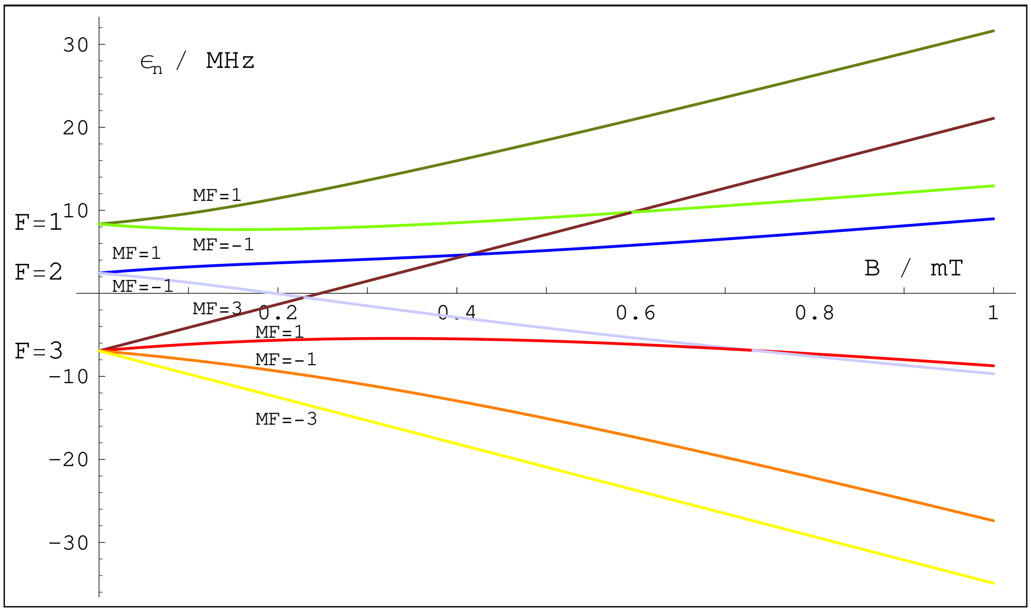

Figure 3.4: Splitting of the $2p\,^2P_{\frac{3}{2}}$ hyperfine energy levels ϵ_n of ^{7}Li in the odd subsystem ($M_F = \text{odd}$) due to the Zeeman effect.

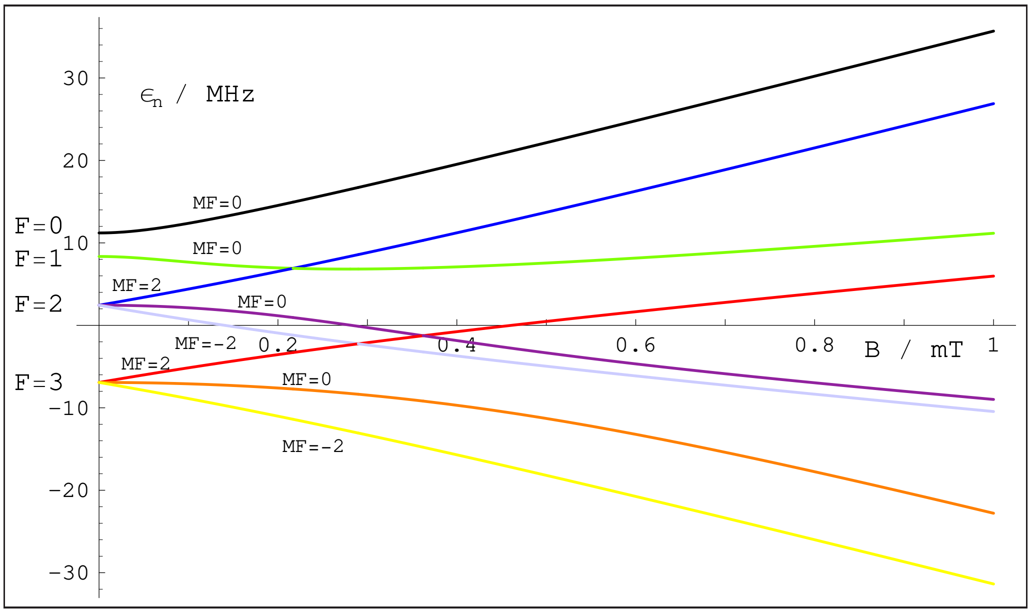

Figure 3.5: Splitting of the $2p\,^2P_{\frac{3}{2}}$ hyperfine energy levels ϵ_n of ^{7}Li in the even subsystem ($M_F = \text{even}$) due to the Zeeman effect.

energy eigenvalues and the designation of the pairs of eigenvectors involved can be found in section 3.7 in this chapter.

3.4 Stark Effect of the $2p\ ^2P_{\frac{3}{2}}$ Level of ^{7}Li

The calculation of energy corrections is carried out analogously to those in the case of the Zeeman effect. Correspondingly the operator

$$\hat{H}_{\text{tot}} = \hat{H}_{\text{hyp}} + \hat{H}_{\text{el,eff}} \tag{3.3}$$

has to be diagonalized for both subsystems.

As explained in chapter 2, the matrix elements of the operator $\hat{H}_{\text{el,eff}}$ are made up of two parts, those of the scalar and the tensorial polarizability

$$\hat{H}_{\text{el,eff}} = \hat{H}^{(0)}_{\text{el,eff}} + \hat{H}^{(2)}_{\text{el,eff}} \,. \tag{3.4}$$

The energy shifts due to the scalar polarizability concern the $2p\ ^2P_{\frac{3}{2}}$ level as a whole and appreciably exceed in magnitude the shifts caused by the tensorial polarizability. This fact hampers the presentation of Stark diagrams. Fig. 3.6 shows the energy corrections of the odd subsystem of ^{7}Li merely as a demonstration of the predominance of the scalar polarizability. In order to suppress this global downward shift of the energy in the diagrams, the scalar polarizability α_0 is simply put to zero before diagonalizing the perturbation matrix. The locations (values of the external fields) of the crossing points are not changed. This is easy to understand because $\hat{H}^{(0)}_{\text{el,eff}}$ is represented by a matrix proportional to the identity matrix in all different bases. With the use of

$$\hat{H}^{(0)}_{\text{el,eff}} = -\frac{1}{2}\alpha_0 E^2\, \hat{1} \tag{3.5}$$

the eigenvalue problem of the operator $\hat{H}_{\text{tot}} = \hat{H}_{\text{hyp}} + \hat{H}_{\text{el,eff}}$ can therefore be written in the following way:

$$\begin{aligned} \hat{H}_{\text{tot}}|\lambda_n\rangle &= \epsilon_n|\lambda_n\rangle, && (3.6)\\ \left[\hat{H}_{\text{hyp}} - \frac{1}{2}\alpha_0 E^2\, \hat{1} + \hat{H}^{(2)}_{\text{el,eff}}\right]|\lambda_n\rangle &= \epsilon_n|\lambda_n\rangle; && (3.7)\\ \Rightarrow \quad \left[\hat{H}_{\text{hyp}} + \hat{H}^{(2)}_{\text{el,eff}}\right]|\lambda_n\rangle &= \underbrace{\left(\epsilon_n + \frac{1}{2}\alpha_0 E^2\right)}_{\epsilon'_n}|\lambda_n\rangle. && (3.8) \end{aligned}$$

Diagonalizing $\hat{H}_{\text{tot}}$ with $\alpha_0 = 0$ leads to the energy eigenvalues ϵ'_n that differ

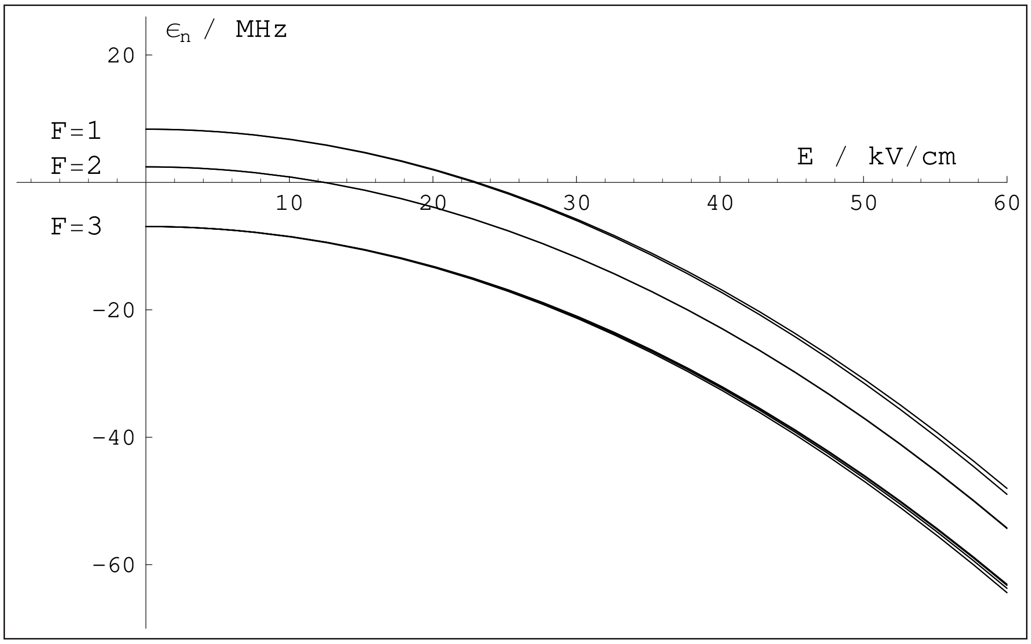

Figure 3.6: Splitting of the $2p\ ^2P_{\frac{3}{2}}$ hyperfine energy levels of $^7\mathsf{Li}$ in the odd subsystem (M_F = odd) according to the Stark effect, demonstrating the predominance of the term proportional to the scalar polarizability α_0. The small shifts separating the levels corresponding to the same value of the quantum number F are due to the term of the tensorial polarizability α_2. This is responsible for the crossing of energy levels due to the Stark effect.

from the actual eigenvalues ϵ_n by the global factor $\frac{1}{2}\alpha_0 E^2$:

$$\epsilon_n = \epsilon_n' - \frac{1}{2}\alpha_0 E^2. \tag{3.9}$$

The differences between energy eigenvalues belonging to the same value of the electric field E don't change by this transition:

$$\epsilon_2' - \epsilon_1' = \left(\epsilon_2 + \frac{1}{2}\alpha_0 E^2\right) - \left(\epsilon_1 + \frac{1}{2}\alpha_0 E^2\right) = \epsilon_2 - \epsilon_1. \tag{3.10}$$

For generating the plots it is advantageous to depict the eigenvalues ϵ_n' instead of the eigenvalues ϵ_n versus the electric field strength E as a single glance on Figs. 3.7 and 3.8 indicates. Besides, in such a diagram it is much easier to locate the points of accidental degeneracies.

The energy corrections caused by the quadratic Stark effect for both subsystems of the $2p\ ^2P_{\frac{3}{2}}$ level are shown in Figs. 3.7 and 3.8. While in the odd subsystem 2 electric crossing points have been located, the even subsystem doesn't contain any electric crossing point. Once more it is refered to the listing of crossing point data in section 3.7.

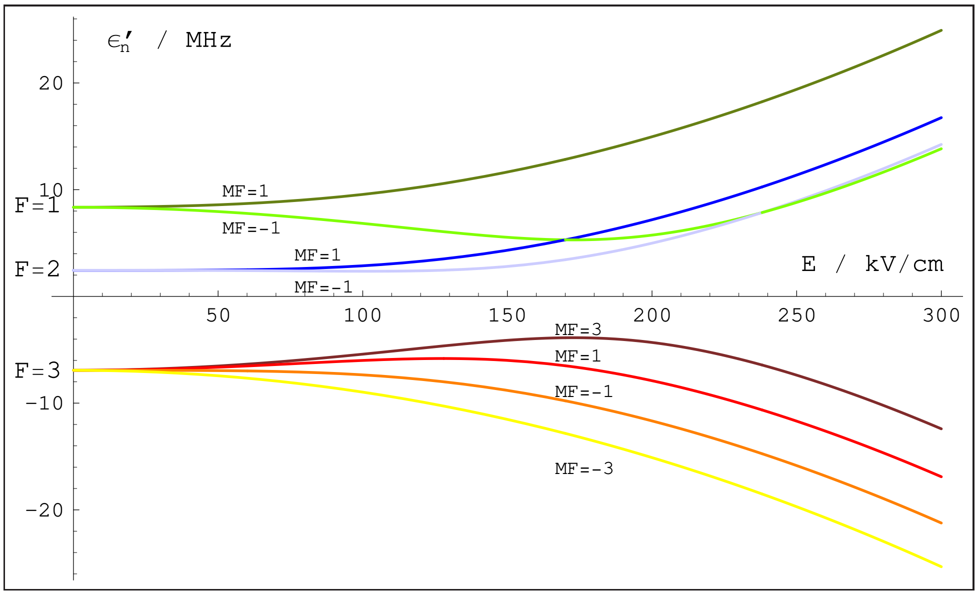

Figure 3.7: Splitting of the $2p\ ^2P_{\frac{3}{2}}$ hyperfine energy levels ϵ'_n of ^{7}Li in the odd subsystem (M_F = odd) due to the Stark effect. The term proportional to the scalar polarizability α_0 was put to zero before diagonalizing the perturbation matrix.

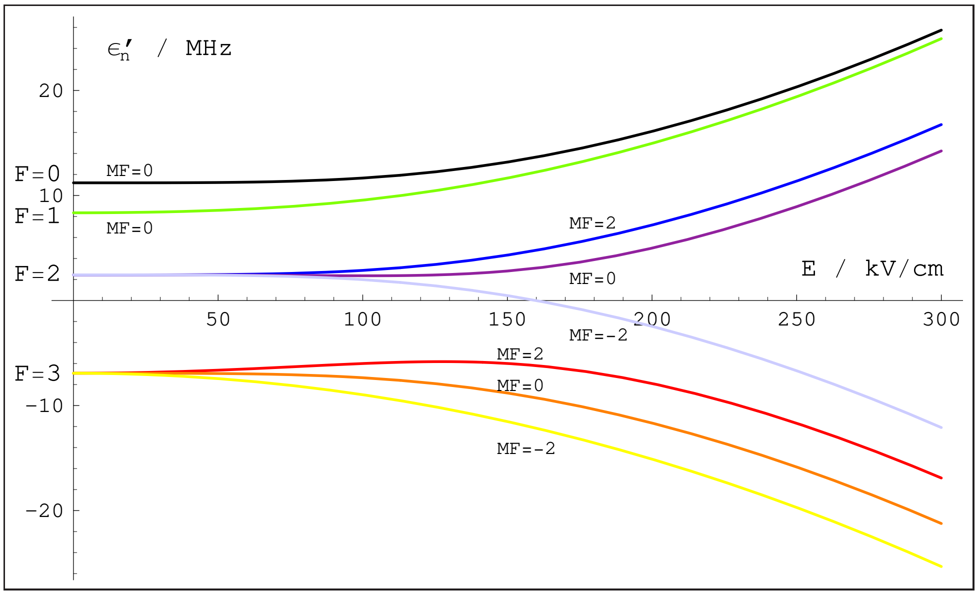

Figure 3.8: Splitting of the $2p\ ^2P_{\frac{3}{2}}$ hyperfine energy levels ϵ'_n of ^{7}Li in the even subsystem (M_F = even) due to the Stark effect. The term proportional to the scalar polarizability α_0 was put to zero before diagonalizing the perturbation matrix.

Figs. 3.7 and 3.8 show 16 curves in total. These are labeled with magnetic quantum numbers M_F such that M_F and $-M_F$ belong to different energies. This observation should be confronted with results known from the usual treatment of the Stark effect. This problem has already been hinted to in the introduction, section 1.2.

In the usual theory, the constant external electric field is aligned with the z-axis (quantization axis). Under this special presupposition and in second order perturbation theory, necessary in this investigation limited to the Hilbert space of the $2p\ ^2P_{\frac{3}{2}}$ level, the energy eigenvalues providing the frequency shifts depend on the square of the electric field strength and on the absolute value $|M_F|$ of the magnetic quantum number M_F. So one obtains 10 curves whose labels are given in Tab. 3.2 below in the column "$E \parallel z-axis$".

The very same number of energy (or frequency) shifts and curves must also turn up if another quantization axis (i.e. another basis for the computation of the elements of the perturbation matrix) is used. Some of these appear twice, once in Fig. 3.7 and once in Fig. 3.8. This explains the apparent redundancy and the labeling of the curves, which differs from that given in the table below in the column "$E \parallel z - axis$".

In fact, diagonalizing the perturbation operator (3.3) for various values of the electric field strength E, plotting the resulting curves and comparing these to the curves contained in Figs. 3.7 and 3.8 leads to the assignments enumerated in the table below.

$\boldsymbol{E \parallel z - axis}$		$\boldsymbol{E \perp z - axis}$			
		Odd Subsystem Fig. 3.7		**Even Subsystem** Fig. 3.8	
F	$\|M_F\|$	F	M_F	F	M_F
0	0			0	0
1	1	1	1	1	0
1	0	1	-1		
2	2	2	1	2	2
2	1	2	-1	2	0
2	0			2	-2
3	0	3	3		
3	1	3	1	3	2
3	2	3	-1	3	0
3	3	3	-3	3	-2

Table 3.2: Comparison of quantum numbers assigned to the energy levels of the Stark effect in ^{7}Li for two different orientations of the electric field.

3.5 Field Cycle Diagrams - Adiabatic Hyperfine Level Transfer in ^{7}Li

In 1994 Musso and Windholz [2] theoretically discovered the possibility of an adiabatic hyperfine level transfer for the $3p\ ^2P_{\frac{3}{2}}$ level of Na. Afterwards, Windholz et.al. [3] performed an experiment, confirming their expectations. For experimental reasons Ga instead of Na atoms were used. The Ga atoms of an atomic beam (whose valence electrons are prepared in a well defined quantum state, characterized by the quantum numbers F and M_F) start in a region of space where no external fields are present and pass through consecutive regions in space with inhomogeneous crossed electric and magnetic fields. This passage has to be carried out adiabatically which guarantees that the evolution of the state vector is such that for any arbitrary instant the state vector remains an eigenvector of the total Hamiltonian corresponding to the prevailing values of the external fields (*Adiabatic Theorem of Quantum Mechanics*). After leaving the regions of nonzero external fields, the valence electrons of the Ga atoms can be found in final quantum states characterized by the quantum numbers F' and M'_F. These quantum numbers may differ from the numbers F and M_F characterizing the initial state. A more detailed description of this effect is given in [2]. An interpretation can be found in [4] and [11] that has once more been confirmed by experiment [3].

The field cycle to which the Ga atoms are exposed can be subdivided into four regions. Region 1 is characterized by a linearly increasing magnetic field and zero electric field. In region 2 the magnetic field is constant whereas now the electric field increases linearly. Regions 3 and 4 finally have decreasing magnetic and electric fields, respectively, while the other field remains constant. Therefore, the whole cycle can be characterized by shifted increasing, constant and decreasing magnetic and electric field strengths.

Figs. 3.9 and 3.10 show the energy corrections corresponding to a specific field cycle characterized by certain maximum values for the field strengths.

With the help of these diagrams it is possible to give an illustrative interpretation of the adiabatic hyperfine structure level transfer: by passing through a closed cycle within the BE-plane adiabatically, that is to say by slow variations of the external fields, the system, initially in an eigenstate of the Hamiltonian, evolves such that for all later times of the adiabatic transition the state vector of the system remains an eigenstate of the Hamiltonian (corresponding to the prevailing external field values). For this reason the static aspect of the field cycle diagrams shown, consisting of a mere enumeration of energy eigenvalues belonging to different field values, is accompanied by a dynamical aspect, that reproduces the variations in the quantum energy of a state in the course of an adiabatically performed field cycle.

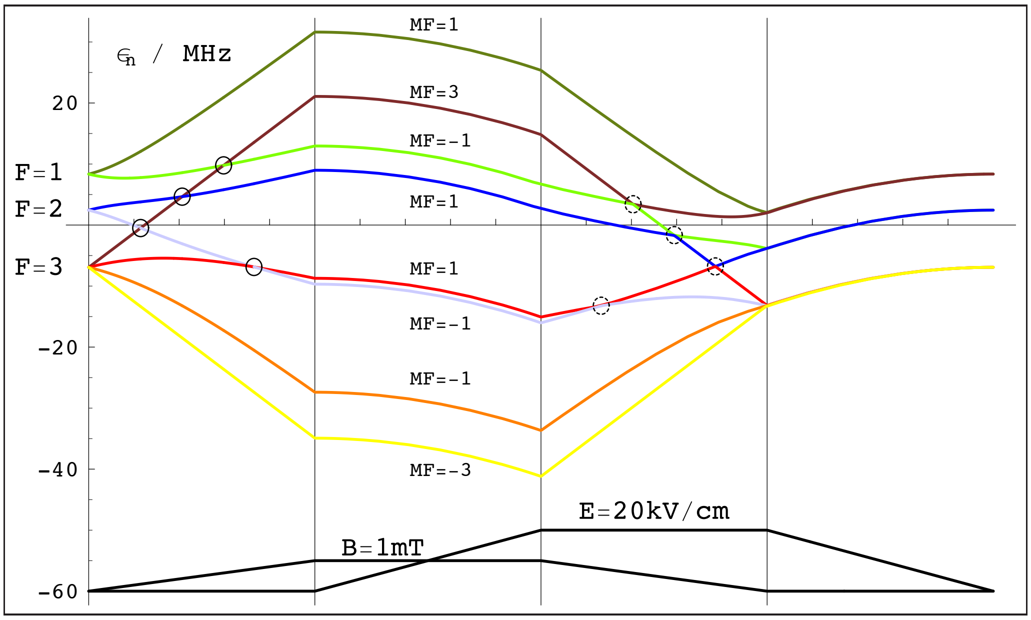

Figure 3.9: Special field cycle of the electromagnetic field with the corresponding splitting of the $2p\,^2P_{\frac{3}{2}}$ hyperfine levels of ^{7}Li in the odd subsystem (M_F = odd). The lists below contain the pairs of field parameters used in the calculations. A semicolon separates magnetic field values from electric ones; the lists are either of the form $\{B_{\text{start}}, B_{\text{end}}, B_{\text{step}}; E\}$ or $\{B; E_{\text{start}}, E_{\text{end}}, E_{\text{step}}\}$; the last entry of three values, separated by commas, is the step size needed in order to resolve the crossings and anticrossings, respectively. The units are mT and kV/cm.

Region 1: {0.001,1,0.001;0} Region 2: {1;0.01,20,0.01}

Region 3: {0.999,0.75,-0,001;20},{0.7499,0.72,-0.00005;20},{0.719,0.593,-0.001;20},
{0.592999,0.592,-0.000001;20},{0.591,0.42,-0.001;20},{0.41998,0.4,-0.00002;20},
{0.399,0.229,-0.001;20},{0.228999,0.228,-0.000001;20},{0.227,0.001,-0.001;20}

Region 4: {0.001;19.99,0,-0.01}

For small field values the color code corresponds to the scheme already introduced. For higher values of the external field strengths, the assignment between quantum states and colors is made by the so-called *analytic continuation of eigenvectors*. According to this method, the system of eigenvectors is computed for neighboring points lying on the curve of the specific field cycle under study. By evaluating the overlap of eigenvectors belonging to consecutive field points, it is possible to extend the assignment between quantum states and colors beyond crossing and anticrossing points. In particular for the identification of the areas of anticrossing in regions 3 of the diagrams the eigenvectors have to be computed for extremely small field increments.

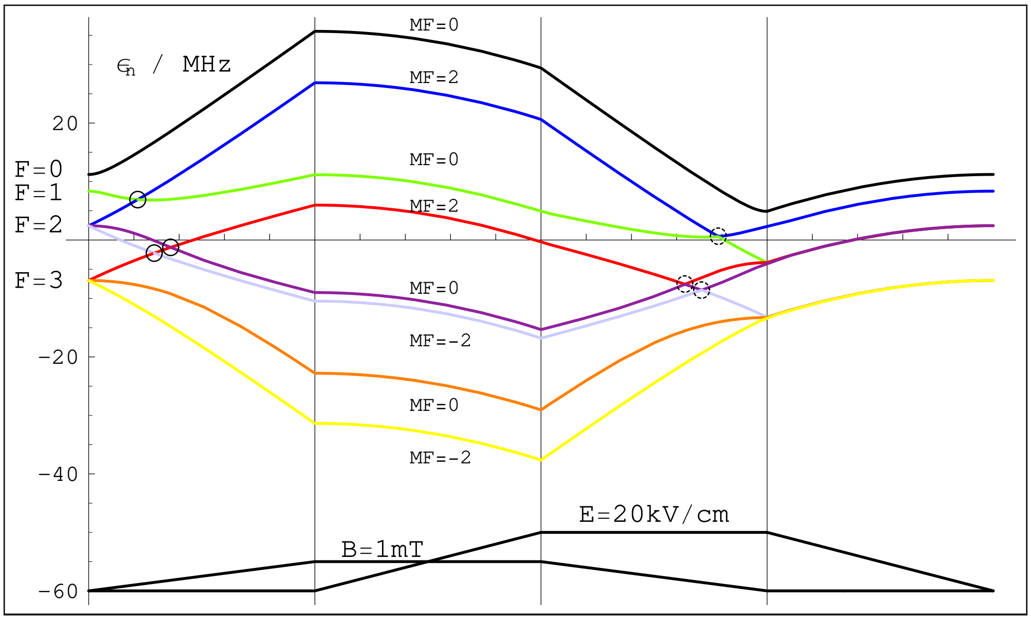

Figure 3.10: Special field cycle of the electromagnetic field with the corresponding splitting of the $2p\ ^2P_{\frac{3}{2}}$ hyperfine levels of ^{7}Li in the even subsystem (M_F = even). The lists below contain the pairs of field parameters used in the calculations. A semicolon separates magnetic field values from electric ones; the lists are either of the form $\{B_{\text{start}},B_{\text{end}},B_{\text{step}};E\}$ or $\{B;E_{\text{start}},E_{\text{end}},E_{\text{step}}\}$; the last entry of three values, separated by commas, is the step size needed in order to resolve the crossings and anticrossings, respectively. The units are mT and kV/cm.

Region 1: {0.001,1,0.001;0} Region 2: {1;0.01,20,0.01}
Region 3: {0.999,0.375,-0,001;20},{0.37499,0.355,-0.00001,20},{0.354,0.29,-0.001;20},
{0.289999,0.2897,-0.000001;20},{0.289,0.23,-0.001;20},{0.22997,0.2,-0.00003;20},
{0.199,0.001,-0.001;20} Region 4: {0.001;19.99,0,-0.01}

The captions of the figures contain the step sizes in the external field values needed to resolve the anticrossings. Regions 1 (magnetic field only) show the magnetic crossing points already discussed in section 3.3. Rendering the diagrams has been done without suppressing the scalar polarizability α_0.

3.6 Structure of Energy Surfaces in $^7\mathsf{Li}$

In order to generalize the investigations on the Stark Zeeman effect of the $2p\ ^2P_{\frac{3}{2}}$ hyperfine structure level, it is obvious to extend the calculations of energy corrections to the whole BE-plane of external field parameters. By symmetry considerations, however, and in the case of $^7\mathsf{Li}$, the treatment can immediately be restricted to the first quadrant of that plane ($B \geq 0, E \geq 0$).

By displaying the energy corrections above this quadrant one obtains for $^7\mathsf{Li}$ in both subsystems two groups of 8 surfaces. The structures and mutual locations of these surfaces are the main subject of this section. In the course of the investigations the existence of one crossing point per subsystem (right as in the case of Na) has been demonstrated for both nonvanishing magnetic and electric field. These points are named **BEo** and **BEe** according to the subsystem they belong to.

Three different methods serve for the task of locating the points of accidental degeneracy. The first one, going back to Heubrandtner, is based on a connection between the appearance of accidental degeneracies and the vanishing of codiagonal elements of the total perturbation matrix, tridiagonalized by the method by Givens. For further details, see [4].

The second method uses the possible appearance of Berry phases accompanying the analytic continuation along an adiabatically passed, closed cycle in the BE-plane around the point of accidental degeneracy. In general the **BE**-crossing points induce such geometric changes in phase, so a successive reduction of the area enclosed by the curve succeeds in locating the crossing point with increasing accuracy.

The third method consists of representing the energy surfaces graphically and performing more accurate investigations where two surfaces seem to approach or intersect. With the help of the FindMinimum[...] command of Mathematica the minima of the differences of two distinct energy surfaces are located. These minima can be identified with the **BE**-crossing points in the case of surfaces intersecting at isolated points. This method lacks the clear-cut aiming inherent to the first method.

As already performed in the case of the pure Stark effect, here too, it is useful to set the scalar polarizability α_0 equal to zero, since this simplification does not change the differences of energy eigenvalues along lines in the BE-plane corresponding to $E = \text{const.}$

The quantities ϵ'_n given in the following figures are the energy eigenvalues of the operator

$$\hat{H}_{\text{tot},\alpha_0\equiv 0} = \hat{H}_{\text{hyp}} + \hat{H}_{\text{mag}} + \hat{H}^{(2)}_{\text{el,eff}} \tag{3.11}$$

and are related to the eigenvalues ϵ_n of the total perturbation operator

$$\hat{H}_{\text{tot}} = \hat{H}_{\text{hyp}} + \hat{H}_{\text{mag}} + \hat{H}_{\text{el,eff}} \tag{3.12}$$

via

$$\epsilon_n = \epsilon'_n - \frac{1}{2}\alpha_0 E^2. \tag{3.13}$$

Especially the graphical visualization of the energy surfaces gains in clarity by putting the scalar polarizability α_0 equal to zero, even if the ranges for the field values are not chosen to be particularly small.

Figs. 3.11 and 3.12 show the energy surfaces of the odd subsystem, Figs. 3.13 and 3.14 those of the even subsystem. Two different viewpoints have been used in rendering the graphics. In order to emphasize the pure Zeeman and Stark splittings located in the coordinate planes ($B\,\epsilon'_n$- and $E\,\epsilon'_n$-planes, respectively) thick lines have been used. The **BE**-crossing points are marked by white arrows in two diagrams. These diagrams also contain the naming of the energy surfaces of the form (F, M_F) (comp. section 3.7).

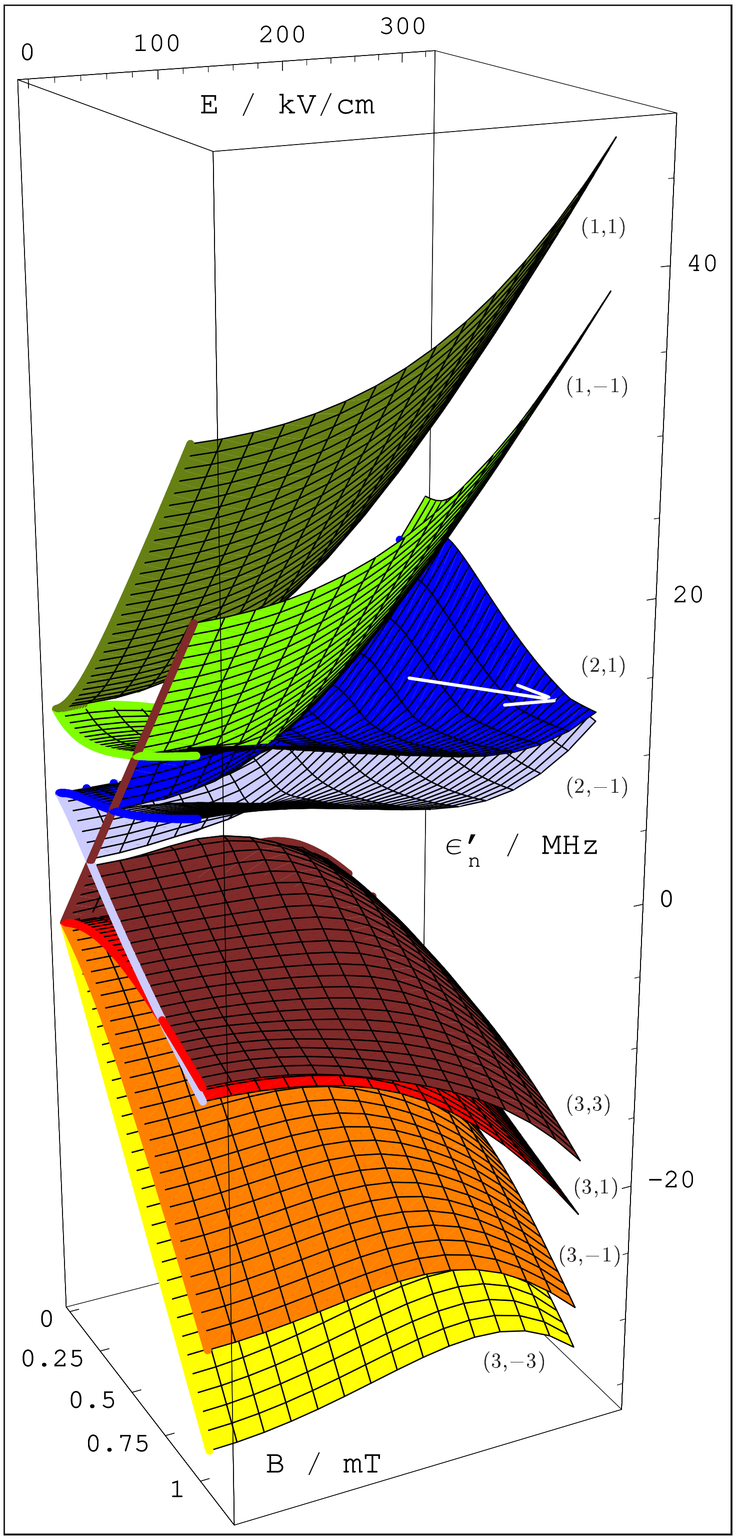

Figure 3.11: Energy surfaces in the odd subsystem of ^{7}Li.

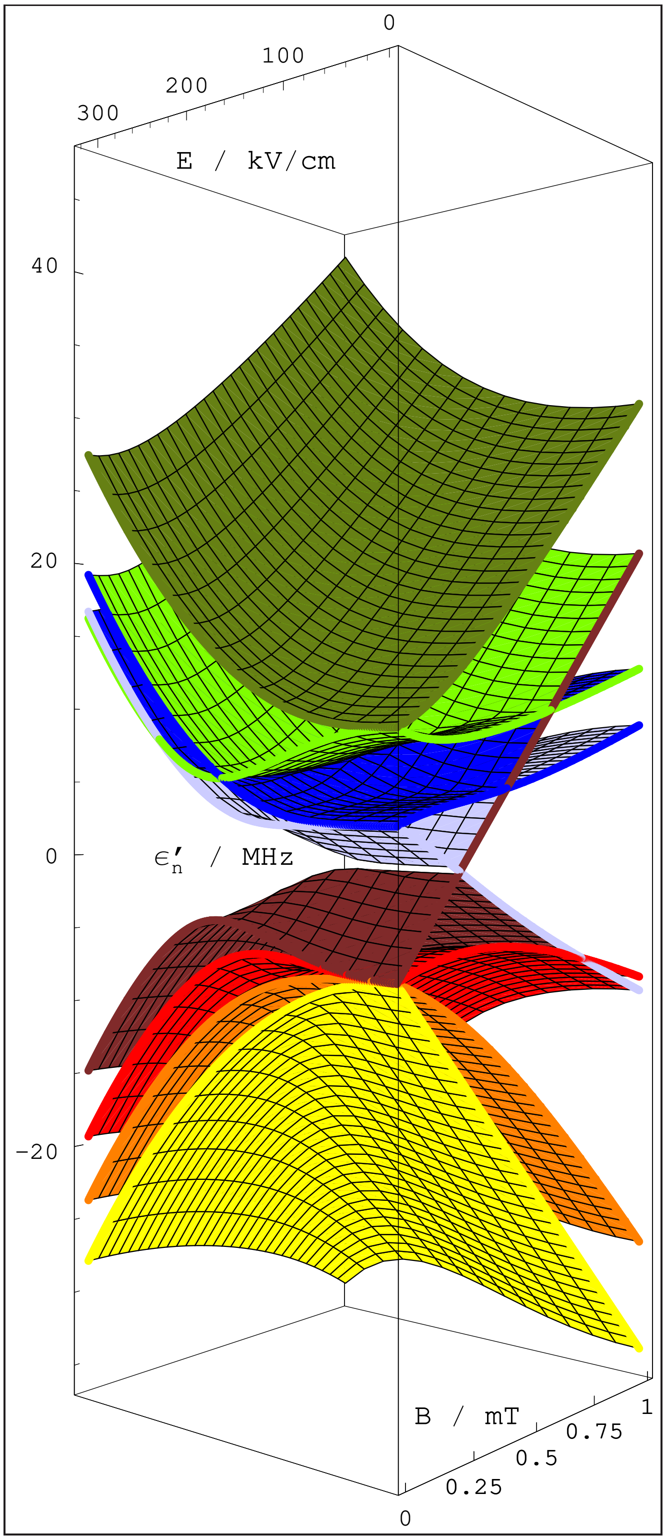

Figure 3.12: Energy surfaces in the odd subsystem of ^{7}Li; view of magnetic and electric crossing points.

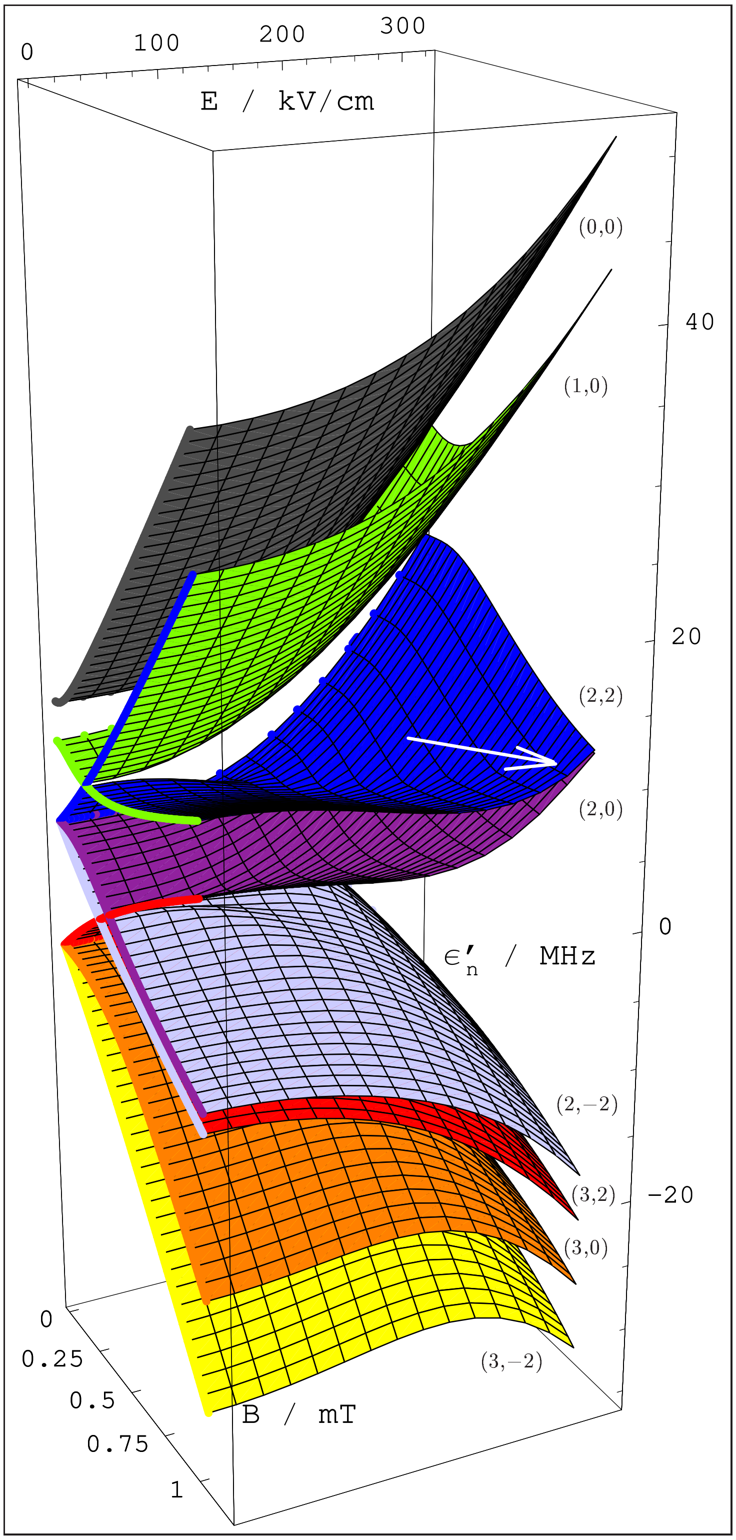

Figure 3.13: Energy surfaces in the even subsystem of ^{7}Li.

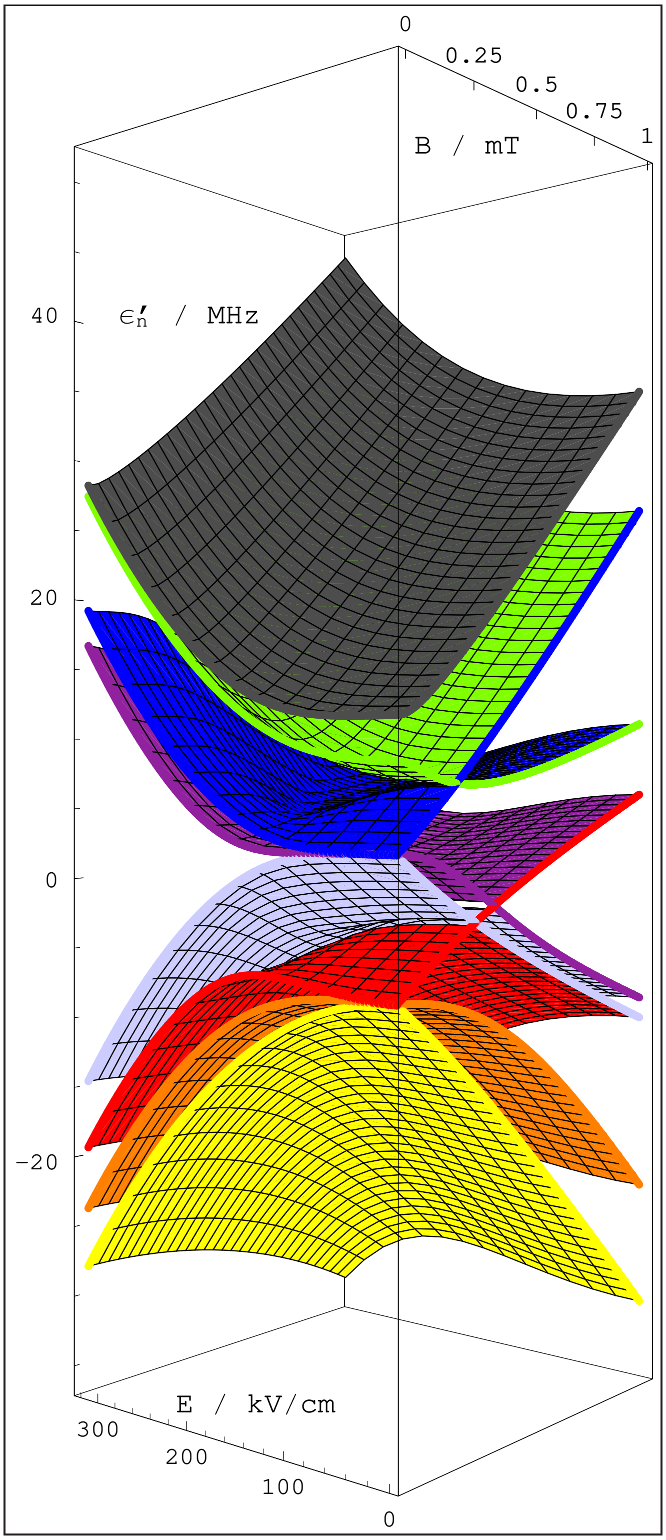

Figure 3.14: Energy surfaces in the even subsystem of ^{7}Li; view of magnetic crossing points.

3.7 Listing of Crossing Point Data for ^{7}Li

This section presents a summary of all the data characterizing the various crossing points that have been found. Names, external field values and energy eigenvalues are listed as well as the pairs of eigenvectors involved. As already mentioned, the eigenvectors corresponding to an arbitrary pair of external field values in the BE-plane are named after the quantum numbers F and M_F characterizing those eigenvectors for very small magnetic fields, from which they can be reproduced by analytic continuation. This convention unambiguously assigns a pair of quantum numbers (F, M_F) to the eigenvectors at all points of the BE-plane. However, this pair (F, M_F) must definitely not be identified with the simultaneous eigenvectors $|FM_F\rangle$ of the operators $\hat{\vec{F}}^2$ and $\hat{F}_z$. Tab. 3.3 contains the data to all 7 points of accidental degeneracy of the odd subsystem, Tab. 3.4 all data to the 4 points of the even subsystem.

Name	**B / mT**	**E / kV/cm**	ϵ **/ MHz**	$(\mathbf{F}, \mathbf{M_F})$-$(\mathbf{F'}, \mathbf{M'_F})$
Bo1	0.2296	0	-0.49324	(2,-1)-(3,3)
Bo2	0.4134	0	4.65259	(2,1)-(3,3)
Bo3	0.5965	0	9.78018	(1,-1)-(3,3)
Bo4	0.7309	0	-6.86793	(2,-1)-(3,1)
Eo1	0	170.029	-450.319	(1,-1)-(2,1)
Eo2	0	238.052	-885.240	(1,-1)-(2,-1)
BEo	0.8239	314.841	-1551.515	(2,-1)-(2,1)

Table 3.3: Listing of crossing point data for the odd subsystem in ^{7}Li

Name	**B / mT**	**E / kV/cm**	ϵ **/ MHz**	$(\mathbf{F}, \mathbf{M_F})$-$(\mathbf{F'}, \mathbf{M'_F})$
Be1	0.2169	0	6.91020	(1,0)-(2,2)
Be2	0.2898	0	-2.24125	(2,-2)-(3,2)
Be3	0.3623	0	-1.25658	(2,0)-(3,2)
BEe	0.9194	301.709	-1425.022	(2,2)-(2,0)

Table 3.4: Listing of crossing point data for the even subsystem in ^{7}Li

The energy eigenvalues given are those of the total perturbation operator, including the term of the scalar polarizability α_0. The following two diagrams in Figs. 3.15 and 3.16 show the mutual locations of the crossing points for the two subsystems. These diagrams are called crossing diagrams for short.

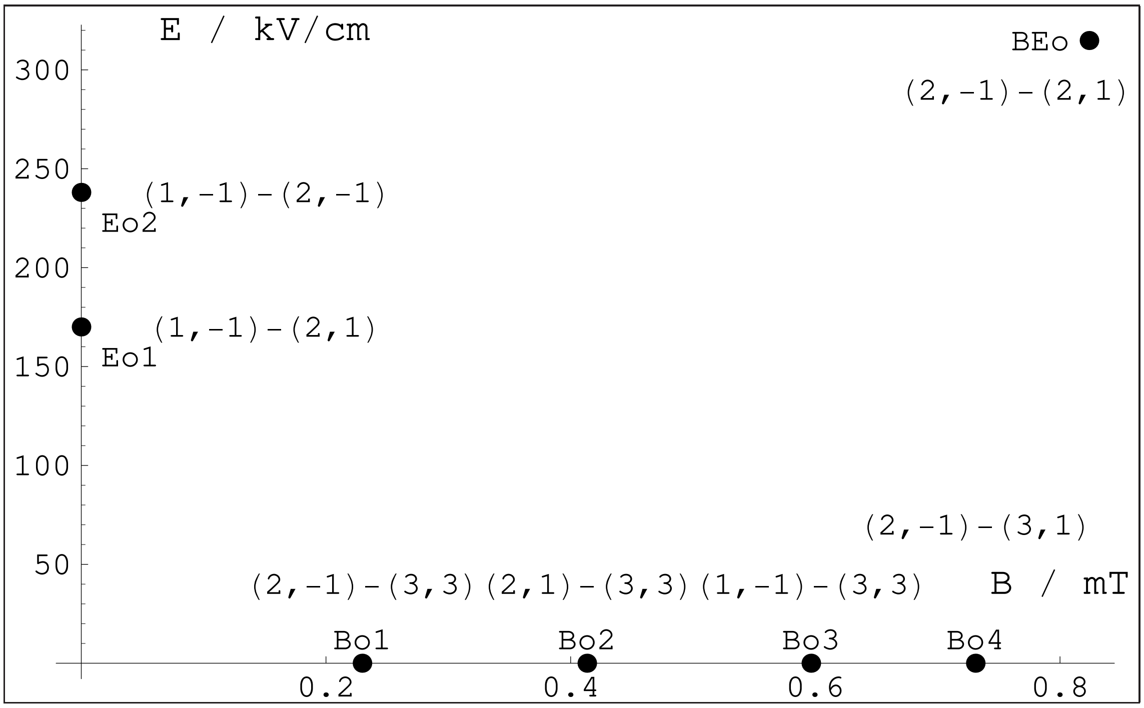

Figure 3.15: Crossing diagram of the odd subsystem in ^{7}Li

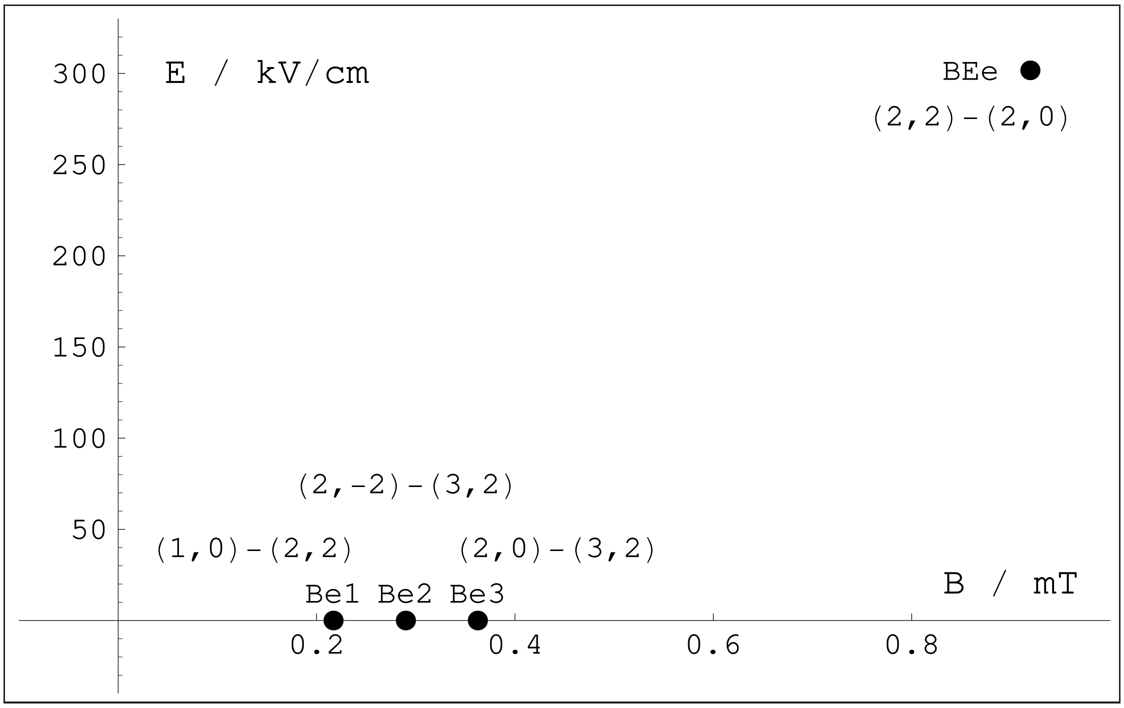

Figure 3.16: Crossing diagram of the even subsystem in ^{7}Li

3.8 Berry Phases in ^{7}Li

As mentioned above, eigenvectors may assume an additional geometric phase factor called Berry phase when the external parameters (in this case the magnetic and the electric field strengths) pass through a closed cycle enclosing a crossing point. Such a cycle is represented in the BE-plane by a closed curve around a certain crossing point. All hermitian perturbation matrices used here are real and therefore all eigenvectors can be represented as linear combinations of the basis vectors with real coefficients. This explains why in this particular case only Berry phases equal to

$$e^{\pi \imath} = -1 \tag{3.14}$$

may appear. For this reason geometric phases manifest themselves merely as changes in sign of the eigenvectors under analytic continuation of the former along closed paths around particular crossing points.

By using a Mathematica-program by Heubrandtner, it was rather easy to find out, whether the continuation of eigenvectors around a particular crossing point leads to a change in sign or not. The program follows the overlap of wavefunctions along closed rectangular paths and finally calculates the overlap of the transported eigenvectors with the original ones.

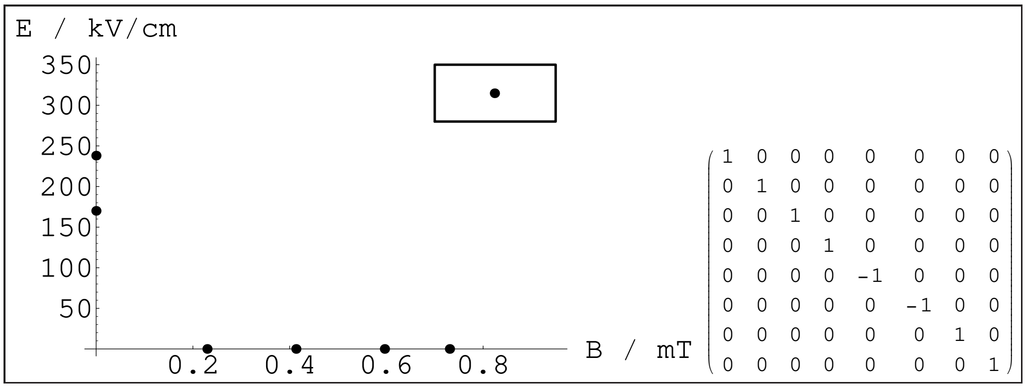

Figure 3.17: Output of the program used in the investigations on the appearance of Berry phases. This diagram shows the rectangular path (within the BE-plane) along which the eigenvectors of the perturbation have been evaluated in the case of the **BEo**-crossing point in ^{7}Li. The overlap matrix indicates which eigenvectors assume a sign change in the adiabatic field cycle corresponding to the rectangular path.

Fig. 3.17 shows the output of this program for the typical example of the **BEo**-crossing point. The matrix in the output indicates, which eigenvectors are affected by the change in sign. Clearly these are only the two eigenvectors whose energy eigenvalues coincide at the point of accidental degeneracy (crossing point). Applying this procedure to all the crossing points found in both subsystems shows that only the two **BE**-crossing points and the point on the E-axis in the BE-plane belonging to the higher field strength induce such changes in sign.

The two Tabs. 3.5 and 3.6 summarize the results found for the odd and the even subsystem, respectively.

	Bo1	**Bo2**	**Bo3**	**Bo4**	**Eo1**	**Eo2**	**BEo**
Berry phase occurs	No	No	No	No	No	Yes	Yes

Table 3.5: Appearance of Berry phases in the odd subsystem of ^{7}Li.

	Be1	**Be2**	**Be3**	**BEe**
Berry phase occurs	No	No	No	Yes

Table 3.6: Appearance of Berry phases in the even subsystem of ^{7}Li.

Chapter 4

^{6}Li

The structure of this chapter is quite the same as that of the preceding one. Once more the discussion starts with the presentation of the matrix elements of the perturbation operators followed by the color code adapted for ^{6}Li.

Thereafter, the Zeeman and the Stark effects of the $2p\ ^2P_{\frac{3}{2}}$ fine structure level of ^{6}Li are discussed separately. Then the combination of these effects is considered in connection with the calculation of energy corrections corresponding to a particular field cycle. Later on the structure of the energy surfaces for the positive and the negative subsystem are investigated and depicted, respectively.

The last three sections are reserved to a summary of the data characterizing the crossing points, to the occurrence of Berry phases and to a presentation of analytic expressions for field values and energy eigenvalues of some crossing points in ^{6}Li.

4.1 Matrix Elements of the Perturbation Operators

As indicated in section 2.2, the total degree of degeneracy of the $2p\ ^2P_{\frac{3}{2}}$ fine structure level of ^{6}Li is 12. Therefore, the perturbation operators are represented in the various bases by 12x12 real, symmetric square matrices. By choosing a particular ordering of the basis states ($|\gamma_I \gamma_J I J F M_F\rangle$ or $|\gamma_I \gamma_J I J M_I M_J\rangle$) these matrices can be reduced. The two blocks arranged along the main diagonal represent the perturbation operators in the positive and the negative subsystem, respectively. The order of the basis vectors is

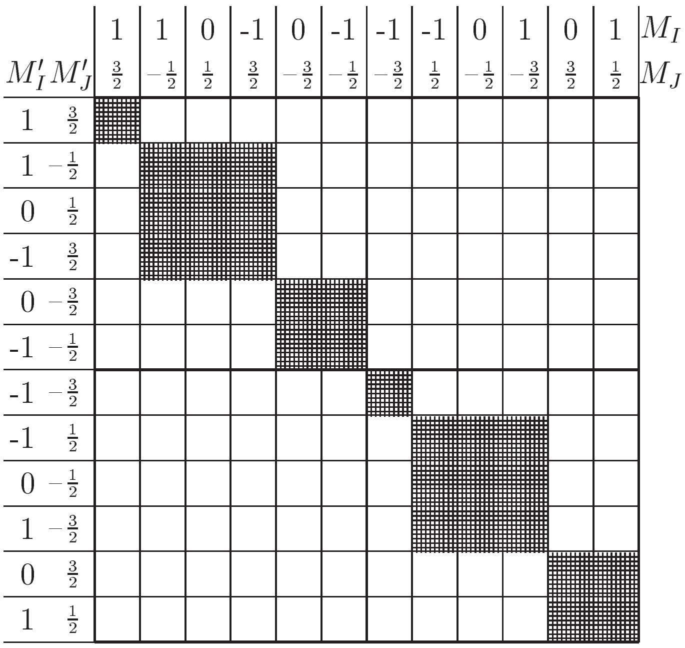

Figure 4.1: Hyperfine matrix elements $\langle \gamma_I \gamma_J I J M_I M_J | \hat{H}_{\mathrm{hyp}} | \gamma_I \gamma_J I J M_I' M_J' \rangle$ of the $2p\ ^2P_{\frac{3}{2}}$ level of ^{6}Li as given in eq. (2.16).

such that those of the positive subsystem are followed by those of the negative subsystem.

The presentation of the structure of the matrices representing the three perturbation operators differs from that used in chapter 3, as the matrix elements for a nuclear spin $I = 1$ have not yet been given explicitly before in the basis $|\gamma_I \gamma_J I J M_I M_J\rangle$. This representation is shown in Figs. 4.1, 4.2 and 4.3. Even in this representation it is possible to divide the whole $2p\ ^2P_{\frac{3}{2}}$ fine structure level into the positive and the negative subspace. According to

$$M_F = M_I + M_J \tag{4.1}$$

each of the basis states $|\gamma_I \gamma_J I J M_I M_J\rangle$ can be assigned unambiguously to only one of the subsystems.

Figs. 4.4, 4.5 and 4.6 describe the structure of the perturbation matrices in the coupled representation using the basis vectors $|\gamma_I \gamma_J I J F M_F\rangle$.

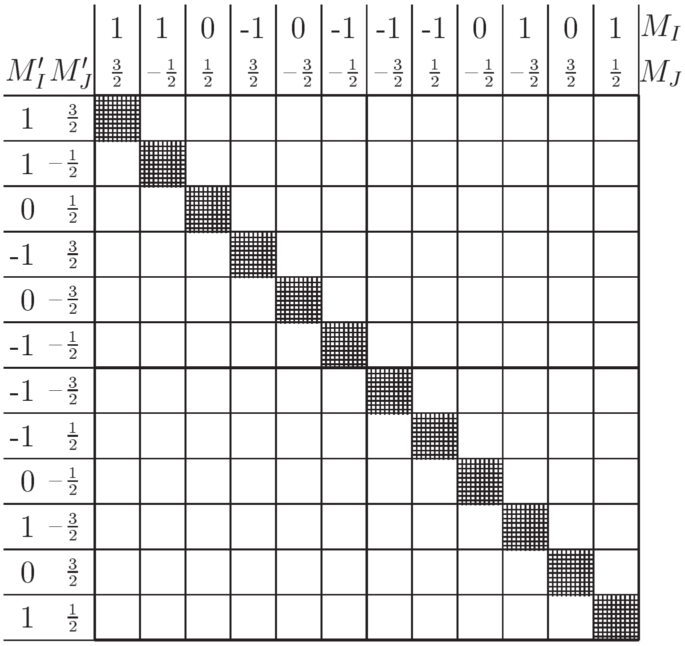

Figure 4.2: Zeeman matrix elements $\langle \gamma_I \gamma_J I J M_I M_J | \hat{H}_{\mathrm{mag}} | \gamma_I \gamma_J I J M_I' M_J' \rangle$ of the $2p\,^2P_{\frac{3}{2}}$ level of ^{6}Li as given in eq. (2.21).

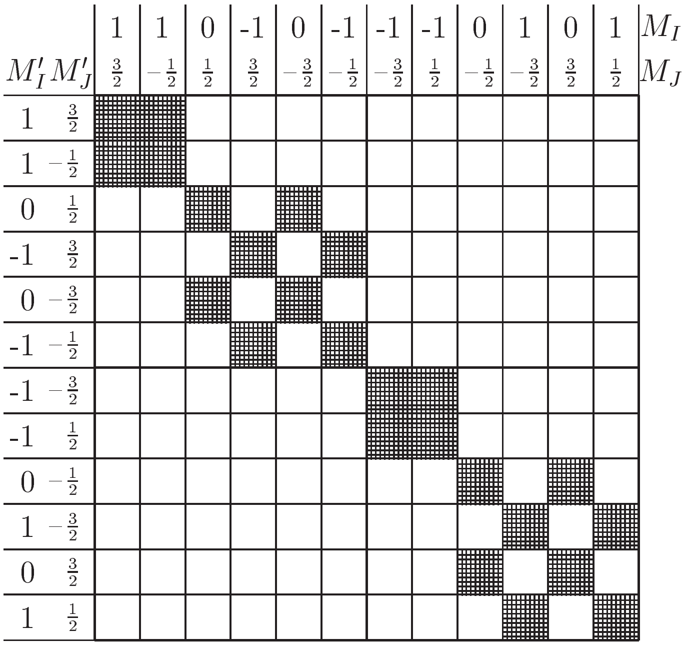

Figure 4.3: Stark matrix elements $\langle \gamma_I \gamma_J I J M_I M_J | \hat{H}_{\mathrm{el,eff}} | \gamma_I \gamma_J I J M_I' M_J' \rangle$ of the $2p\,^2P_{\frac{3}{2}}$ level of ^{6}Li as given in eqs. (2.37) and (2.38).

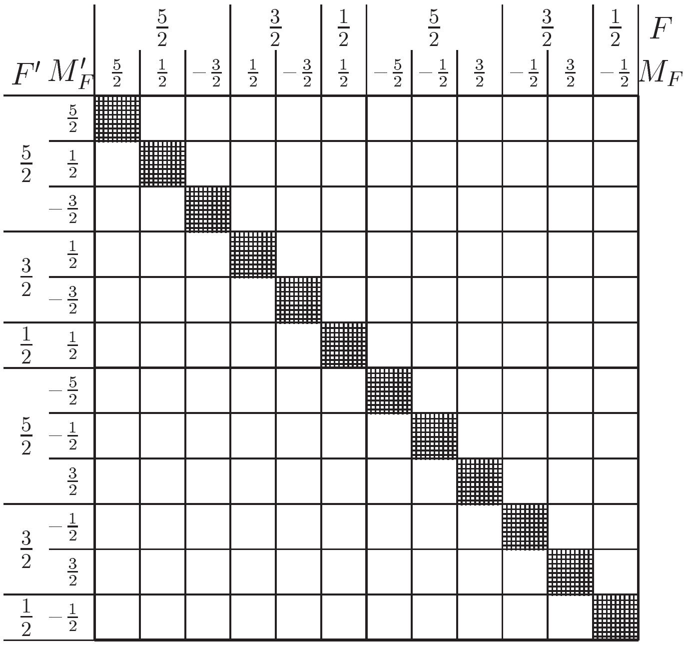

Figure 4.4: Hyperfine matrix elements $\langle \gamma_I \gamma_J I J F M_F | \hat{H}_{\text{hyp}} | \gamma_I \gamma_J I J F' M_F' \rangle$ of the $2p\ ^2P_{\frac{3}{2}}$ level of ^{6}Li as given in eq. (2.14). F...total atomic angular momentum; M_F...corresponding magnetic quantum number $-F \leq M_F \leq +F$

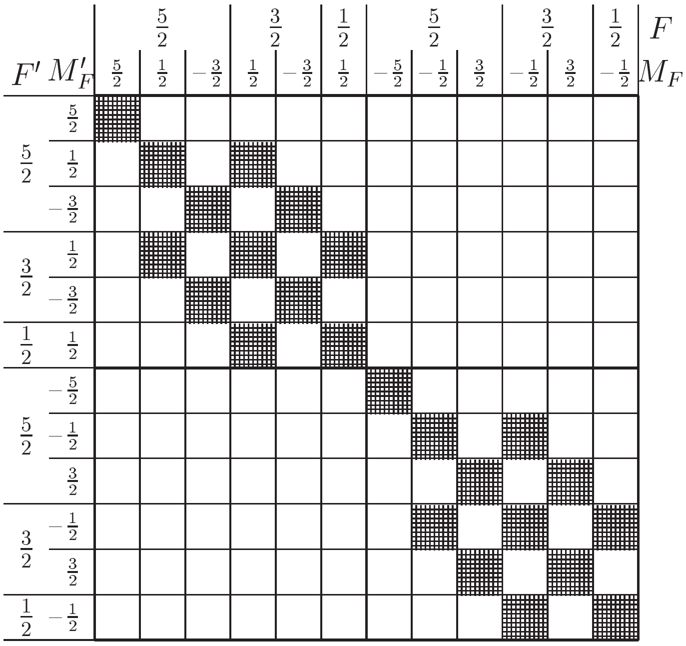

Figure 4.5: Zeeman matrix elements $\langle \gamma_I \gamma_J I J F M_F | \hat{H}_{\text{mag}} | \gamma_I \gamma_J I J F' M_F' \rangle$ of the $2p\ ^2P_{\frac{3}{2}}$ level of ^{6}Li as given in eq. (2.20). F...total atomic angular momentum; M_F...corresponding magnetic quantum number $-F \leq M_F \leq +F$

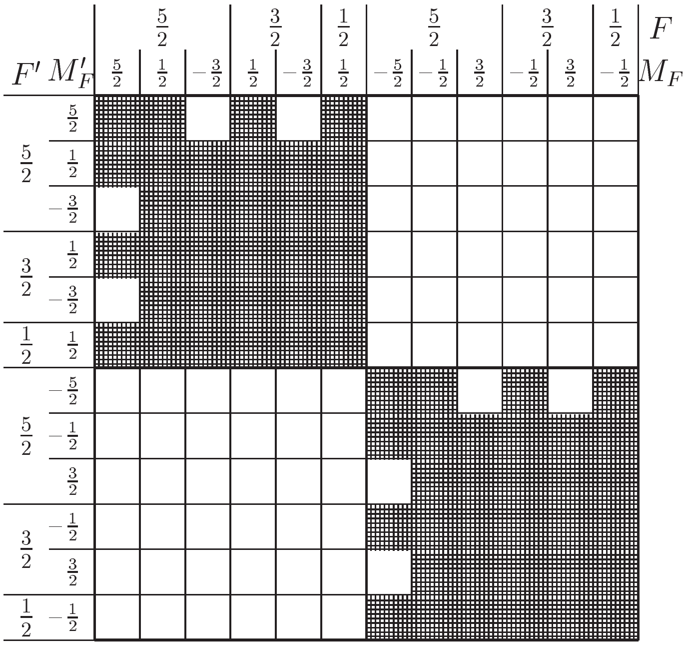

Figure 4.6: Stark matrix elements $\langle \gamma_I \gamma_J I J F M_F | \hat{H}_{\mathrm{el,eff}} | \gamma_I \gamma_J I J F' M'_F \rangle$ of the $2p\ ^2P_{\frac{3}{2}}$ level of $^6\mathsf{Li}$ as given in eqs. (2.34) and (2.35). F...total atomic angular momentum; M_F...corresponding magnetic quantum number $-F \leq M_F \leq +F$

4.2 Relation between Quantum Numbers and Colors for ^{6}Li

The convention to use one shade of colors for one hyperfine level characterized by the quantum number F is maintained for ^{6}Li but, for reasons of symmetry, not the convention to use darker shades for higher values of the quantum number M_F. The details are shown in Tab. 4.1 below.

Positive Subsystem			Negative Subsystem		
F	M_F	Color	F	M_F	Color
$\frac{5}{2}$	$\frac{5}{2}$		$\frac{5}{2}$	$-\frac{5}{2}$	
$\frac{5}{2}$	$\frac{1}{2}$		$\frac{5}{2}$	$-\frac{1}{2}$	
$\frac{5}{2}$	$-\frac{3}{2}$		$\frac{5}{2}$	$\frac{3}{2}$	
$\frac{3}{2}$	$\frac{1}{2}$		$\frac{3}{2}$	$-\frac{1}{2}$	
$\frac{3}{2}$	$-\frac{3}{2}$		$\frac{3}{2}$	$\frac{3}{2}$	
$\frac{1}{2}$	$\frac{1}{2}$		$\frac{1}{2}$	$-\frac{1}{2}$	

Table 4.1: Color code used for the positive and the negative subsystems of the energy levels in ^{6}Li

4.3 Zeeman Effect of the $2p\ ^2P_{\frac{3}{2}}$ Level of ^{6}Li

The magnetic field totally removes the natural degeneracy of the hyperfine structure. The energy eigenvalues for small magnetic field strengths are ordered according to the magnetic quantum number M_F of the corresponding states. Fig. 4.7 gives the details for the positive, Fig. 4.8 for the negative subsystem.

In contrast to the corresponding diagrams for ^{7}Li in section 3.3, here it is necessary to depict the energy eigenvalues for both positive and negative magnetic field strengths because the Zeeman diagrams for the two subsystems of ^{6}Li are not symmetric with respect to a change of the direction of the magnetic field. As a result, the crossing points of one subsystem for negative magnetic field (in z-direction) are definitely not located opposite (with respect to the E-axis of the BE-plane) to the crossing points of the same subsystem for positive field values, as it is the case for ^{7}Li. This fact is treated in more detail in chapter 6.

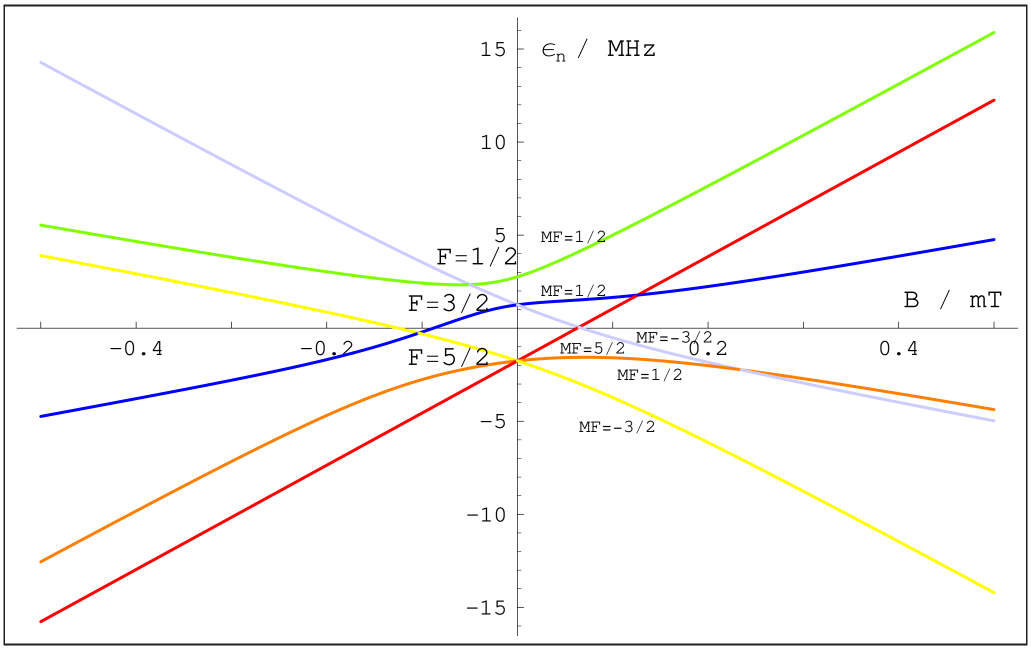

Figure 4.7: Splitting of the $2p\ ^2P_{\frac{3}{2}}$ hyperfine energy levels ϵ_n of ^{6}Li in the positive subsystem due to the Zeeman effect.

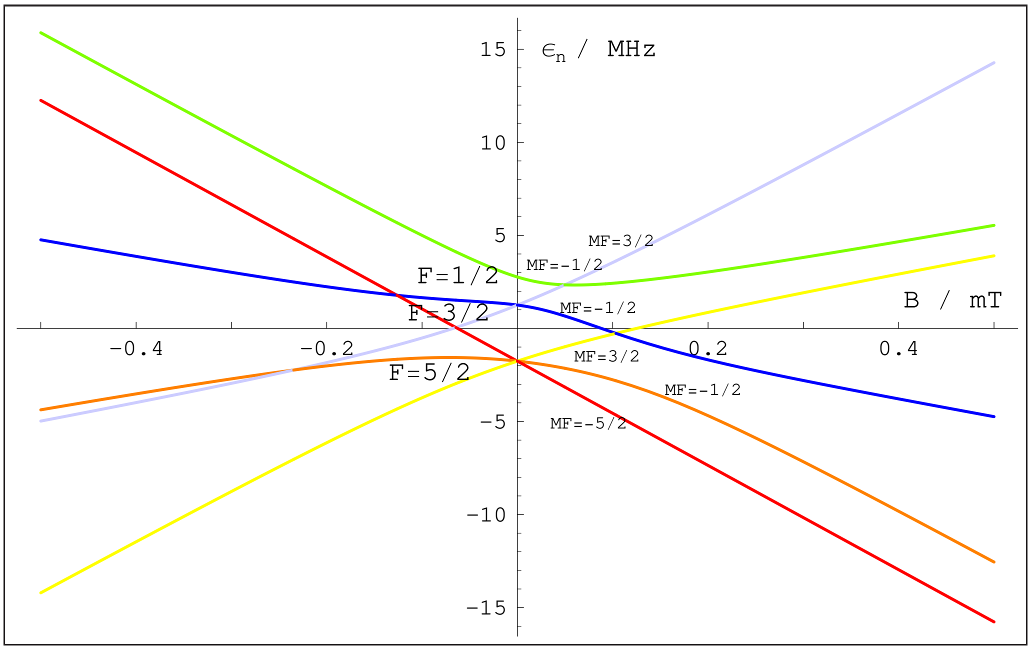

Figure 4.8: Splitting of the $2p\ ^2P_{\frac{3}{2}}$ hyperfine energy levels ϵ_n of ^{6}Li in the negative subsystem due to the Zeeman effect.

The positive subsystem contains 5 magnetic crossing points **Bpn**, 3 at positive values of the magnetic field, 2 at negative values. The point **Bp1** is located at a negative magnetic field value. The negative subsystem has the same number of magnetic crossing points, denoted by **Bnn** (where the second **n** numbers the points), with the same energy values, but with the signs of the magnetic field values reversed.

The data to the whole set of crossing points found in ^{6}Li is presented in section 4.7.

4.4 Stark Effect of the $2p\ ^2P_{\frac{3}{2}}$ Level of ^{6}Li

The diagonalization of the operator

$$\hat{H}_{\text{hyp}} + \hat{H}_{\text{el,eff}} \tag{4.2}$$

provides the Stark energy corrections of the hyperfine levels under study. As discussed in detail in section 3.4, omitting the term proportional to the

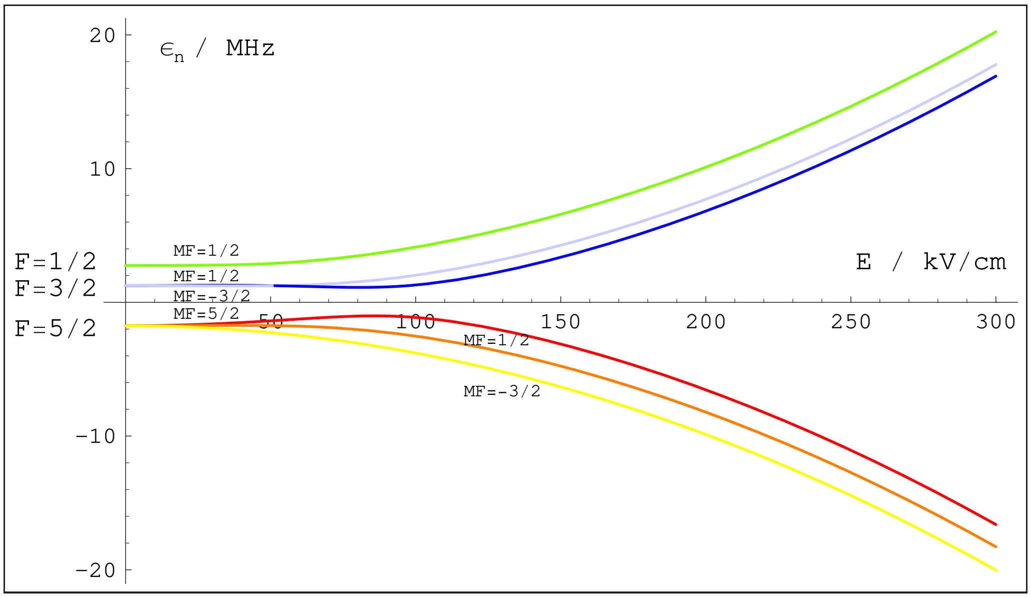

Figure 4.9: Splitting of the $2p\ ^2P_{\frac{3}{2}}$ hyperfine energy levels ϵ'_n of ^{6}Li in the positive subsystem due to the Stark effect. The term proportional to the scalar polarizability α_0 was put to zero before diagonalizing the perturbation matrix.

scalar polarizability α_0 doesn't change the differences of eigenvalues corresponding to a given value of the electric field strength. By such a simplification, the locations of the electric crossing points (within the BE-plane) are

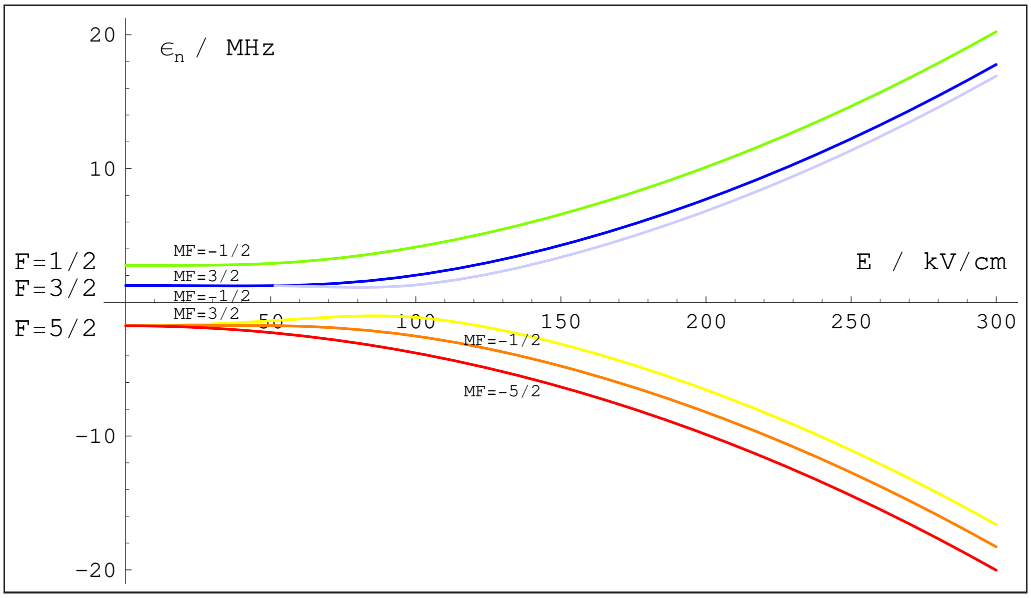

Figure 4.10: Splitting of the $2p\ ^2P_{\frac{3}{2}}$ hyperfine energy levels ϵ_n' of ^{6}Li in the negative subsystem due to the Stark effect. The term proportional to the scalar polarizability α_0 was put to zero before diagonalizing the perturbation matrix.

not altered. Moreover, the Stark diagrams (energy eigenvalues versus electric field strength) gain greatly in clarity by suppressing the overall downward shift due to α_0.

Therefore, all the diagrams below show the eigenvalues ϵ_n' of the operator

$$\hat{H}_{\text{hyp}} + \hat{H}^{(2)}_{\text{el,eff}} \tag{4.3}$$

in place of ϵ_n, those of the operator given in eq. (4.2). (see section 3.4).

The Stark diagram of the positive subsystem of ^{6}Li is shown in Fig. 4.9, those of the negative subsystem in Fig. 4.10. The two diagrams are identical, a fact that will be clarified together with the differences in the symmetries of Zeeman diagrams for ^{7}Li and ^{6}Li in chapter 6.

Even in these diagrams (with α_0 suppressed) it is hard to locate the one existing electric crossing point in each of the two systems. In fact these two crossing points have been overlooked in a first run and only the investigations on Berry phases revealed their existence (see also the list of crossing points in section 4.7).

In the introduction, section 1.2, and at the end of section 3.4, the different labeling resulting from the use of different quantization axes of the perturbation Hamiltonian (comprising the hyperfine interaction and the effective electric interaction) has been discussed. As the total angular momentum F is half-odd integer (and so are the corresponding magnetic quantum numbers M_F), there is no comparable redundancy inherent to the Stark splitting diagrams of ^{6}Li as inherent to the diagrams of ^{7}Li, given in Figs. 3.7 and 3.8 of section 3.4. The labeling of the curves, however, still depends on the directions of the quantization axis and that of the electric field. This is again summarized in the corresponding Tab. 4.2 below.

$\boldsymbol{E \parallel z - axis}$		$\boldsymbol{E \perp z - axis}$			
		Positive Subsystem Fig. 4.9		**Negative Subsystem** Fig. 4.10	
F	$\|M_F\|$	F	M_F	F	M_F
$\frac{1}{2}$	$\frac{1}{2}$	$\frac{1}{2}$	$\frac{1}{2}$	$\frac{1}{2}$	$-\frac{1}{2}$
$\frac{3}{2}$	$\frac{1}{2}$	$\frac{3}{2}$	$\frac{1}{2}$	$\frac{3}{2}$	$\frac{3}{2}$
$\frac{3}{2}$	$\frac{3}{2}$	$\frac{3}{2}$	$-\frac{3}{2}$	$\frac{3}{2}$	$-\frac{1}{2}$
$\frac{5}{2}$	$\frac{1}{2}$	$\frac{5}{2}$	$\frac{5}{2}$	$\frac{5}{2}$	$\frac{3}{2}$
$\frac{5}{2}$	$\frac{3}{2}$	$\frac{5}{2}$	$\frac{1}{2}$	$\frac{5}{2}$	$-\frac{1}{2}$
$\frac{5}{2}$	$\frac{5}{2}$	$\frac{5}{2}$	$-\frac{3}{2}$	$\frac{5}{2}$	$-\frac{5}{2}$

Table 4.2: Comparison of quantum numbers assigned to the energy levels of the Stark effect in ^{6}Li for two different orientations of the electric field.

4.5 Field Cycle Diagrams - Adiabatic Hyperfine Level Transfer in ^{6}Li

This section contains a treatment of specific field cycle diagrams for both, the positive and the negative subsystem in ^{6}Li. As in ^{7}Li, a hyperfine level transfer discussed in detail in section 3.5 may occur in ^{6}Li. See Figs. 4.11 and 4.12 for specific field cycles in the positive and the negative subsystem,

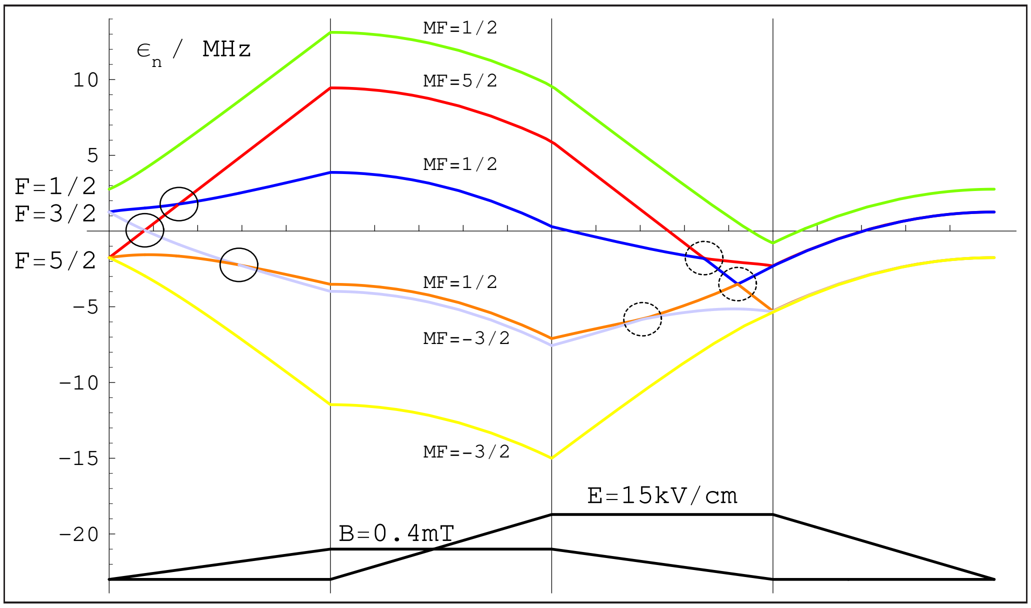

Figure 4.11: Special field cycle of the electromagnetic field with the corresponding splitting of the $2p\,^2P_{\frac{3}{2}}$ hyperfine levels of ^{6}Li in the positive subsystem. The lists below contain the pairs of field parameters used in the calculations. A semicolon separates magnetic field values from electric ones; the lists are either of the form $\{B_{\text{start}},B_{\text{end}},B_{\text{step}};E\}$ or $\{B;E_{\text{start}},E_{\text{end}},E_{\text{step}}\}$; the last entry of three values, separated by commas, is the step size needed in order to resolve the crossings and anticrossings, respectively. The units are mT and kV/cm.
Region 1: {0.001,0.4,0.001;0} Region 2: {0.4;0.01,15,0.01}
Region 3: {0.399,0.24,-0,001;15},{0.23995,0.228,-0.00005,15},{0.227,0.128,-0.001;15}, {0.12799,0.116,-0.00001;15},{0.115,0.064,-0.001;15},{0.063999,0.0638,-0.000001;15}, {0.0637,0.001,-0.0001;15} Region 4: {0.001;14.99,0,-0.01}

respectively.

Once more it is confirmed that crossing points appear exclusively in region 1, anticrossing points in region 3 of the diagrams mentioned above. Crossing points are marked by bold black circles, anticrossing points by dashed circles.

Figs. 4.13 and 4.14 show the typical behavior of the two energy eigenvalues in the immediate vicinity of one crossing point and one anticrossing point

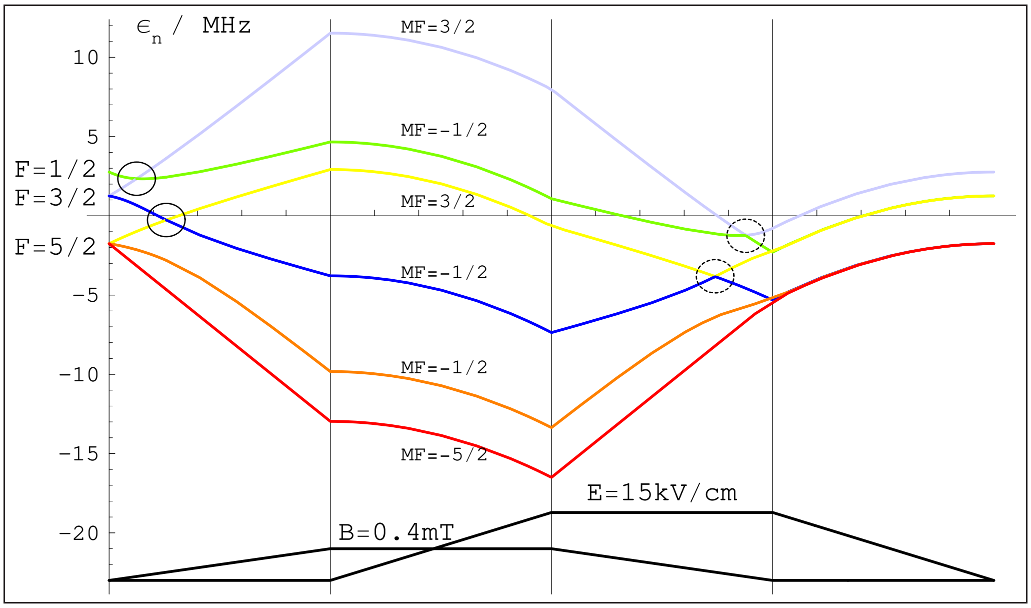

Figure 4.12: Special field cycle of the electromagnetic field with the corresponding splitting of the $2p\ ^2P_{\frac{3}{2}}$ hyperfine levels of ^{6}Li in the negative subsystem. The lists below contain the pairs of field parameters used in the calculations. A semicolon separates magnetic field values from electric ones; the lists are either of the form $\{B_{\text{start}},B_{\text{end}},B_{\text{step}};E\}$ or $\{B;E_{\text{start}},E_{\text{end}},E_{\text{step}}\}$; the last entry of three values, separated by commas, is the step size needed in order to resolve the crossings and anticrossings, respectively. The units are mT and kV/cm.
Region 1: {0.001,0.4,0.001;0} Region 2: {0.4;0.01,15,0.01}
Region 3: {0.399,0.108,-0,001;15},{0.10795,0.1,-0.00005;15},{0.099,0.056,-0.001;15},
{0.05595,0.04,-0.00005;15},{0.039,0.001,-0.001;15} Region 4: {0.001;14.99,0,-0.01}

in the positive subsystem. Compare the scale in the anticrossing diagram with the corresponding step size for the magnetic field strength necessary to resolve the anticrossing point as given in the caption of Fig. 4.11.

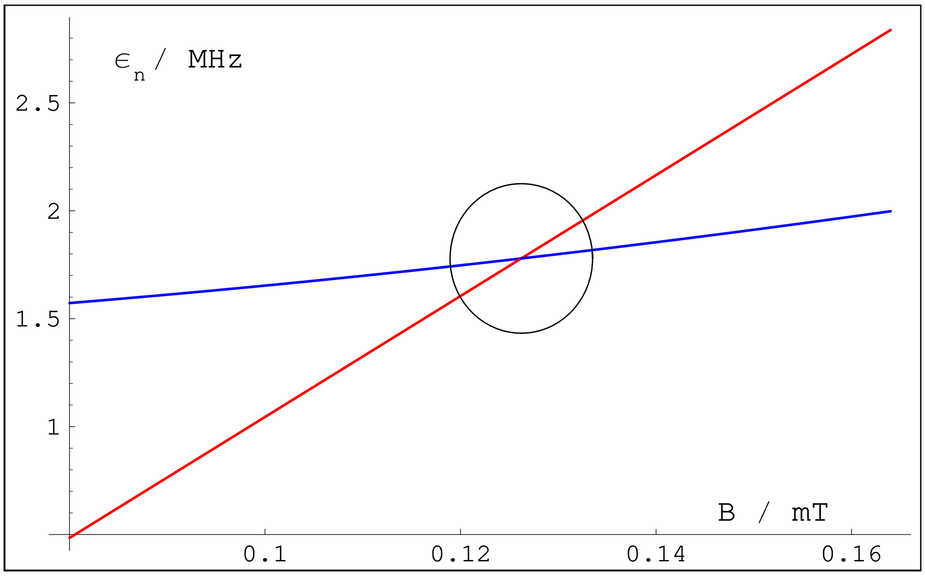

Figure 4.13: Behavior of the energy eigenvalues in the vicinity of the **Bp4**-crossing point in ^{6}Li for the field cycle given in Fig. 4.11. The crossing point can easily be identified by the appropriate use of colors in the figures.

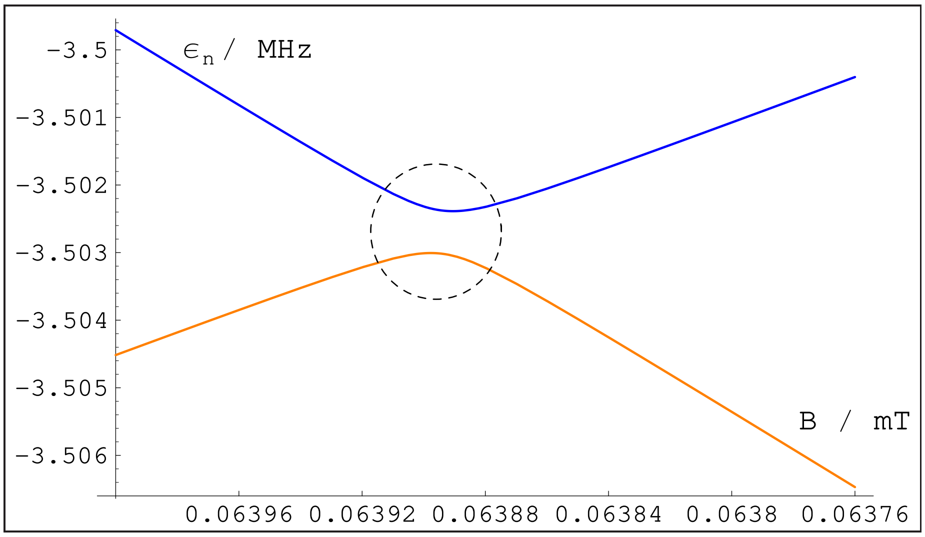

Figure 4.14: Behavior of the energy eigenvalues in the vicinity of an anticrossing point in ^{6}Li for the field cycle given in Fig. 4.11. The anticrossing point shown corresponds to the lowest value of the magnetic field strength amongst the three points in Fig. 4.11. It can also be identified by the appropriate use of colors. Observe the small energy gap between the two levels.

4.6 Structure of Energy Surfaces in ^{6}Li

For ^{7}Li the investigations on the structure of the energy surfaces have been limited to the first quadrant of the BE-plane. This restriction is no longer applicable for ^{6}Li since already the energy corrections due to the Zeeman effect of the two subsystems of ^{6}Li are not symmetric with respect to a magnetic field reversal. The Stark effect, however, is considered here only in its quadratic form, so a change of the direction of the electric field has no effect on the energy eigenvalues. Therefore, the considerations can at least be restricted to the closed half-plane $E \geq 0$ of the BE-plane. However, as shown in chapter 6, the structure of the energy surfaces of the positive system for negative magnetic field strengths is identical to the structure of the energy surfaces of the negative system for positive magnetic field strengths. For this reason, the calculations have only been carried out for the first quadrant $(B \geq 0, E \geq 0)$ of the BE-plane.

The naming of the crossing points follows the naming used for ^{7}Li; the preceding letters **BE** express the fact that the corresponding crossing points belong to both, nonvanishing magnetic field and nonvanishing electric field. A subsequent **p** or **n** symbolizes the subsystem to which the particular crossing point belongs to.

From the three methods for searching the crossing points presented in section 3.6 only the last two ones are used for ^{6}Li: the method of visualizing the energy surfaces by Mathematica plots and the method of Berry phases.

The following Figs. 4.15-4.18 show the energy surfaces of the positive and the negative subsystem of ^{6}Li. As explained in section 3.6 the scalar polarizability α_0 is put to zero in preparing the diagrams. The quantities ϵ'_n are the eigenvalues of the operator given in eq. (3.11) which are related to the energy eigenvalues of the total Hamiltonian (3.12) by eq. (3.13).

Figs. 4.15 and 4.17 show one crossing point for the negative subsystem, denoted **BEn**, but none for the positive subsystem. The corresponding **BEp**-point of the positive subsystem is located at the same energy eigenvalue and electric field value as the point **BEn**, but with the magnetic field value reversed. These two pictures show the names of the energy surfaces of the form (F, M_F). The other pictures present different views of the energy surfaces and show the magnetic and the electric crossing points in the planes $E = 0$ and $B = 0$.

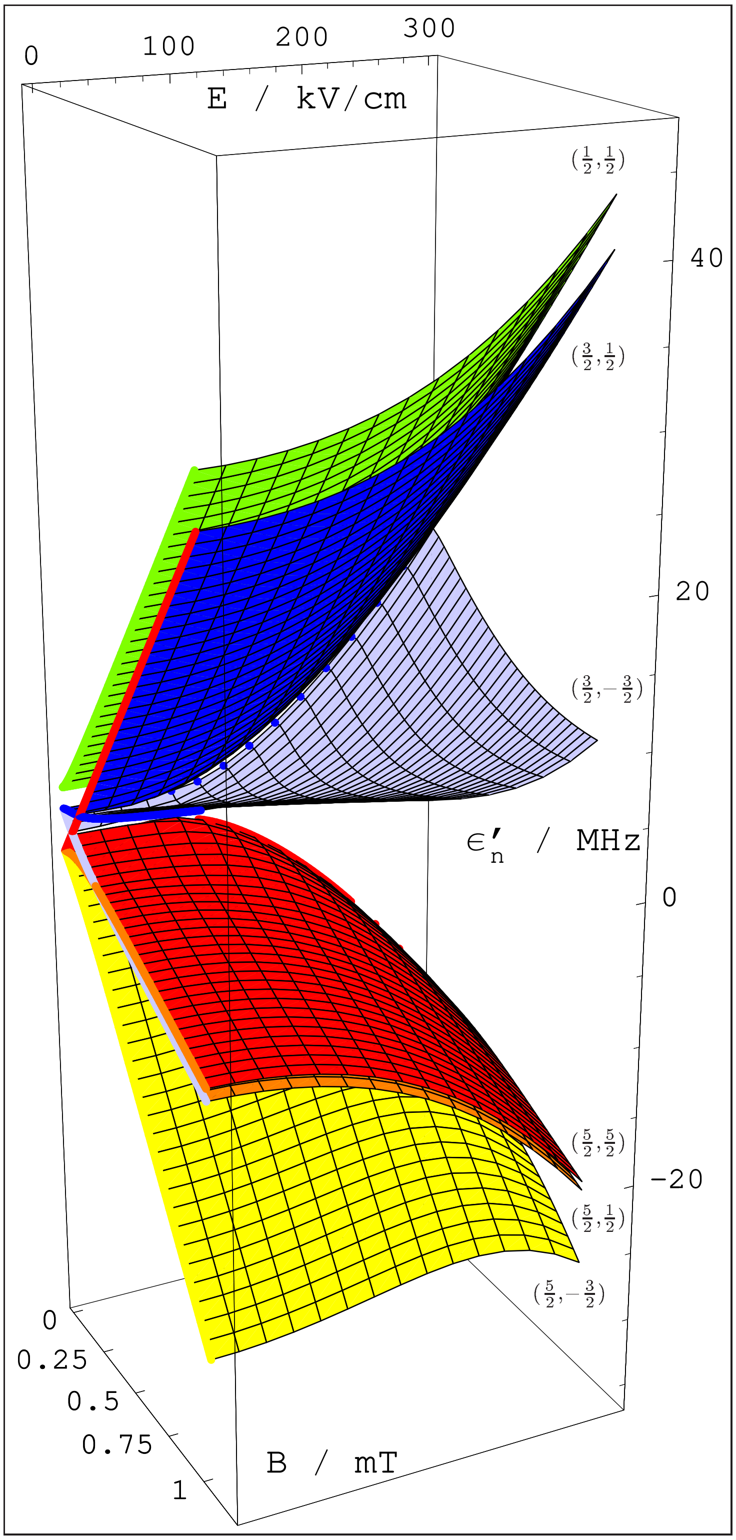

Figure 4.15: Energy surfaces in the positive subsystem of ^{6}Li.

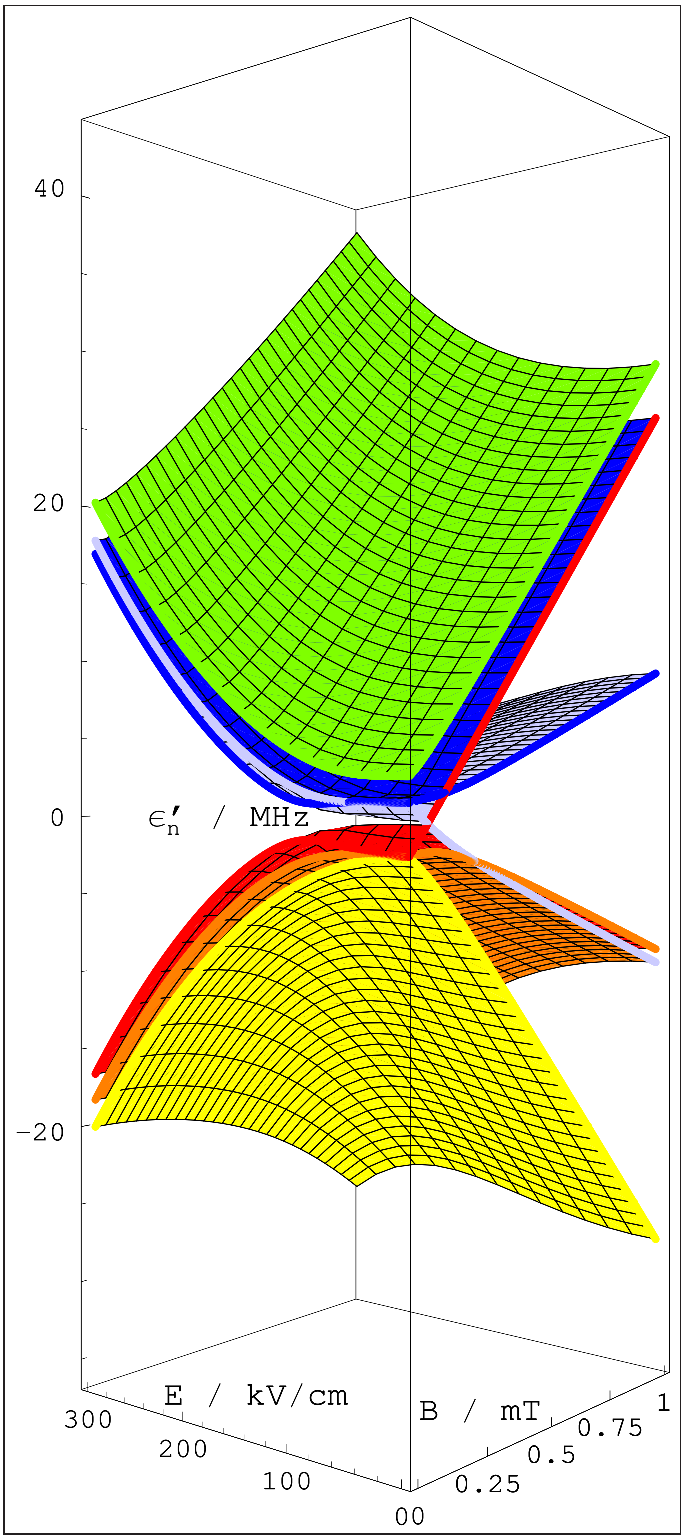

Figure 4.16: Energy surfaces in the positive subsystem of ^{6}Li; view of magnetic and electric crossing points.

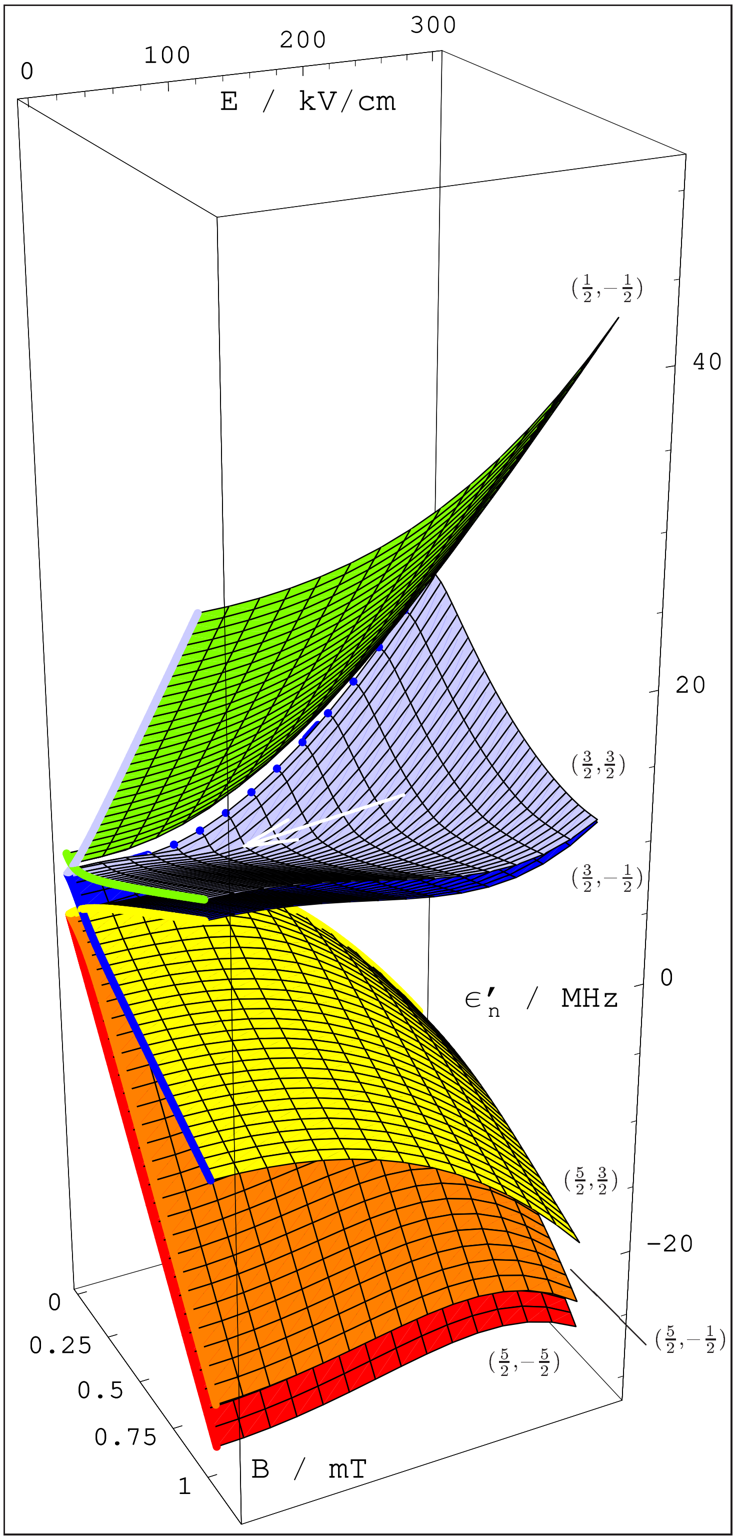

Figure 4.17: Energy surfaces in the negative subsystem of ^{6}Li.

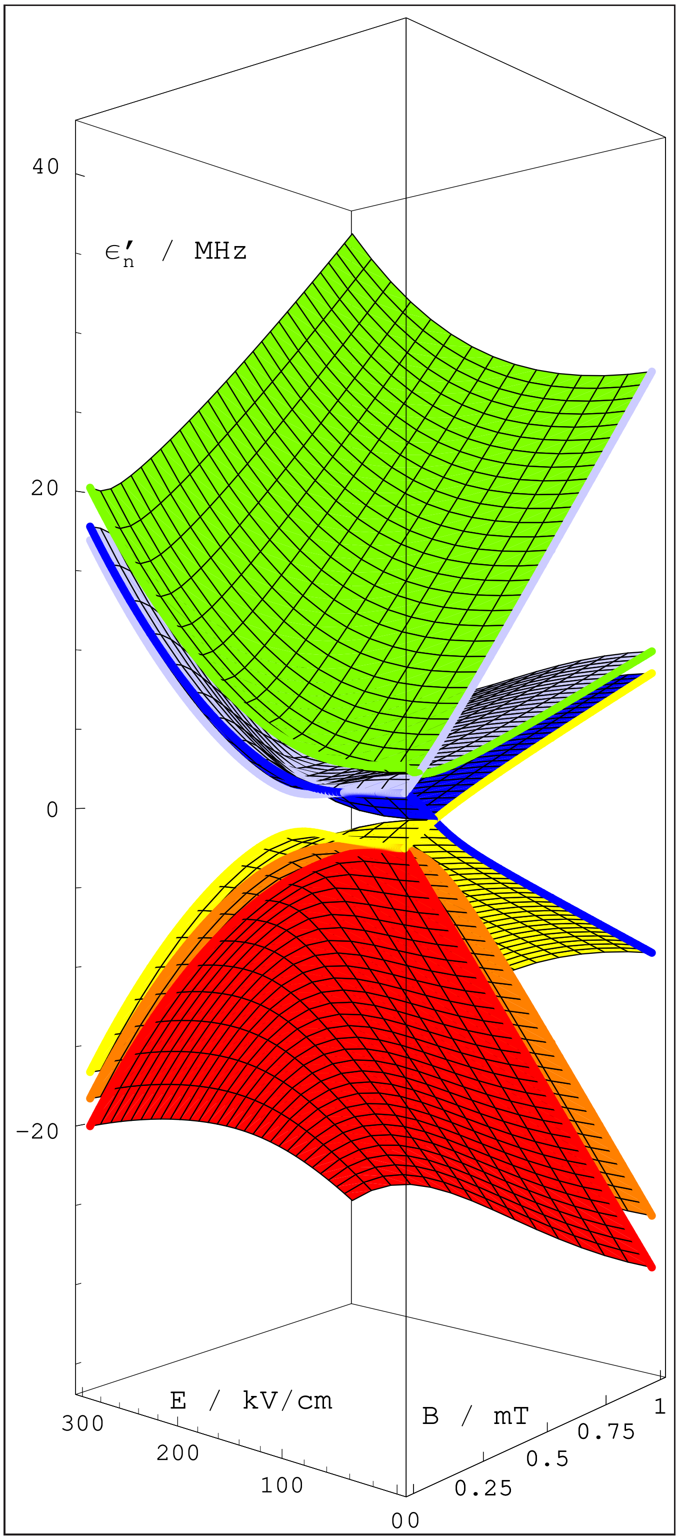

Figure 4.18: Energy surfaces in the negative subsystem of ^{6}Li; view of magnetic and electric crossing points.

4.7 Listing of Crossing Point Data for ^{6}Li

The following two Tabs. 4.3 and 4.4 list all the data that characterize the various crossing points in ^{6}Li: names, field values, energy eigenvalues and the pairs of quantum numbers (F, M_F) assigned to the corresponding eigenvectors by analytic continuation (see section 3.7). The energies given are the eigenvalues of the total perturbation operator ϵ_n, including the term proportional to the scalar polarizability α_0, belonging to the field values of the corresponding crossing points.

Name	**B / mT**	**E / kV/cm**	**ϵ / MHz**	$(\mathbf{F}, \mathbf{M_F})$-$(\mathbf{F'}, \mathbf{M'_F})$
Bp1	-0.10335	0.	-0.26564	$(\frac{3}{2}, \frac{1}{2})$-$(\frac{5}{2}, -\frac{3}{2})$
Bp2	-0.04978	0.	2.34180	$(\frac{1}{2}, \frac{1}{2})$-$(\frac{3}{2}, -\frac{3}{2})$
Bp3	0.06451	0.	0.05000	$(\frac{3}{2}, -\frac{3}{2})$-$(\frac{5}{2}, \frac{5}{2})$
Bp4	0.12622	0.	1.77922	$(\frac{3}{2}, \frac{1}{2})$-$(\frac{5}{2}, \frac{5}{2})$
Bp5	0.23458	0.	-2.23480	$(\frac{3}{2}, -\frac{3}{2})$-$(\frac{5}{2}, \frac{1}{2})$
Ep1	0.	51.390	-40.52359	$(\frac{3}{2}, \frac{1}{2})$-$(\frac{3}{2}, -\frac{3}{2})$
BEp	-0.13029	127.430	-254.8313	$(\frac{3}{2}, \frac{1}{2})$-$(\frac{3}{2}, -\frac{3}{2})$

Table 4.3: Listing of crossing point data for the positive subsystem in ^{6}Li

Name	**B / mT**	**E / kV/cm**	**ϵ / MHz**	$(\mathbf{F}, \mathbf{M_F})$-$(\mathbf{F'}, \mathbf{M'_F})$
Bn1	0.10335	0.	-0.26564	$(\frac{3}{2}, -\frac{1}{2})$-$(\frac{5}{2}, \frac{3}{2})$
Bn2	0.04978	0.	2.34180	$(\frac{1}{2}, -\frac{1}{2})$-$(\frac{3}{2}, \frac{3}{2})$
Bn3	-0.06451	0.	0.05000	$(\frac{3}{2}, \frac{3}{2})$-$(\frac{5}{2}, -\frac{5}{2})$
Bn4	-0.12622	0.	1.77922	$(\frac{3}{2}, -\frac{1}{2})$-$(\frac{5}{2}, -\frac{5}{2})$
Bn5	-0.23458	0.	-2.23480	$(\frac{3}{2}, \frac{3}{2})$-$(\frac{5}{2}, -\frac{1}{2})$
En1	0.	51.390	-40.52359	$(\frac{3}{2}, \frac{3}{2})$-$(\frac{3}{2}, -\frac{1}{2})$
BEn	0.13029	127.430	-254.8313	$(\frac{3}{2}, \frac{3}{2})$-$(\frac{3}{2}, -\frac{1}{2})$

Table 4.4: Listing of crossing point data for the negative subsystem in ^{6}Li

As discussed in section 4.3 and chapter 6 the Zeeman diagrams of each of the two subsystems of ^{6}Li are not symmetric with respect to a change of the direction of the magnetic field. Therefore, the crossing diagrams for ^{6}Li have to be extended to negative magnetic field values. The relative locations (in the BE-plane) of the various crossing points are shown in the two Figs. 4.19 and 4.20.

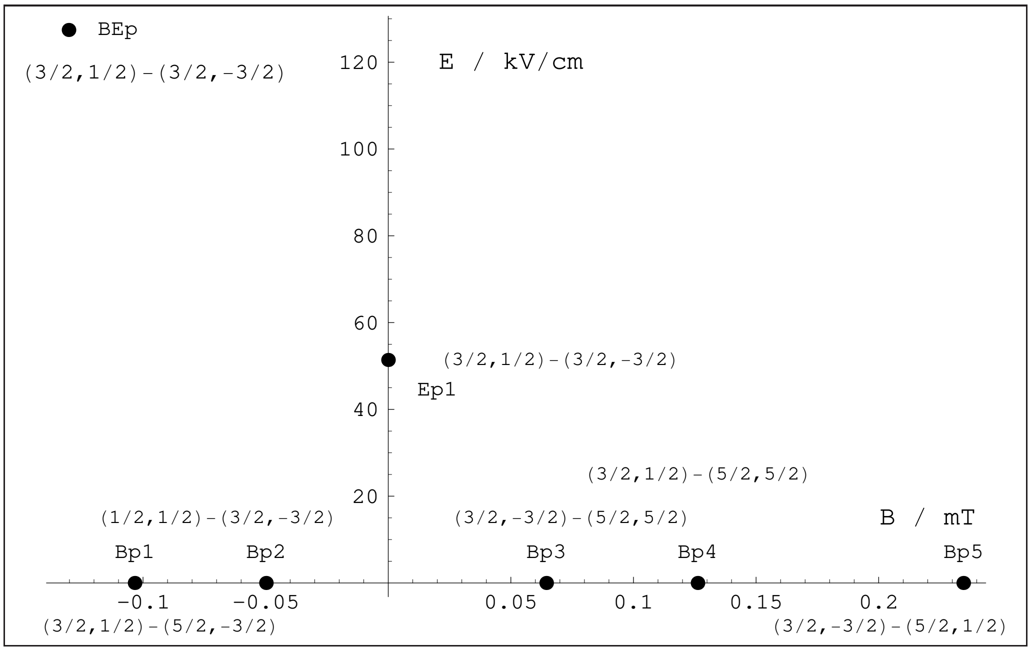

Figure 4.19: Crossing diagram of the positive subsystem of ^{6}Li

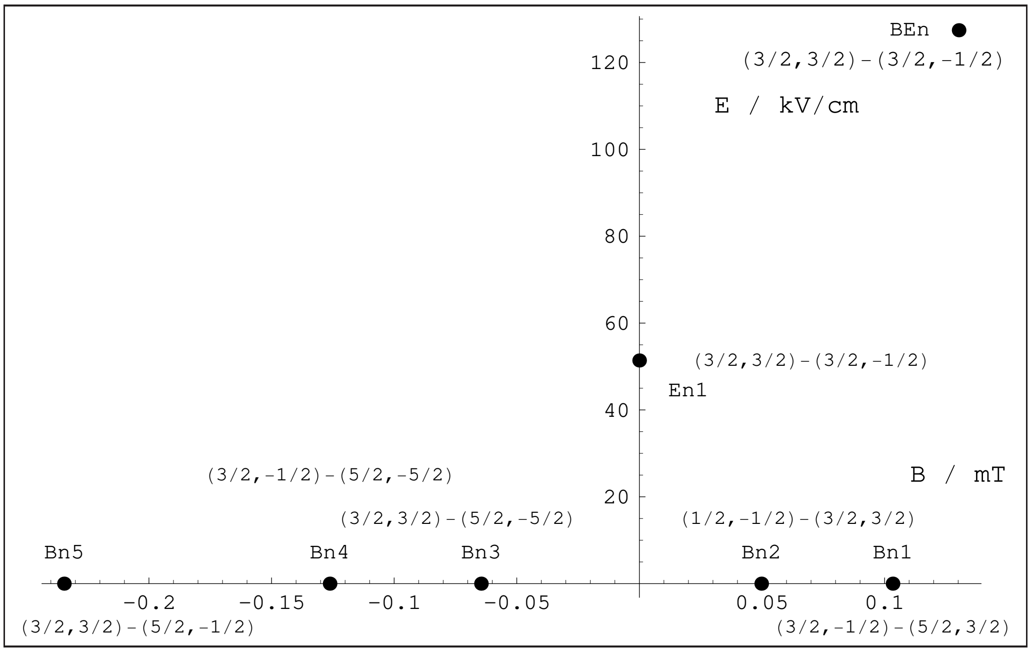

Figure 4.20: Crossing diagram of the negative subsystem of ^{6}Li

4.8 Berry Phases in ^{6}Li

It has already been mentioned in section 4.4 that only the investigations on Berry phases revealed the existence of the two electric crossing points **Ep1** and **En1**, one in each subsystem. Even though the **BE**-crossing point has been found by the FindMinimum command of Mathematica, this point also induces changes in sign of the eigenvectors under analytic continuation of the former (comp. section 3.8). Fig. 4.21 shows the output of the Mathematica program by Heubrandtner for the **BEn**-crossing point. Tabs. 4.5 and 4.6

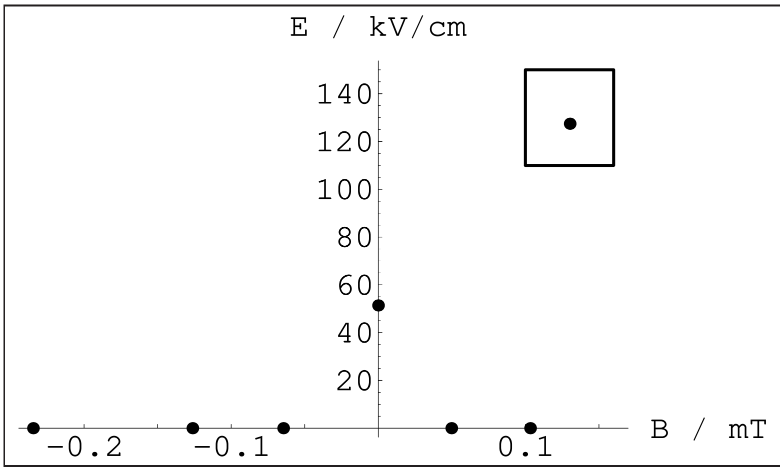

$$\begin{pmatrix} 1 & 0 & 0 & 0 & 0 & 0 \\ 0 & 1 & 0 & 0 & 0 & 0 \\ 0 & 0 & 1 & 0 & 0 & 0 \\ 0 & 0 & 0 & -1 & 0 & 0 \\ 0 & 0 & 0 & 0 & -1 & 0 \\ 0 & 0 & 0 & 0 & 0 & 1 \end{pmatrix}$$

Figure 4.21: Output of the program used in the investigations on the appearance of Berry phases. This diagram shows the rectangular path (within the BE-plane) along which the eigenvectors of the perturbation have been evaluated in the case of the **BEn**-crossing point in ^{6}Li. The overlap matrix indicates which eigenvectors assume a sign change in the adiabatic field cycle corresponding to the rectangular path.

summarize the results on Berry phases for all crossing points in ^{6}Li.

	Bp1	**Bp2**	**Bp3**	**Bp4**	**Bp5**	**Ep1**	**BEp**
Berry phase occurs	No	No	No	No	No	Yes	Yes

Table 4.5: Appearance of Berry phases in the positive subsystem of ^{6}Li.

	Bn1	**Bn2**	**Bn3**	**Bn4**	**Bn5**	**En1**	**BEn**
Berry phase occurs	No	No	No	No	No	Yes	Yes

Table 4.6: Appearance of Berry phases in the negative subsystem of ^{6}Li.

4.9 Analytic Expressions for the Energies and Field Values of Certain Crossing Points in ^{6}Li

It is possible to find analytic expressions for the energy eigenvalues and the field values of certain crossing points in ^{6}Li. That is to say, that the locations of crossing points can easily be found from the atomic constants of the particular atom under study, without ever calculating explicitly any matrix elements.

This computation has been performed by Heubrandtner and Schnizer in the case of Na. These expressions can be used (with some care) also for other elements, as ^{69}Ga, ^{71}Ga or ^{7}Li, characterized by the quantum numbers $I = \frac{3}{2}$ and $J = \frac{3}{2}$.

In the case of ^{6}Li, however, these expressions are of course not applicable. This section presents in brief the method to obtain such analytic expressions and the results in the case of some crossing points in ^{6}Li.

4.9.1 The Resultant of two Characteristic Equations

Because of the strong similarities between the two subsystems in ^{6}Li, it is sufficient to limit the investigations e.g. to the positive subsystem. Inspecting the structures of the matrix elements of that subsystem in the $|\gamma_I \gamma_J I J M_I M_J\rangle$ basis, given in Figs. 4.1, 4.2 and 4.3, leads to the following observation: the characteristic equation of the perturbation matrix including the hyperfine structure and the magnetic interaction decouples into three characteristic equations of order 1, 2 and 3, respectively. The evaluation (for arbitrary magnetic field strength) of the resultant of two of these polynomials is used to find analytic expressions for the wanted field values B from the zeros of the resultant. For two polynomials with a common factor the resultant is zero (see, e.g. [12]). These zeros then correspond to the magnetic field values of the magnetic crossing points **Bpn** or **Bnn**. The success of this method depends on the order of the resultant. Theoretically, one should be able to obtain in a similar way expressions for the electric crossing points and the **BE**-points. In ^{6}Li, however, only for the points **Bp3**, **Bn3**, **Bp4** and **Bn4** practicable analytic expressions could be found. The expressions obtained for the field values of all other magnetic crossing points in ^{6}Li (**Bp1**, **Bn1**, **Bp2**, **Bn2**, **Bp5**, **Bn5**) are too lengthy to be of any use.

4.9.2 Analytic Expressions for the Points Bp3 and Bn3

The energy eigenvalues of the crossing points **Bp3** and **Bn3** are the same, the magnetic field values are the negatives of each other. These points appear at magnetic field strengths given by

$$B_{\mathbf{Bp3,Bn3}} = \pm \frac{(2\hat{g}_I - 3g_J)\,(2a+b)}{2\,\mu_B\,(\hat{g}_I - 3g_J)\,(\hat{g}_I - g_J)}. \tag{4.4}$$

Their common energy is

$$\epsilon_{\mathbf{Bp3,Bn3}} = \frac{1}{4}\left[6a + b - \frac{(2\hat{g}_I - 3g_J)^2\,(2a+b)}{(\hat{g}_I - 3g_J)\,(\hat{g}_I - g_J)}\right]. \tag{4.5}$$

4.9.3 Analytic Expressions for the Points Bp4 and Bn4

The crossing points **Bp4** and **Bn4** appear at magnetic field values given by

$$B_{\mathbf{Bp4,Bn4}} = \pm \tfrac{1}{16\hat{g}_I(\hat{g}_I - g_J)g_J\mu_B}\Big\{ -8\hat{g}_I^2 a + 32\hat{g}_I g_J a - 12 g_J^2 a - 2\hat{g}_I^2 b - \tag{4.6}$$
$$-\sqrt{32\hat{g}_I\,(2\hat{g}_I - 3g_J)\,(\hat{g}_I - g_J)\,g_J\,(8a^2 + 2ab - b^2) + 4\left[-16\hat{g}_I g_J a + 6g_J^2 a + \hat{g}_I^2\,(4a+b)\right]^2}\Big\}$$

Their energy is

$$\epsilon_{\mathbf{Bp4,Bn4}} = \tfrac{1}{4}\,(6a+b) + \tfrac{1}{32\hat{g}_I g_J(\hat{g}_I - g_J)}\cdot \tag{4.7}$$
$$\Big\{(2\hat{g}_I - 3g_J)\Big[2\,(4a+b)\,\hat{g}_I^2 - 32 g_J a \hat{g}_I + 12 g_J^2 a +$$
$$+\sqrt{4\left[\,(4a+b)\,\hat{g}_I^2 - 16 g_J a \hat{g}_I + 6 g_J^2 a\right]^2 + 32\hat{g}_I g_J\,(\hat{g}_I - g_J)\,(2\hat{g}_I - 3g_J)\,(8a^2 + 2ab - b^2)}\,\Big]\Big\}.$$

In the four expressions above, a and b denote the hyperfine structure constants of the $2p\ {}^2P_{\frac{3}{2}}$ level (cf. App. B).

Chapter 5

Influence of the nearby $2p\ ^2P_{\frac{1}{2}}$ Fine Structure Level on the Crossing Points of the $2p\ ^2P_{\frac{3}{2}}$ Level in ^{7}Li

5.1 General Preliminaries

The purpose of this chapter is to work out the influence of the nearby $2p\ ^2P_{\frac{1}{2}}$ fine structure level on the field values and on the energy eigenvalues of the crossing points of the $2p\ ^2P_{\frac{3}{2}}$ fine structure level of ^{7}Li, discussed in chapter 4. In other words, the validity of the approximation of neglecting nondiagonal matrix elements in J (matrix elements of the perturbation operators between eigenstates of the operator $\hat{\vec{J}}^2$ with different eigenvalues, in this case $J(J+1)$ with quantum numbers $J = \frac{1}{2}$ or $J = \frac{3}{2}$) is examined. This examination is required by the low energy splitting between the two fine structure levels $2p\ ^2P_{\frac{3}{2}}$ and $2p\ ^2P_{\frac{1}{2}}$ in Li, which is the lowest value (appr. 10 GHz) amongst all alkalines.

First of all, such considerations require an extension of the state space and of the basis. The degree of degeneracy of the $2p\ ^2P_{\frac{3}{2}}$ fine structure level of

^{7}Li (with nuclear spin $I = \frac{3}{2}$) is 16, that of the lower $2p\ ^2P_{\frac{1}{2}}$ level is 8;

$$\begin{array}{lclcl} 2p\ ^2P_{\frac{3}{2}} & : & F = 3, 2, 1, 0 & \sum\limits_{F=0}^{3} (2F+1) & = & 16 \\ 2p\ ^2P_{\frac{1}{2}} & : & F = 2, 1 & \sum\limits_{F=1}^{2} (2F+1) & = & 8. \end{array} \tag{5.1}$$

Therefore, the state space of the $2p\ ^2P$ configuration of ^{7}Li is 24-dimensional. In consequence, the inclusion of the $2p\ ^2P_{\frac{1}{2}}$ fine structure level necessitates to include also the fine structure Hamiltonian (Hamiltonian of the spin-orbit interaction) among the operators describing the perturbation of the $2p\ ^2P$ level. In the following sections the formulae and the structure of the matrix elements of the various perturbation operators are presented. The four different contributions to the hyperfine Hamiltonian are discussed independently of each other.

Thereafter, section 5.3 is dedicated to the presentation of the results of the numerical calculation of the eigenvalues. The main purpose is to compare the field values and the energy eigenvalues of the crossing points (of the $2p\ ^2P_{\frac{3}{2}}$ level) found while neglecting the nondiagonal matrix elements in the quantum number J, with the corresponding values found while taking the influence of the $2p\ ^2P_{\frac{1}{2}}$ level into account. According to the selection rule

$$\Delta M_F = \text{even} \tag{5.2}$$

for nonvanishing matrix elements of the hyperfine, the Zeeman and the Stark Hamiltonians (in the basis of common eigenstates of $\hat{\vec{F}}^2$ and $\hat{F}_z$) and because of

$$M_F = M_I + M_S + M_L, \tag{5.3}$$

the 24-dimensional matrix can be reduced to two blocks arranged along the main diagonal (odd and even subsystems, each having the dimension 12). The task to numerically compute the energy eigenvalues of a 24-dimensional square matrix is thus reduced to computing the eigenvalues of two 12-dimensional square matrices.

5.2 Representation of the Perturbation Operators in the $2p\ ^2P$ Configuration of ^{7}Li

Eqs. (2.14) and (2.16) of the hyperfine matrix elements in section 2.2.1 of chapter 2 don't contain any information about matrix elements between eigenstates of the operator $\hat{\vec{J}}^2$ corresponding to different eigenvalues. Therefore, those matrix elements have to be calculated right from the beginning. However, for this task another basis is used, since the same calculations have already been performed by Umfer [13]. None of the two bases $|\gamma_I \gamma_J I(SL)JFM_F\rangle$ and $|\gamma_I \gamma_J IM_I(SL)JM_J\rangle$ already introduced is used, but the basis of common eigenvectors of the operators $\hat{\vec{I}}^2$, $\hat{I}_z$, $\hat{\vec{S}}^2$, $\hat{S}_z$, $\hat{\vec{L}}^2$ and $\hat{L}_z$ denoted by $|\gamma_I \gamma_L IM_I SM_S LM_L\rangle$. γ_I and γ_L again represent the eigenvalues of all the other operators which together with the operators given above form a complete set of commuting observables.

5.2.1 The Fine Structure Hamiltonian

The perturbation operator of the fine structure

$$\hat{H}_{\text{fs}} = \xi\left(\hat{r}\right) \hat{\vec{L}} \cdot \hat{\vec{S}} \tag{5.4}$$

takes the interaction between the spin and the orbital angular momentum of the valence electron into account. $\xi\left(r\right)$ is a function that depends only on the radial coordinate of the valence electron.

The computations of the matrix elements of the fine structure operator above and of those of all the other perturbation operators are rather lengthy and time-consuming even though they present no major difficulties. For the sake of clarity these calculations are omitted and only the resulting formulae are given explicitly here. All the computations can be carried out easily with the help of the algebra of spherical tensor operators, especially the Wigner-Eckart-theorem, treated in great detail in [6] or [7].

The matrix elements of the fine structure operator in the basis with the basis states $|\gamma_I \gamma_L IM_I SM_S LM_L\rangle$ are obtained by applying the Wigner-Eckart theorem twice and by evaluating the resulting reduced matrix elements:

$$\begin{aligned} &\langle \gamma_I \gamma_L IM_I SM_S LM_L | \hat{H}_{\text{fs}} | \gamma_I \gamma_L IM_I' SM_S' LM_L' \rangle = \\ &= \zeta_{nl} \delta_{M_I M_I'} (-1)^{L-M_L+S-M_S} \sqrt{(2L+1)(L+1)L(2S+1)(S+1)S} \cdot \\ &\cdot \sum_{q=-1}^{1} (-1)^q \begin{pmatrix} L & 1 & L \\ -M_L & q & M_L' \end{pmatrix} \begin{pmatrix} S & 1 & S \\ -M_S & -q & M_S' \end{pmatrix} \end{aligned} \tag{5.5}$$

The number ζ_{nl} is the so called fine structure constant and depends on the configuration under study. For its numerical value for the $2p\,^2P$ configuration of ^{7}Li see the listing of atomic constants in App. B.

In the above and the following formulae all but the magnetic quantum numbers remain fixed since the configuration $2p\ ^2P$ of $^7\mathsf{Li}$ is characterized by given values of the quantum numbers γ_I, γ_L, I, S and L.

5.2.2 The Hyperfine Structure Hamiltonian

The various terms of the Hyperfine Hamiltonian are discussed separately. Those are: the orbital term, the spin dipole term and (Fermi's) contact term in the case of the magnetic interaction and the quadrupole term in the case of the electric interaction. (see eqs. (2.2)-(2.7)). The physical origins of these terms have been discussed in section 2.2.1.

The Orbital Term

The Hamiltonian of the orbital term is

$$\hat{H}_{\text{orb}} = g_L \hat{g}_I \mu_B^2 \frac{2\mu_0}{4\pi} \frac{\hat{\vec{I}} \cdot \hat{\vec{L}}}{\hat{r}^3}. \tag{5.6}$$

Its matrix elements in the $|\gamma_I \gamma_L I M_I S M_S L M_L\rangle$-representation are given by

$$\begin{aligned} &\langle \gamma_I \gamma_L I M_I S M_S L M_L | \hat{H}_{\text{orb}} | \gamma_I \gamma_L I M_I' S M_S' L M_L' \rangle = \\ &= a_{\text{o}}\, \delta_{M_S M_S'} \tfrac{L+S}{L} (-1)^{L-M_L+I-M_I} \sqrt{(2L+1)(L+1)L(2I+1)(I+1)I} \cdot \\ &\cdot \sum_{q=-1}^{1} (-1)^q \begin{pmatrix} L & 1 & L \\ -M_L & -q & M_L' \end{pmatrix} \begin{pmatrix} I & 1 & I \\ -M_I & q & M_I' \end{pmatrix} \end{aligned} \tag{5.7}$$

where a_{o} is the so-called orbital hyperfine structure constant defined by

$$a_{\text{o}} = \frac{\langle \gamma_I \gamma_L I M_I = I S M_S = S L M_L = L | \hat{H}_{\text{orb}} | \gamma_I \gamma_L I M_I' = I S M_S' = S L M_L' = L \rangle}{I\,(L+S)}. \tag{5.8}$$

a_{o} consists above all of the reduced matrix element and can be determined empirically.

The Dipole Term

The operator that corresponds to the dipole term is

$$\hat{H}_{\text{dip}} = \frac{\mu_0}{4\pi} \hat{g}_I g_S \mu_B^2 \frac{1}{\hat{r}^3} \left[3 \frac{\hat{\vec{S}} \cdot \hat{\vec{r}}}{\hat{r}^2} \hat{\vec{r}} - \hat{\vec{S}} \right] \cdot \hat{\vec{I}}. \tag{5.9}$$

In order to calculate the matrix elements it is convenient to rewrite this operator in the following form

$$\hat{H}_{\rm dip} = -\frac{g_S \mu_0}{4\pi} \sqrt{10} \hat{g}_I \mu_B^2 \frac{1}{\hat{r}^3} \left[\hat{\mathbf{C}}^{(2)} \times \hat{\mathbf{S}}^{(1)} \right] \cdot \hat{\mathbf{I}}^{(1)}. \tag{5.10}$$

For the details see, for example, [14]. The matrix elements of the operator in eq. (5.10) are

$$\begin{aligned} &\langle \gamma_I \gamma_L I M_I S M_S L M_L | \hat{H}_{\rm dip} | \gamma_I \gamma_L I M_I' S M_S' L M_L' \rangle = \qquad (5.11) \\ &= a_{\rm d} (-1)^{I - M_I + 3L + 3S - M_L - M_S + 1} \sqrt{\tfrac{15}{2}} \tfrac{L+S}{2SL(2L-1)} \sqrt{(2I+1)(I+1)I(2S+1)(S+1)S} \cdot \\ &\cdot \sqrt{(2L+3)(2L+2)(2L+1)(2L)(2L-1)} \sum_{q=-1}^{1} (-1)^q \begin{pmatrix} I & 1 & I \\ -M_I & q & M_I' \end{pmatrix} \cdot \\ &\cdot \sum_{q_1=-1}^{1} \sum_{q_2=-2}^{2} \begin{pmatrix} 1 & 2 & 1 \\ q_1 & q_2 & -q \end{pmatrix} \begin{pmatrix} L & 2 & L \\ M_L & q_2 & -M_L' \end{pmatrix} \begin{pmatrix} S & 1 & S \\ M_S & q_1 & -M_S' \end{pmatrix} \end{aligned}$$

where the dipole hyperfine structure constant $a_{\rm d}$ is defined (similarly to $a_{\rm o}$) by

$$a_{\rm d} = \frac{\langle \gamma_I \gamma_L I M_I = I S M_S = S L M_L = L | \hat{H}_{\rm dip} | \gamma_I \gamma_L I M_I' = I S M_S' = S L M_L' = L \rangle}{I\,(L+S)}. \tag{5.12}$$

The Contact Term

The Hamiltonian of the contact term is

$$\hat{H}_{\rm con} = \frac{\mu_0 g_S}{4\pi} \hat{g}_I \mu_B^2 \delta\left(\hat{r}\right) \frac{2}{3} \hat{\vec{S}} \cdot \hat{\vec{I}} \tag{5.13}$$

and its matrix elements are

$$\begin{aligned} &\langle \gamma_I \gamma_L I M_I S M_S L M_L | \hat{H}_{\rm con} | \gamma_I \gamma_L I M_I' S M_S' L M_L' \rangle = \\ &= a_{\rm c}\, \delta_{M_L M_L'} \tfrac{L+S}{S} (-1)^{I - M_I + S - M_S} \sqrt{(2I+1)(I+1)I(2S+1)(S+1)S} \cdot \\ &\cdot \sum_{q=-1}^{1} (-1)^q \begin{pmatrix} I & 1 & I \\ -M_I & q & M_I' \end{pmatrix} \begin{pmatrix} S & 1 & S \\ -M_S & -q & M_S' \end{pmatrix} \qquad (5.14) \end{aligned}$$

with analog definition of the contact hyperfine structure constant $a_{\rm c}$:

$$a_{\rm c} = \frac{\langle \gamma_I \gamma_L I M_I = I S M_S = S L M_L = L | \hat{H}_{\rm con} | \gamma_I \gamma_L I M_I' = I S M_S' = S L M_L' = L \rangle}{I\,(L+S)}. \tag{5.15}$$

The definitions of the hyperfine structure constants a_o, a_d, a_c are such that the relations

$$\begin{array}{ccccccc} a_{\frac{3}{2}} & = & a_\mathrm{o} & + & a_\mathrm{d} & + & a_\mathrm{c} \\ a_{\frac{1}{2}} & = & 2a_\mathrm{o} & - & 10a_\mathrm{d} & - & a_\mathrm{c} \end{array} \tag{5.16}$$

hold (see e.g. [15]) where $a_{\frac{3}{2}}$ and $a_{\frac{1}{2}}$ are the hyperfine structure constants of the fine structure levels $2p\ {}^2P_{\frac{3}{2}}$ and $2p\ {}^2P_{\frac{1}{2}}$, respectively.

The Electric Quadrupole Term

The perturbation operator that takes into account the interaction between the electric field gradient induced by the valence electron at the position of the nucleus with the quadrupole moment of the former is

$$\hat{H}_\mathrm{qua} = -\frac{e^2}{4\pi\epsilon_0} \cdot \frac{\sqrt{6}}{2} \cdot \frac{Q}{I(2I-1)} \cdot \frac{1}{\hat{r}^3} \cdot \hat{\mathbf{C}}^{(2)}(\theta,\phi) \cdot \left[\hat{\mathbf{I}} \cdot \hat{\mathbf{I}}\right]^{(2)}, \tag{5.17}$$

where Q is the quadrupole moment of the nucleus defined by

$$Q := \langle IM_I = I | Q_{zz} | IM_I' = I \rangle. \tag{5.18}$$

For the details see again [14]. The matrix elements of this operator are

$$\begin{aligned} &\langle \gamma_I \gamma_L I M_I S M_S L M_L | \hat{H}_\mathrm{qua} | \gamma_I \gamma_L I M_I' S M_S' L M_L' \rangle = \\ &= b(-1)^{I-M_I+L-M_L} \delta_{M_S M_S'} \frac{\sqrt{(2L+3)(2L+2)(2L+1)(2L)(2L-1)(2I+3)(2I+2)(2I+1)(2I)(2I-1)}}{4\cdot 2L(2L-1)\cdot 2I(2I-1)} \cdot \\ &\sum_{q=-2}^{2} (-1)^q \begin{pmatrix} I & 2 & I \\ -M_I & q & M_I' \end{pmatrix} \begin{pmatrix} L & 2 & L \\ -M_L & -q & M_L' \end{pmatrix} \end{aligned} \tag{5.19}$$

with the traditional hyperfine structure constant b defined by

$$b = \langle \gamma_I \gamma_L I M_I = I S M_S = S L M_L = L | \hat{H}_\mathrm{qua} | \gamma_I \gamma_L I M_I' = I S M_S' = S L M_L' = L \rangle. \tag{5.20}$$

5.2.3 The Hamiltonian of the External Magnetic Field

In comparison with the laborious computations needed for finding the matrix elements of the various terms of the hyperfine operator, the matrix elements of the magnetic perturbation operator given in eq. (2.17) are found easily as

$$\begin{aligned} &\langle \gamma_I \gamma_L I M_I S M_S L M_L | \hat{H}_\mathrm{mag} | \gamma_I \gamma_L I M_I' S M_S' L M_L' \rangle = \\ &= \mu_B B_z \left[g_L M_L + g_S M_S - \hat{g}_I M_I \right] \delta_{M_I M_I'} \cdot \delta_{M_S M_S'} \cdot \delta_{M_L M_L'} \end{aligned} \tag{5.21}$$

with the relation

$$\hat{\vec{\mu}} = \hat{\vec{\mu}}_L + \hat{\vec{\mu}}_S + \hat{\vec{\mu}}_I \tag{5.22}$$

together with

$$\begin{aligned} \hat{\vec{\mu}}_L &= -g_L \mu_B \hat{\vec{L}} \\ \hat{\vec{\mu}}_S &= -g_S \mu_B \hat{\vec{S}} \\ \hat{\vec{\mu}}_I &= +g_I \mu_N \hat{\vec{I}} = \hat{g}_I \mu_B \hat{\vec{I}}. \end{aligned} \tag{5.23}$$

The matrix representing the magnetic interaction is diagonal in all the magnetic quantum numbers M_I, M_S and M_L.

5.2.4 The Effective Hamiltonian of the External Electric Field

Finding the matrix elements of the effective electric perturbation operator given in eq. (2.30) in the basis $|\gamma_I \gamma_L I M_I S M_S L M_L\rangle$ proceeds in two steps. Since it is necessary to generalize eqs. (2.34) and (2.35) to matrix elements nondiagonal in the quantum number J, it is first of all convenient to use the corresponding formula given explicitly, for example, in [16]. Then, finding the matrix elements in the basis $|\gamma_I \gamma_L I M_I S M_S L M_L\rangle$ simply amounts to a unitary change of basis via Clebsch-Gordan-coefficients.

The matrix elements of the two terms of the operator $\hat{H}_{\text{el,eff}}$ in the basis $|\gamma_I \gamma_J I(SL)JFM_F\rangle$ given in [16] are

$$\begin{aligned} &\langle \gamma_I \gamma_J I(SL)JFM_F | \hat{H}^{(0)}_{\text{el,eff}} | \gamma_I \gamma_J I(SL)J'F'M'_F \rangle = \\ &\quad = -\tfrac{1}{2}\alpha_0 E^2 \delta_{JJ'} \cdot \delta_{FF'} \cdot \delta_{M_F M'_F} \end{aligned} \tag{5.24}$$

and

$$\begin{aligned} &\langle \gamma_I \gamma_J I(SL)JFM_F | \hat{H}^{(2)}_{\text{el,eff}} | \gamma_I \gamma_J I(SL)J'F'M'_F \rangle = \\ &= -\tfrac{\sqrt{4}}{6}\alpha_2 (-1)^{F-M_F} (-1)^{I+J'+F} \sqrt{(2F+1)(2F'+1)} \begin{Bmatrix} J & F & I \\ F' & J' & 2 \end{Bmatrix} \cdot \\ &\cdot (-1)^{S+L+J} \sqrt{\left[\tfrac{(2L+3)(2L+2)(2L+1)(2J+1)(2J'+1)}{2L(2L-1)}\right]} \begin{Bmatrix} L & J & S \\ J' & L & 2 \end{Bmatrix} \cdot \\ &\cdot \sum_{Q=-2}^{2} (-1)^Q \begin{pmatrix} F & 2 & F' \\ -M_F & Q & M'_F \end{pmatrix} \{\mathbf{E}\,\mathbf{E}\}^2_{-Q}\,; \end{aligned} \tag{5.25}$$

the last braces are defined in terms of Clebsch-Gordan-coefficients by

$$\{\mathbf{E}\,\mathbf{E}\}^K_Q = \sum_{q=-1}^{1} \sum_{q'=-1}^{1} \langle 11qq' | 11KQ \rangle E^1_q E^1_{q'}. \tag{5.26}$$

The corresponding formulae in [16] contain some misprints; these have been found by redoing the calculations. This explains the differences between the given expressions and those of [16]. The spherical components E^1_q of the electric field strength are given in (2.36).

The subsequent change of basis actually consists of two unitary transformations. For the sake of simplicity, the quantum numbers γ_I, γ_J and γ_L are omitted in the following. Expressing the basis vectors $|I(SL)JFM_F\rangle$ by linear combinations of the vectors of the intermediate basis $|IM_I(SL)JM_J\rangle$ via

$$|I(SL)JFM_F\rangle = \sum_{M_I=-I}^{I} \sum_{M_J=-J}^{J} |IM_I(SL)JM_J\rangle\langle IJM_IM_J|IJFM_F\rangle \quad (5.27)$$

and analogously expressing the basis vectors $|IM_I(SL)JM_J\rangle$ of the intermediate basis by the basis vectors $|IM_ISM_SLM_L\rangle$ via

$$|IM_I(SL)JM_J\rangle = \sum_{M_S=-S}^{S} \sum_{M_L=-L}^{L} |IM_ISM_SLM_L\rangle\langle SLM_SM_L|SLJM_J\rangle \quad (5.28)$$

and combining the above two equations leads to

$$\begin{aligned} |I(SL)JFM_F\rangle = &\sum_{M_I=-I}^{I} \sum_{M_J=-J}^{J} \sum_{M_S=-S}^{S} \sum_{M_L=-L}^{L} |IM_ISM_SLM_L\rangle \cdot \\ &\cdot \langle SLM_SM_L|SLJM_J\rangle\langle IJM_IM_J|IJFM_F\rangle. \end{aligned} \quad (5.29)$$

This represents the vectors of the "old" basis $|I(SL)JFM_F\rangle$ by linear combinations of the vectors of the "new" basis. The elements of the transformation matrix are therefore

$$\begin{aligned} t_{ij} &= \langle IM_ISM_SLM_L|I(SL)JFM_F\rangle = \\ &= \sum_{M_J=-J}^{J} \langle SLM_SM_L|SLJM_J\rangle\langle IJM_IM_J|IJFM_F\rangle. \end{aligned} \quad (5.30)$$

The real unitary matrix T with elements t_{ij} can now be used to find the matrix representation of the operator $\hat{H}_{\text{el,eff}}$ in the basis $|IM_ISM_SLM_L\rangle$ according to the matrix equation

$$\hat{H}_{\text{el,eff}}^{\{|IM_ISM_SLM_L\rangle\}} = S^{\mathsf{T}} \hat{H}_{\text{el,eff}}^{\{|I(SL)JFM_F\rangle\}} S \qquad \text{with} \qquad S = T^{-1}. \quad (5.31)$$

5.2.5 The Structure of the Matrix Elements

Even though the matrix elements have only been given in the $|IM_ISM_SLM_L\rangle$ basis, the matrices representing the perturbation operators in the two other sets of basis vectors have been evaluated by means of unitary transformations as discussed at the end of the preceding subsection in the case of the effective electric operator. However, it makes no sense to give even the structure of the matrix elements in all three bases. This subsection therefore presents the structure of the matrix elements only in the $|IM_ISM_SLM_L\rangle$ basis where the basis vectors are ordered such that the states of the even subsystem are followed by those of the odd subsystem.

Fig. 5.1 shows the structure of the matrix elements of the fine structure operator given in eq. (5.5), Figs. 5.2-5.6 those of the various terms of the hyperfine structure operator at first each one alone, their sum at the end.

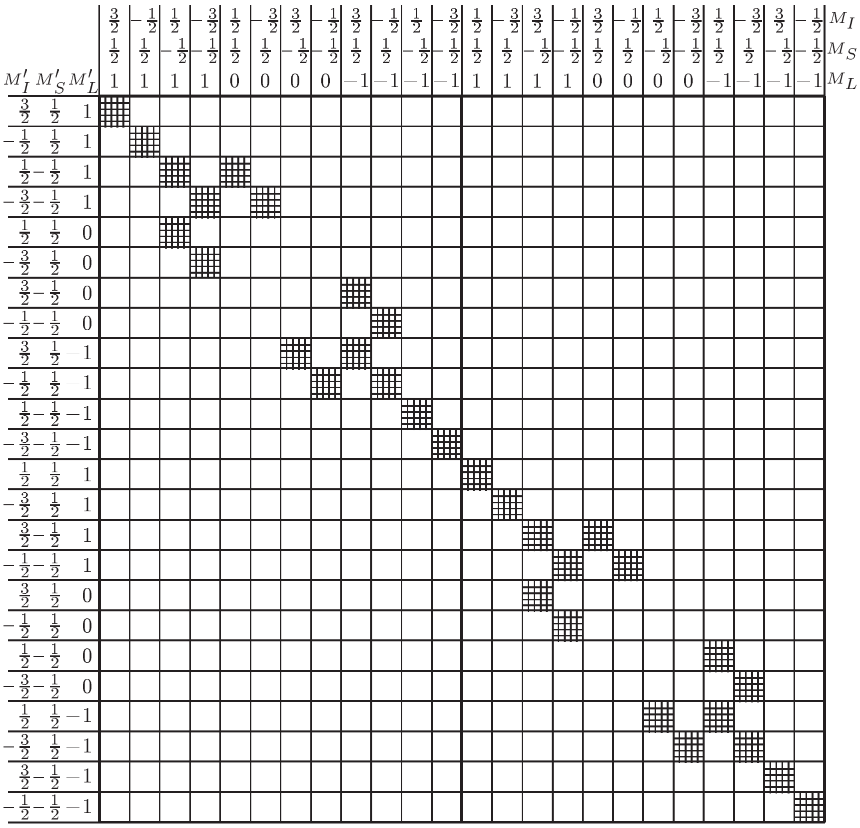

Figure 5.1: Fine Structure matrix elements $\langle\gamma_I\gamma_L IM_ISM_SLM_L|\hat{H}_{\mathrm{fs}}|\gamma_I\gamma_L IM'_ISM'_SLM'_L\rangle$ of the whole $2p\ ^2P$ level of ^{7}Li as given in eq. (5.5). M_I, M_S, M_L...magnetic quantum numbers of the nuclear spin, the electronic spin and the orbital angular momentum.

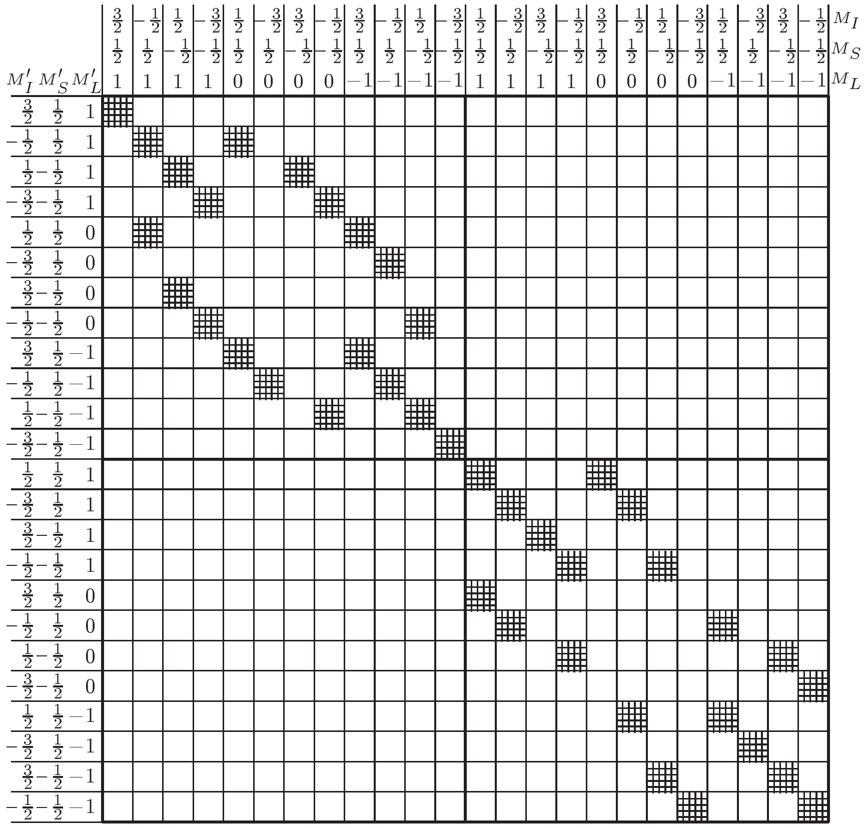

Figure 5.2: Matrix elements of the orbital term of the hyperfine interaction $\langle \gamma_I \gamma_L I M_I S M_S L M_L | \hat{H}_{\mathrm{orb}} | \gamma_I \gamma_L I M'_I S M'_S L M'_L \rangle$ of the whole $2p\ {}^2P$ level of ${}^7\mathsf{Li}$ as given in eq. (5.7). M_I, M_S, M_L...magnetic quantum numbers of the nuclear spin, the electronic spin and the orbital angular momentum.

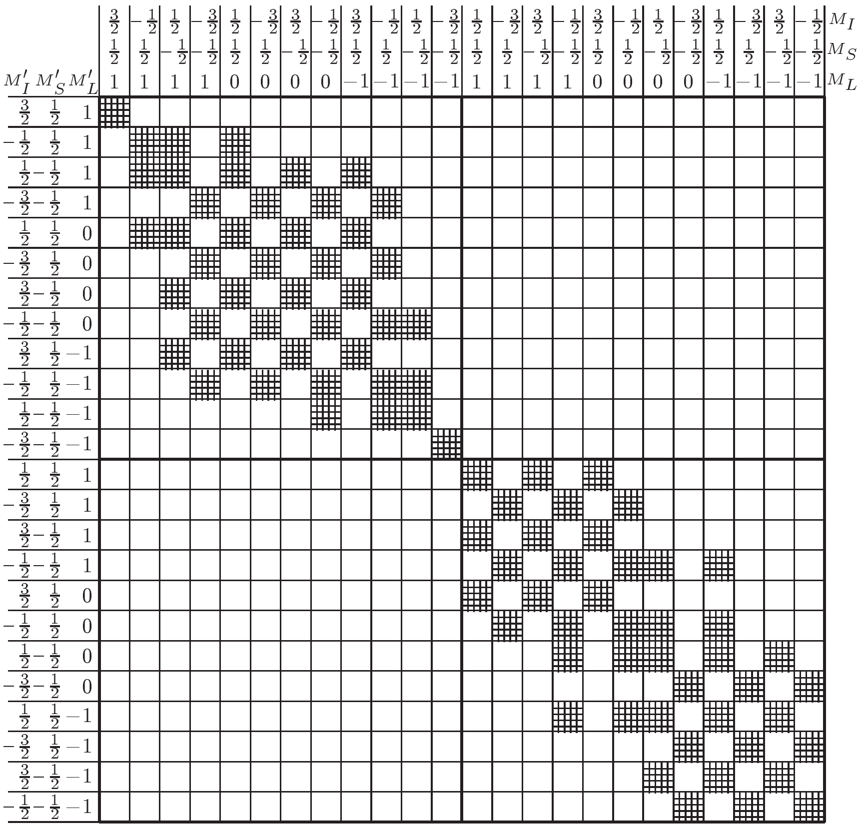

Figure 5.3: Matrix elements of the dipole term of the hyperfine interaction $\langle \gamma_I \gamma_L I M_I S M_S L M_L | \hat{H}_{\text{dip}} | \gamma_I \gamma_L I M'_I S M'_S L M'_L \rangle$ of the whole $2p\ ^2P$ level of $^7\mathsf{Li}$ as given in eq. (5.11). M_I, M_S, M_L...magnetic quantum numbers of the nuclear spin, the electronic spin and the orbital angular momentum.

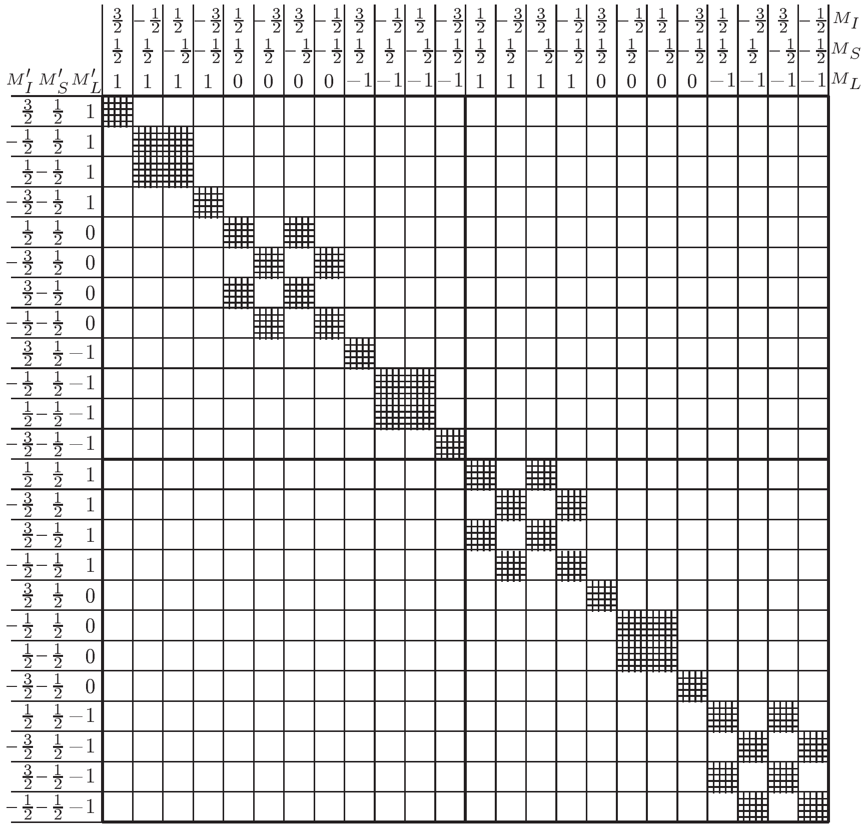

Figure 5.4: Matrix elements of the contact term of the hyperfine interaction $\langle \gamma_I \gamma_L I M_I S M_S L M_L | \hat{H}_{\mathrm{con}} | \gamma_I \gamma_L I M_I' S M_S' L M_L' \rangle$ of the whole $2p\ ^2P$ level of $^7\mathsf{Li}$ as given in eq. (5.14). M_I, M_S, M_L...magnetic quantum numbers of the nuclear spin, the electronic spin and the orbital angular momentum.

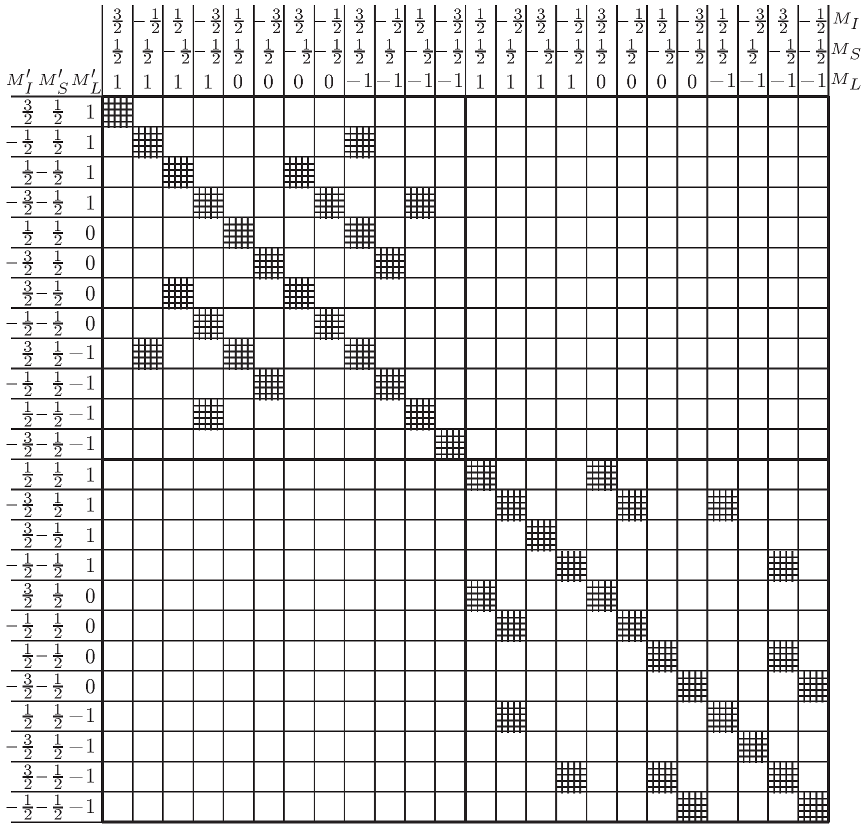

Figure 5.5: Matrix elements of the quadrupole term of the hyperfine interaction $\langle \gamma_I \gamma_L I M_I S M_S L M_L | \hat{H}_{\text{qua}} | \gamma_I \gamma_L I M_I' S M_S' L M_L' \rangle$ of the whole $2p\,^2P$ level of $^7\mathsf{Li}$ as given in eq. (5.19). M_I, M_S, M_L...magnetic quantum numbers of the nuclear spin, the electronic spin and the orbital angular momentum.

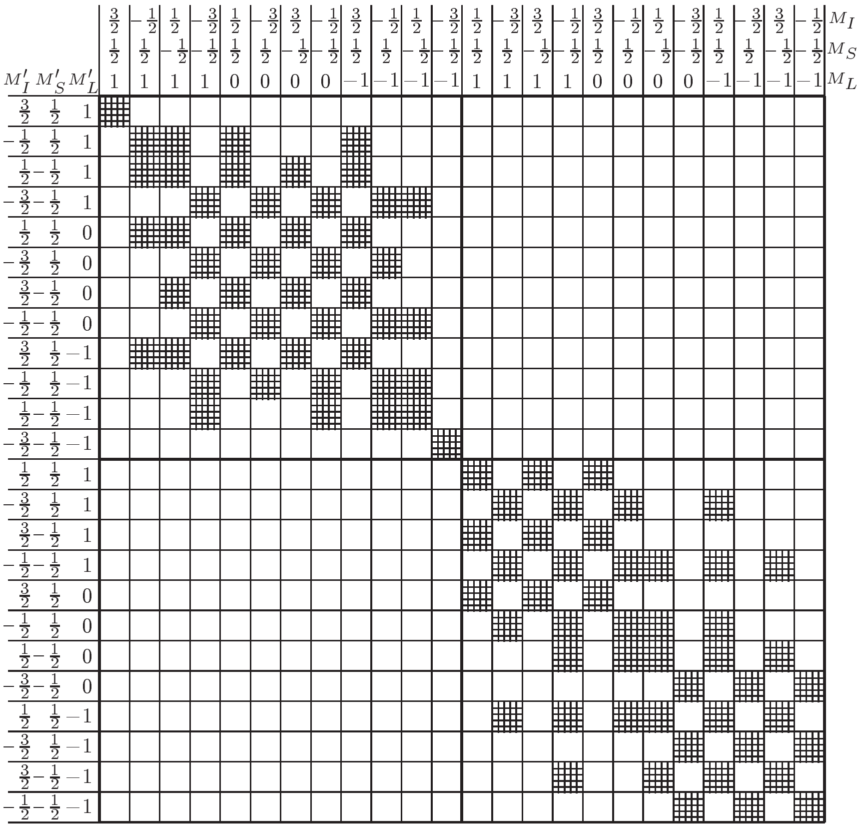

Figure 5.6: Matrix elements of the total hyperfine interaction $\langle \gamma_I \gamma_L I M_I S M_S L M_L | \hat{H}_{\text{hyp}} | \gamma_I \gamma_L I M_I' S M_S' L M_L' \rangle$ of the whole $2p\ ^2P$ level of ^{7}Li. M_I, M_S, M_L...magnetic quantum numbers of the nuclear spin, the electronic spin and the orbital angular momentum.

The following two Figs. 5.7 and 5.8 finally give the matrix structure of the operators of external fields.

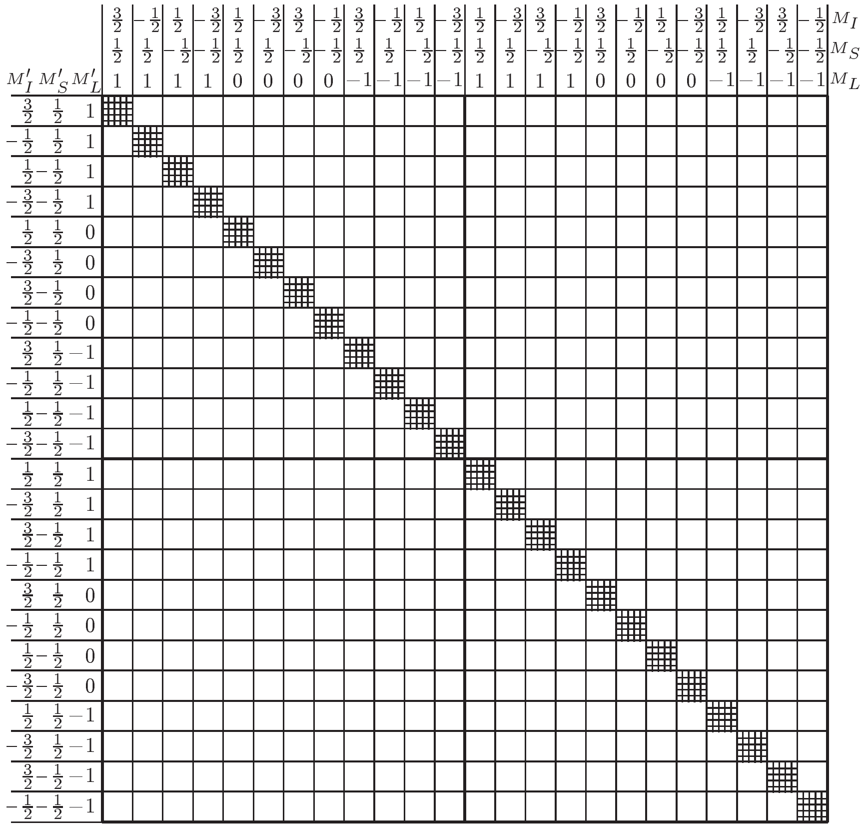

Figure 5.7: Matrix elements of the magnetic perturbation operator $\langle \gamma_I \gamma_L I M_I S M_S L M_L | \hat{H}_{\mathrm{mag}} | \gamma_I \gamma_L I M_I' S M_S' L M_L' \rangle$ of the whole $2p\ ^2P$ level of $^7\mathsf{Li}$ as given in eq. (5.21). M_I, M_S, M_L...magnetic quantum numbers of the nuclear spin, the electronic spin and the orbital angular momentum.

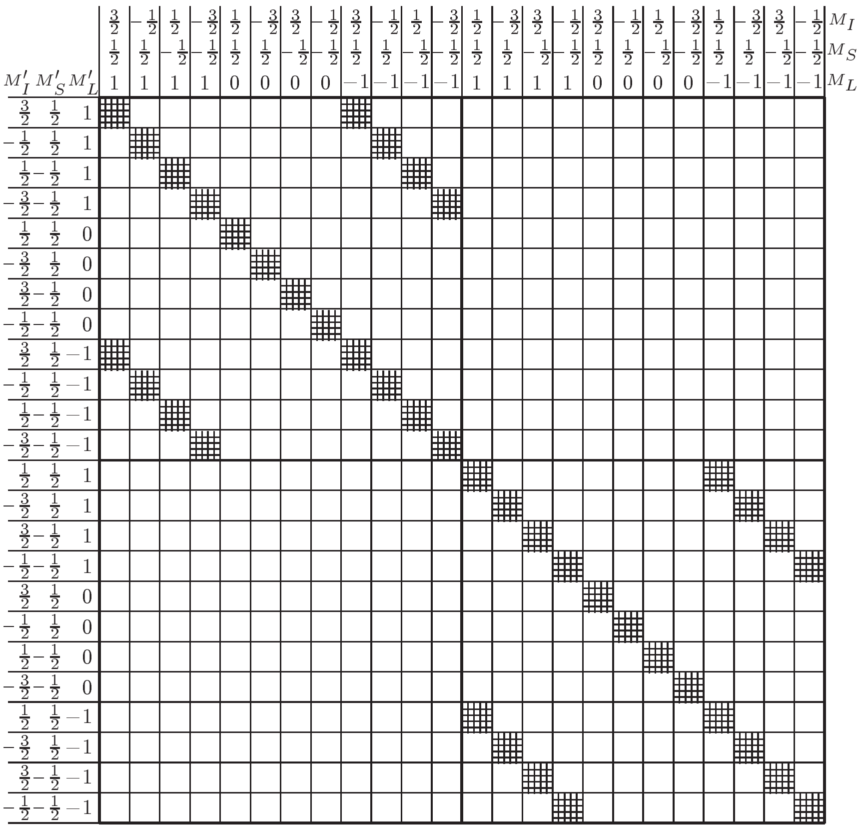

Figure 5.8: Matrix elements of electric perturbation operator $\langle \gamma_I \gamma_L I M_I S M_S L M_L | \hat{H}_{\text{el,eff}} | \gamma_I \gamma_L I M_I' S M_S' L M_L' \rangle$ of the whole $2p\ ^2P$ level of ^7Li as given in eqs. (5.24) and (5.25). M_I, M_S, M_L...magnetic quantum numbers of the nuclear spin, the electronic spin and the orbital angular momentum.

5.3 Comparison of Crossing Point Data

By diagonalizing the sum of all the perturbation operators

$$\hat{H}_{\text{fs}} + \hat{H}_{\text{hyp}} + \hat{H}_{\text{mag}} + \hat{H}_{\text{el,eff}} \tag{5.32}$$

the energy eigenvalues of the total Hamiltonian can be determined for the odd and the even subsystems separately. Since both subsystems have dimension 12 one obtains in the case of moderate field strengths 8 eigenvalues that can be assigned to the $2p\ ^2P_{\frac{3}{2}}$ fine structure level and 4 eigenvalues that can be assigned to the $2p\ ^2P_{\frac{1}{2}}$ fine structure level. The latter are of no interest in these considerations.

By use of the methods for the determination of crossing points, discussed in section 3.6, the energy eigenvalues, the magnetic and the electric field values of the crossing points can be recalculated in this extended formalism. All results for the crossing points of ^{7}Li are given in Tabs. 5.1 and 5.2.

Name	B / mT	E / kV/cm	ϵ / MHz	$(\mathbf{F}, \mathbf{M_F})$-$(\mathbf{F'}, \mathbf{M'_F})$
Bo1	0.2317	0	-0.41939	(2,-1)-(3,3)
Bo2	0.4160	0	4.73782	(2,1)-(3,3)
Bo3	0.6004	0	9.89598	(1,-1)-(3,3)
Bo4	0.7386	0	-6.87388	(2,-1)-(3,1)
Eo1	0	169.359	-446.716	(1,-1)-(2,1)
Eo2	0	235.024	-862.887	(1,-1)-(2,-1)
BEo	0.6746	290.452	-1320.262	(2,-1)-(2,1)

Table 5.1: Listing of crossing point data for the odd subsystem in ^{7}Li. All numerical values have been obtained by diagonalizing the sum of the perturbation operators given in eq. (5.32) within the whole $2p\ ^2P$ level.

Name	B / mT	E / kV/cm	ϵ / MHz	$(\mathbf{F}, \mathbf{M_F})$-$(\mathbf{F'}, \mathbf{M'_F})$
Be1	0.2143	0	6.95709	(1,0)-(2,2)
Be2	0.2935	0	-2.16845	(2,-2)-(3,2)
Be3	0.3636	0	-1.21886	(2,0)-(3,2)
BEe	0.7700	275.686	-1189.642	(2,2)-(2,0)

Table 5.2: Listing of crossing point data for the even subsystem in ^{7}Li. All numerical values have been obtained by diagonalizing the sum of the perturbation operators given in eq. (5.32) within the whole $2p\ ^2P$ level.

By comparing this data with the one given in Tabs. 3.3 and 3.4 of section 3.7, one recognizes that the influence of the $2p\ ^2P_{\frac{1}{2}}$ fine structure level on the crossing points of the $2p\ ^2P_{\frac{3}{2}}$ level consists above all of a shift towards lower electric and higher magnetic field values and higher energy values. The energy corrections don't exceed about 17 %, a value obtained for the **BEe**-crossing point. The influence on the location of crossing points increases for lower crossing point energies.

Chapter 6

On Certain Symmetries of the Zeeman and Stark Effect Operators

The main purpose of this last chapter is to work out the reasons for the different symmetries of Zeeman diagrams under a change of the direction of the magnetic field for the two subsystems of the $2p\,^2P_{\frac{3}{2}}$ fine structure level in $^6\mathsf{Li}$ and $^7\mathsf{Li}$, respectively. Section 6.1 is devoted only to this task. In section 6.2 an explanation for the identical Stark effects of the two subsystems in $^6\mathsf{Li}$ is given. Section 6.3 presents a justification for the restriction of the considerations on the energy surfaces on the first quadrant of the BE-plane in the case of $^6\mathsf{Li}$.

At first sight these issues don't seem to have much in common. Since their theoretical background, however, is quite the same (a certain symmetry or antisymmetry of the perturbation operators of the external fields), they are treated together in this chapter.

6.1 Symmetries of Zeeman Diagrams in the Subsystems of $^6\mathsf{Li}$ and $^7\mathsf{Li}$

All considerations of this chapter are performed in the $|\gamma_I \gamma_J I J M_I M_J\rangle$ basis (abbreviated by $|M_I M_J\rangle$ for simplicity). Since the observed effects don't depend on the representation in which the calculations are performed, this is a matter of choice.

Figs. 6.1 and 6.2 on the following two pages demonstrate the differences in the Zeeman diagrams of ^{6}Li and ^{7}Li: whereas all three diagrams of ^{7}Li are symmetric with respect to a magnetic field reversal, in ^{6}Li only the diagram for the total $2p\ ^2P_{\frac{3}{2}}$ fine structure level has this property. The symmetric Zeeman effect of the total $2p\ ^2P_{\frac{3}{2}}$ fine structure level is simply a consequence of ordinary rotational invariance.

6.1.1 Symmetries of the Perturbation Operators

The explanations of the different behavior stated above are based on the symmetries of the matrix elements of the perturbation operators with respect to the following simultaneous changes in the signs of the magnetic quantum numbers M_I and M_J characterizing the bras and kets:

$$\begin{aligned} \langle M_I M_J| &\longrightarrow \langle -M_I - M_J| \\ |M_I M_J\rangle &\longrightarrow |-M_I - M_J\rangle. \end{aligned} \tag{6.1}$$

The corresponding relation for the matrix elements of the hyperfine perturbation operator is:

$$\begin{aligned} \langle \gamma_I \gamma_J I J (-M_I)(-M_J)|\hat{H}_{\text{hyp}}|\gamma_I \gamma_J I J (-M_I')(-M_J')\rangle &= \\ = \langle \gamma_I \gamma_J I J M_I M_J|\hat{H}_{\text{hyp}}|\gamma_I \gamma_J I J M_I' M_J'\rangle \end{aligned} \tag{6.2}$$

The somewhat lengthy manipulations to obtain this result are presented in detail in App. A. For the magnetic perturbation operator given in eq. (2.19) the calculations are straightforward:

$$\begin{aligned} \langle \gamma_I \gamma_J I J (-M_I)(-M_J)|\hat{H}_{\text{mag}}|\gamma_I \gamma_J I J (-M_I')(-M_J')\rangle &= \\ = [g_J(-M_J) - \hat{g}_I(-M_I)]\,\mu_B B_z \cdot \delta_{(-M_I)(-M_I')}\delta_{(-M_J)(-M_J')} &= \\ = -\left(g_J M_J - \hat{g}_I M_I\right)\mu_B B_z \delta_{M_I M_I'}\delta_{M_J M_J'} &= \\ = -\langle \gamma_I \gamma_J I J M_I M_J|\hat{H}_{\text{mag}}|\gamma_I \gamma_J I J M_I' M_J'\rangle. \end{aligned} \tag{6.3}$$

For the effective electric operator one obtains

$$\begin{aligned} \langle \gamma_I \gamma_J I J (-M_I)(-M_J)|\hat{H}_{\text{el,eff}}|\gamma_I \gamma_J I J (-M_I')(-M_J')\rangle &= \\ = \langle \gamma_I \gamma_J I J M_I M_J|\hat{H}_{\text{el,eff}}|\gamma_I \gamma_J I J M_I' M_J'\rangle. \end{aligned} \tag{6.4}$$

This result can easily be verified form eqs. (2.37) and (2.38) if $E_y = E_z = 0$. From symmetry considerations it should apply as long as just $E_z = 0$, but checking this was omitted. The matrix elements of the hyperfine and the

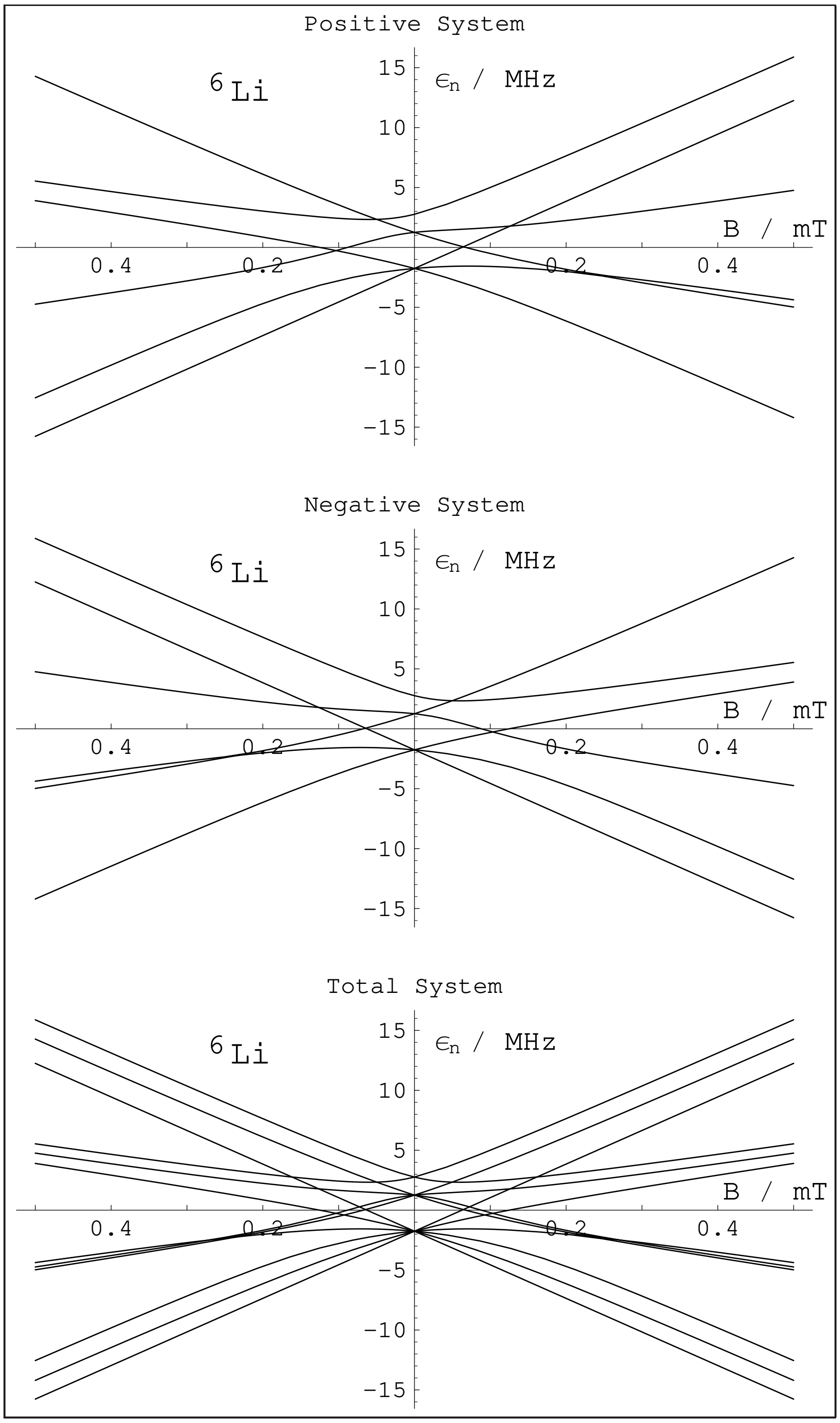

Figure 6.1: Splitting of energy levels of the $2p\ ^2P_{\frac{3}{2}}$ fine structure levels due to the Zeeman effect in ^{6}Li for the total system of levels and the positive and negative subsystems separately. Only the diagram showing the splitting of the total level is symmetric with respect to the energy axis (i.e. a magnetic field reversal).

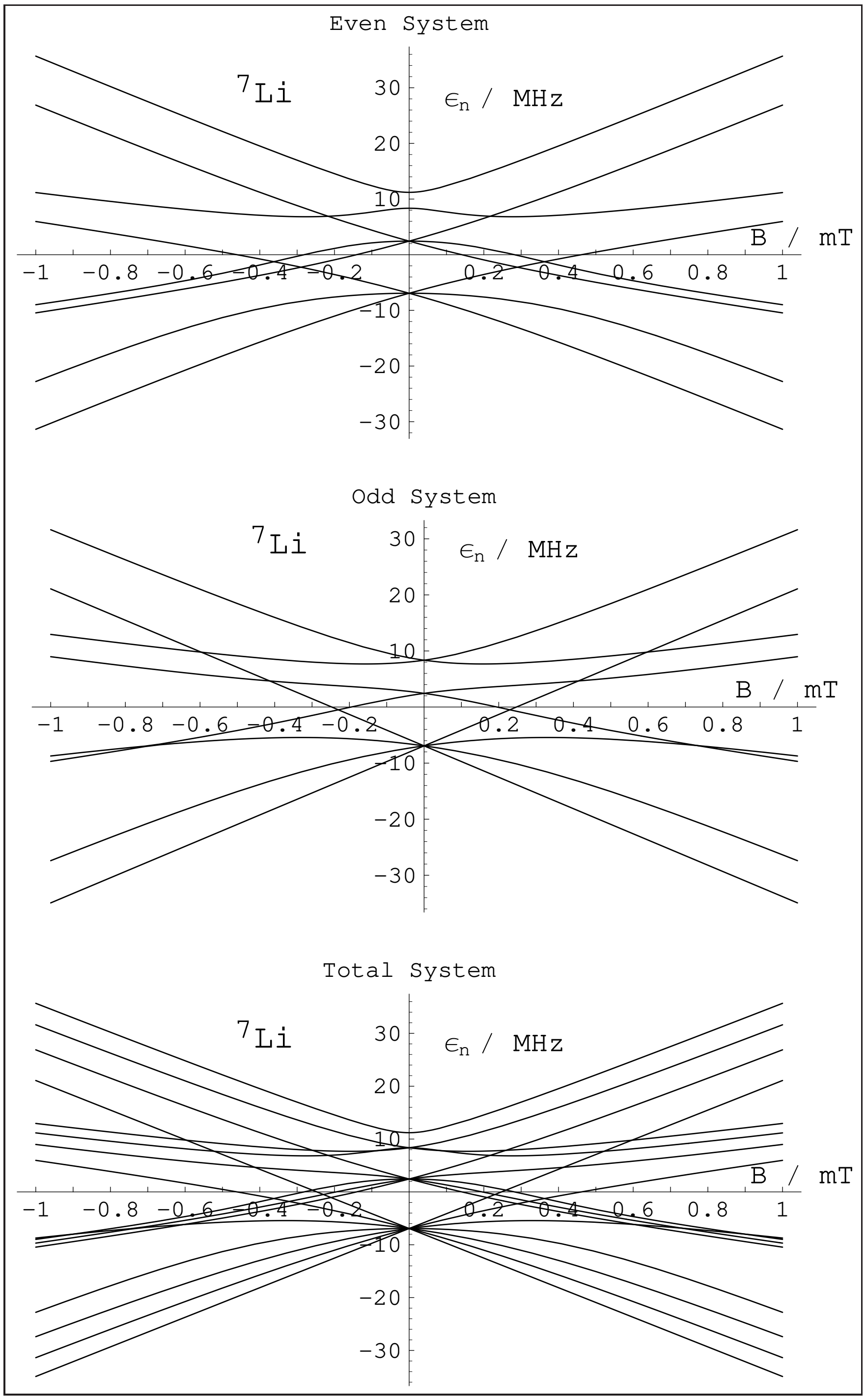

Figure 6.2: Splitting of energy levels of the $2p\,^2P_{\frac{3}{2}}$ fine structure levels due to the Zeeman effect in ^{7}Li for the total system of levels and the odd and even subsystems separately. All three diagrams are symmetric with respect to the energy axis (i.e. a magnetic field reversal).

Stark operators are therefore independent of the operation (6.1), those of the Zeeman operator change in sign. This particular fact is responsible for the symmetry and the antisymmetry of the Zeeman diagrams and the equality of the Stark diagrams of the two subsystems in ^{6}Li. Furthermore, it justifies the restriction of the considerations on the energy surfaces in ^{6}Li to positive field values.

6.1.2 Comparison between ^{6}Li and ^{7}Li

Tab. 6.1 contains a comparison between the properties of the $2p\ ^2P_{\frac{3}{2}}$ fine structure level in ^{6}Li and ^{7}Li. Quantum numbers are shown as well as bases of the state space and of the corresponding subspaces (positive and negative subspaces for ^{6}Li; odd and even subspaces for ^{7}Li). The basis vectors $|\gamma_I \gamma_J I J F M_F\rangle$ are abbreviated by $|FM_F\rangle$ in the table. One significant dif-

	^{6}Li		**^{7}Li**	
I	1		$\frac{3}{2}$	
J	$\frac{3}{2}$		$\frac{3}{2}$	
F	$\frac{5}{2};\ \frac{3}{2};\ \frac{1}{2}$		3;2;1;0	
	Coupling $\Longleftrightarrow$ $\Delta M_F = \text{even}$ $\Rightarrow$ Separation into two subsystems			
	Positive System	Negative System	Odd System	Even System
	$M_F = \frac{5}{2}, \frac{1}{2}, -\frac{3}{2}$	$M_F = \frac{3}{2}, -\frac{1}{2}, -\frac{5}{2}$	$M_F = 3, 1, -1, -3$	$M_F = 2, 0, -2$
$\|FM_F\rangle$	$\|\frac{5}{2},\frac{5}{2}\rangle;\|\frac{5}{2},\frac{1}{2}\rangle;\|\frac{5}{2},-\frac{3}{2}\rangle;$ $\|\frac{3}{2},\frac{1}{2}\rangle;\|\frac{3}{2},-\frac{3}{2}\rangle;\|\frac{1}{2},\frac{1}{2}\rangle;$	$\|\frac{5}{2},\frac{3}{2}\rangle;\|\frac{5}{2},-\frac{1}{2}\rangle;\|\frac{5}{2},-\frac{5}{2}\rangle;$ $\|\frac{3}{2},\frac{3}{2}\rangle;\|\frac{3}{2},-\frac{1}{2}\rangle;\|\frac{1}{2},-\frac{1}{2}\rangle;$	$\|3,3\rangle;\|3,1\rangle;\|3,-1\rangle;\|3,-3\rangle;$ $\|2,1\rangle;\|2,-1\rangle;\|1,1\rangle;\|1,-1\rangle;$	$\|3,2\rangle;\|3,0\rangle;\|3,-2\rangle;\|2,2\rangle;$ $\|2,0\rangle;\|2,-2\rangle;\|1,0\rangle;\|00\rangle;$

Table 6.1: Comparison between the properties of the separation into two subsystems of the $2p\ ^2P_{\frac{3}{2}}$ level in ^{6}Li and ^{7}Li.

ference between the two isotopes comes out clearly: the two state vectors $|FM_F\rangle$ and $|F - M_F\rangle$ always belong to different subsystems in the case of ^{6}Li whereas they always belong to the same subsystem in the case of ^{7}Li. This fact has already been stated in section 2.3 (see eq. (2.46)).

6.1.3 The Reflection Operator $\hat{S}$

The operator $\hat{S}$ is defined within the space $2p\ ^2P_{\frac{3}{2}}$ (for ^{6}Li and ^{7}Li) by its action on the basis states $|M_I M_J\rangle$. Considerations similar to the following can also be performed in the case of ^{7}Li with the operators $\hat{S}^{\mathrm{o}}$ and $\hat{S}^{\mathrm{e}}$ defined in the odd and even subsystems of the $2p\ ^2P_{\frac{3}{2}}$ fine structure level, respectively. The definition of $\hat{S}$ is:

$$\hat{S}\,|M_I M_J\rangle := |-M_I - M_J\rangle. \tag{6.5}$$

By acting with $\hat{S}$ on both sides of eq. (6.5) one obtains:

$$\hat{S}^2\,|M_I M_J\rangle = |M_I M_J\rangle. \tag{6.6}$$

Therefore, $\hat{S}^2$ is the identity operator, i.e. $\hat{S}$ equals its inverse $\hat{S}^{-1}$:

$$\hat{S}^2 = \hat{\mathbb{1}} \quad \text{or} \quad \hat{S} = \hat{S}^{-1}. \tag{6.7}$$

Considering the matrix elements of the $\hat{S}$ operator (in the $|M_I M_J\rangle$ basis)

$$\begin{aligned}\langle M_I' M_J'|\hat{S}|\ M_I M_J\rangle &= \langle M_I' M_J'| - M_I - M_J\rangle = \delta_{M_I' - M_I} \cdot \delta_{M_J' - M_J} = \\ &= \delta_{-M_I' M_I} \cdot \delta_{-M_J' M_J} = \langle -M_I' - M_J'|M_I M_J\rangle \end{aligned} \tag{6.8}$$

leads to

$$\langle M_I' M_J'|\hat{S}\cdot = \langle -M_I' - M_J'|\cdot \quad . \tag{6.9}$$

Comparing this to the Hermitian conjugate of eq. (6.5) and taking into account that the kets $|M_I M_J\rangle$ form a complete basis of the state space, gives

$$\hat{S} = \hat{S}^{\dagger}. \tag{6.10}$$

The $\hat{S}$ operator is therefore unitary.

In the following, the two expressions $\hat{H}_{\mathrm{mag}}\,\hat{S}$ and $\hat{S}\,\hat{H}_{\mathrm{mag}}$ are evaluated, where $\hat{H}_{\mathrm{mag}}$ is used in the form (2.19).

$$\begin{aligned}\hat{H}_{\mathrm{mag}}\,\hat{S}|M_I M_J\rangle &= \hat{H}_{\mathrm{mag}}\,| - M_I - M_J\rangle = \\ &= -\mu_B B_z\,(g_J M_J - \hat{g}_I M_I)\,| - M_I - M_J\rangle \end{aligned} \tag{6.11}$$

$$\begin{aligned}\hat{S}\,\hat{H}_{\mathrm{mag}}|M_I M_J\rangle &= \mu_B B_z\,(g_J M_J - \hat{g}_I M_I)\,\hat{S}|M_I M_J\rangle = \\ &= \mu_B B_z\,(g_J M_J - \hat{g}_I M_I)\,| - M_I - M_J\rangle \end{aligned} \tag{6.12}$$

The two expressions above differ only in sign, the two operators therefore anticommute:

$$\left\{\hat{H}_{\text{mag}},\, \hat{S}\right\} = 0 \quad \text{or} \quad \hat{H}_{\text{mag}} = -\hat{S}\,\hat{H}_{\text{mag}}\,\hat{S}. \tag{6.13}$$

This is used to establish a certain relation for the matrix elements of the sum of the hyperfine operator and the Zeeman operator $\hat{H}_{\text{hyp}} + \hat{H}_{\text{mag}}$:

$$\begin{aligned} &\langle M_I M_J|\hat{H}_{\text{hyp}} + \hat{H}_{\text{mag}}(+B_z)|M_I' M_J'\rangle = \\ &\langle M_I M_J|\hat{H}_{\text{hyp}}|M_I' M_J'\rangle + \langle M_I M_J|\hat{H}_{\text{mag}}(+B_z)|M_I' M_J'\rangle. \end{aligned} \tag{6.14}$$

- For the elements of $\hat{H}_{\text{hyp}}$ one obtains

$$\begin{aligned} \langle M_I M_J|\hat{H}_{\text{hyp}}|M_I' M_J'\rangle &= \langle -M_I - M_J|\hat{H}_{\text{hyp}}| - M_I' - M_J'\rangle = \\ &= \langle M_I M_J|\hat{S}\,\hat{H}_{\text{hyp}}\,\hat{S}|M_I' M_J'\rangle \end{aligned} \tag{6.15}$$

  by taking (6.2) and the definition of the unitary operator $\hat{S}$ into account.

- For the elements of $\hat{H}_{\text{mag}}$ consecutive use of eq. (6.13) and of the identity

$$\hat{H}_{\text{mag}}(+B_z) = -\hat{H}_{\text{mag}}(-B_z) \tag{6.16}$$

  gives

$$\begin{aligned} \langle M_I M_J|\hat{H}_{\text{mag}}(+B_z)|M_I' M_J'\rangle &= -\langle M_I M_J|\hat{S}\,\hat{H}_{\text{mag}}(+B_z)\,\hat{S}|M_I' M_J'\rangle = \\ &= \langle M_I M_J|\hat{S}\,\hat{H}_{\text{mag}}(-B_z)\,\hat{S}|M_I' M_J'\rangle. \end{aligned} \tag{6.17}$$

The combination of these two formulae leads to

$$\begin{aligned} &\langle M_I M_J|\hat{H}_{\text{hyp}} + \hat{H}_{\text{mag}}(+B_z)|M_I' M_J'\rangle = \\ &= \langle M_I M_J|\hat{S}\left[\hat{H}_{\text{hyp}} + \hat{H}_{\text{mag}}(-B_z)\right]\hat{S}|M_I' M_J'\rangle \end{aligned} \tag{6.18}$$

and since $|M_I M_J\rangle$ constitutes a basis

$$\hat{H}_{\text{hyp}} + \hat{H}_{\text{mag}}(+B_z) = \hat{S}\left[\hat{H}_{\text{hyp}} + \hat{H}_{\text{mag}}(-B_z)\right]\hat{S}. \tag{6.19}$$

Since $\hat{S}$ is unitary, the operators $\hat{H}_{\text{hyp}} + \hat{H}_{\text{mag}}(+B_z)$ and $\hat{H}_{\text{hyp}} + \hat{H}_{\text{mag}}(-B_z)$ have the same energy eigenvalues for a given value of B_z. This guarantees a symmetric Zeeman diagram.

6.1.4 Explanation for the Differences in Symmetry

A prerequisite for the validity of the line of reasoning presented in the preceding subsections is the possibility of the definition of the operator $\hat{S}$, whose action has to be closed with respect to the space it is defined on. Therefore, the existence of an operator $\hat{S}$ guarantees a symmetric Zeeman diagram.

In the total space $2p\ ^2P_{\frac{3}{2}}$ the definition of the operator $\hat{S}$ is possible for both isotopes. Therefore, the Zeeman diagrams of the total $2p\ ^2P_{\frac{3}{2}}$ fine structure level possess the mentioned symmetry.

1. ^{7}*Li* In this case it is possible to define operators $\hat{S}^{\mathrm{o}}$ and $\hat{S}^{\mathrm{e}}$, acting in the odd and even subspaces, respectively.

   (a) *odd system:* $M_F = M_I + M_J = \text{odd}$

   $$\hat{S}^{\mathrm{o}}\,|M_I M_J\rangle = |-M_I - M_J\rangle \tag{6.20}$$

   (b) *even system:* $M_F = M_I + M_J = \text{even}$

   $$\hat{S}^{\mathrm{e}}\,|M_I M_J\rangle = |-M_I - M_J\rangle \tag{6.21}$$

   The action of the operator $\hat{S}^{\mathrm{o}}$ ($\hat{S}^{\mathrm{e}}$) on a vector with $M_F = M_I + M_J =$ odd (even) leads to a vector belonging to the odd (even) subsystem (since $M'_F = -M_I - M_J$ is odd (even) too). They map the subsystems onto themselves. Therefore, the Zeeman diagrams of the odd and even subsystems in ^{7}Li (as well as those of ^{23}Na, ^{69}Ga and ^{71}Ga) are symmetric with respect to a change of the direction of the magnetic field.

2. ^{6}*Li* Here, a definition of the operator $\hat{S}$ via

   $$\hat{S}|M_I M_J\rangle = |-M_I - M_J\rangle \tag{6.22}$$

   fails, since in this case the action of the operator $\hat{S}$ on a basis vector $|M_I M_J\rangle$ belonging to the positive subsystem ($M_F = M_I + M_J \equiv 1(4)$) gives a basis vector belonging to the negative subsystem and vice versa since

   $$M'_F = -M_I - M_J = -M_F \equiv -1(4). \tag{6.23}$$

   The line of reasoning presented in the former subsections is not applicable for the two subsystems of ^{6}Li and therefore it is impossible to deduce the symmetry of the corresponding Zeeman diagrams.

6.2 Stark Effect Symmetries in ^{6}Li

The Stark diagrams of the two subsystems in ^{6}Li (positive and negative subsystem) are identical (comp. Fig. 4.9 and 4.10 in section 4.4). This fact can easily be explained with the help of the relations for the matrix elements of the hyperfine structure operator and the effective electric perturbation operator given in section 6.1.1. Combining eqs. (6.2) and (6.4) gives

$$\begin{aligned} &\langle -M_I - M_J | \hat{H}_{\text{hyp}} + \hat{H}_{\text{el,eff}} | -M_I' - M_J' \rangle = \\ &\quad = \langle M_I M_J | \hat{H}_{\text{hyp}} + \hat{H}_{\text{el,eff}} | M_I' M_J' \rangle. \end{aligned} \tag{6.24}$$

Because of the fact that $|M_I M_J\rangle$ and $|-M_I - M_J\rangle$ belong to different subsystems, the last equation suggests the possibility of identical matrix representations of the perturbation operators within the two subsystems assuming an appropriate ordering of the basis states. For this reason, the energy eigenvalues of the operator $\hat{H}_{\text{hyp}} + \hat{H}_{\text{el,eff}}$ corresponding to a given electric field strength E are the same in the positive and the negative subsystem of ^{6}Li.

6.3 Symmetries of the Energy Surfaces in ^{6}Li

The investigations on the energy surfaces of the two sublevels of ^{6}Li were limited to the first quadrant of the BE-plane of field parameters. This section clarifies why this is possible.

Once more the symmetries of the matrix elements of the perturbation operators given in eqs. (6.2)-(6.4) can be used. Combining these three equations and taking relation (6.16) into account leads to

$$\begin{aligned} &\langle -M_I - M_J | \hat{H}_{\text{hyp}} + \hat{H}_{\text{mag}}(+B_z) + \hat{H}_{\text{el,eff}} | -M_I' - M_J' \rangle = \\ &\quad = \langle M_I M_J | \hat{H}_{\text{hyp}} + \hat{H}_{\text{mag}}(-B_z) + \hat{H}_{\text{el,eff}} | M_I' M_J' \rangle. \end{aligned} \tag{6.25}$$

Now the line of arguing is identical to the one given in the preceding section. Because of the fact that $|M_I M_J\rangle$ and $|-M_I - M_J\rangle$ always belong to different subsystems in ^{6}Li, it is possible to obtain identical matrix representations of the total perturbation within the two subsystems, again assuming an appropriate ordering of the basis states. Therefore, the structure of the energy surfaces of the positive subsystem in ^{6}Li for positive magnetic field values equals the structure of the energy surfaces of the negative subsystem for negative magnetic field values and vice versa, i.e. all crossing points of the total $2p\ ^2P_{\frac{3}{2}}$ fine structure level in ^{6}Li have to appear (anti-) symmetrically (with respect to the magnetic field values) within the two subsystems.

Chapter 7

Conclusions

In this diploma thesis it has been shown, that for both isotopes of lithium ($^6\mathsf{Li}$ and $^7\mathsf{Li}$), the theory predicts an adiabatic hyperfine level transfer within the $2p\ ^2P_{\frac{3}{2}}$ fine structure level for perpendicular electric and magnetic fields. For this special field geometry a symmetry remains, which entails the selection rule $\Delta M_F =$ even for the elements of the perturbation matrix, comprising the hyperfine, the magnetic and the electric interactions, within the basis of common eigenvectors of the operators $\hat{\vec{F}}^2$ and $\hat{F}_z$. Therefore, these matrices as well as the system of energy levels separate into two subsystems. These are the odd and the even subsystem for $^7\mathsf{Li}$ (as for $^{23}\mathsf{Na}$, $^{69}\mathsf{Ga}$ and $^{71}\mathsf{Ga}$); all aforementioned atoms have nuclear spin $I = \frac{3}{2}$. For $^6\mathsf{Li}$ ($I = 1$), the two subsystems are called the positive subsystem with

$$M_F = \left\{\frac{5}{2}, \frac{1}{2}, -\frac{3}{2}\right\} \tag{7.1}$$

and the negative subsystem with

$$M_F = \left\{\frac{3}{2}, -\frac{1}{2}, -\frac{5}{2}\right\}. \tag{7.2}$$

Diagrams of the energy surfaces $\epsilon\,(E, B)$ are given for both isotopes.

Within the odd and the even subsystems of $^7\mathsf{Li}$ ($I = \frac{3}{2}$) there exist the same number of crossing points as in the corresponding subsystems of Na with similar relative locations; 7 in the case of the odd subsystem, 4 in the case of the even subsystem. Their field values and energy eigenvalues, however, are smaller than those of Na or Ga, since both, the effects of fine- and hyperfine structure are less significant for lithium.

For $^6\mathsf{Li}$ ($I = 1$), the two subsystems (positive and negative subsystem) have identical electric and magnetic splitting properties for opposite magnetic field strengths. To each of the 7 crossing points of the positive subsystem, there corresponds exactly one crossing point of the negative subsystem. This high similarity between the two subsystems in ^{6}Li was traced back to its origin, a certain symmetry inherent to the perturbation (hyperfine, Stark and Zeeman interactions). The same symmetry properties are also responsible for the symmetries and the antisymmetries of the Zeeman splitting diagrams (with respect to a magnetic field reversal) of the subsystems in ^{7}Li and ^{6}Li, respectively.

By using the method of the resultant, analytic expressions for the field values and the energy eigenvalues of the crossing points **Bp3**, **Bn3**, **Bp4** and **Bn4** in ^{6}Li were obtained. These expressions contain only the atomic constants for the $2p\ ^2P_{\frac{3}{2}}$ fine structure level of the particular atom (with $I = 1$) under study.

Finally, the occurrence of Berry phases accompanying closed adiabatic field cycles was demonstrated for all **BE**-crossing points and for the electric crossing points **Ep1**, **En1** (in ^{6}Li) and **Eo2** (in the odd subsystem of ^{7}Li).

Appendix A

Proof of Symmetry Relations

A.1 Verification of Eq. (6.2)

In order to establish relation (6.2), eq. (2.16) is used at first:

$$\begin{aligned}
&\langle\gamma_I\gamma_J IJ(-M_I)(-M_J)|\hat{H}_{\text{hyp}}|\gamma_I\gamma_J IJ(-M_I')(-M_J')\rangle = \\
&= ha(J)(-1)^{-(M_J-M_J')}(-1)^{J+I-(-M_J-M_I)}\sqrt{(2J+1)(J+1)J(2I+1)(I+1)I}\cdot \\
&\cdot\begin{pmatrix} J & 1 & J \\ M_J & -(M_J-M_J') & -M_J' \end{pmatrix}\begin{pmatrix} I & 1 & I \\ M_I & -(M_J'-M_J) & -M_I' \end{pmatrix}+ \\
&+ hb(J)(-1)^{-(M_J-M_J')}(-1)^{J+I-(-M_J-M_I)}\frac{\sqrt{(2J+3)(J+1)(2J+1)J(2J-1)(2I+3)(I+1)(2I+1)I(2I-1)}}{4IJ(2I-1)(2J-1)}\cdot \\
&\cdot\begin{pmatrix} J & 2 & J \\ M_J & -(M_J-M_J') & -M_J' \end{pmatrix}\begin{pmatrix} I & 2 & I \\ M_I & -(M_J'-M_J) & -M_I' \end{pmatrix}.
\end{aligned} \tag{A.1}$$

With the help of the symmetry relation for the 3j-Symbols (see. [6], eq. (3.7.6))

$$\begin{pmatrix} j_1 & j_2 & j_3 \\ m_1 & m_2 & m_3 \end{pmatrix} = (-1)^{j_1+j_2+j_3}\begin{pmatrix} j_1 & j_2 & j_3 \\ -m_1 & -m_2 & -m_3 \end{pmatrix} \tag{A.2}$$

one finds by rearranging terms in order to use eq. (2.16) again

$$\begin{aligned}
&\langle\gamma_I\gamma_J IJ(-M_I)(-M_J)|\hat{H}_{\text{hyp}}|\gamma_I\gamma_J IJ(-M_I')(-M_J')\rangle = \qquad (A.3)\\
&= ha(J)(-1)^{-(M_J-M_J')}(-1)^{J+I-(-M_J-M_I)}\sqrt{(2J+1)(J+1)J(2I+1)(I+1)I}\cdot \\
&\cdot(-1)^{2J+1}\begin{pmatrix} J & 1 & J \\ -M_J & M_J-M_J' & M_J' \end{pmatrix}(-1)^{2I+1}\begin{pmatrix} I & 1 & I \\ -M_I & M_J'-M_J & M_I' \end{pmatrix}+ \\
&+hb(J)(-1)^{-(M_J-M_J')}(-1)^{J+I-(-M_J-M_I)}\frac{\sqrt{(2J+3)(J+1)(2J+1)J(2J-1)(2I+3)(I+1)(2I+1)I(2I-1)}}{4IJ(2I-1)(2J-1)}\cdot
\end{aligned}$$

$$
\cdot(-1)^{2J+2}\begin{pmatrix} J & 2 & J \\ -M_J & M_J-M'_J & M'_J \end{pmatrix}(-1)^{2I+2}\begin{pmatrix} I & 2 & I \\ -M_I & M'_J-M_J & M'_I \end{pmatrix}=
$$

$$
\begin{aligned}
&= ha(J)(-1)^{M_J-M'_J}(-1)^{J+I-M_J-M_I}\sqrt{(2J+1)(J+1)J(2I+1)(I+1)I}\cdot \\
&\quad\cdot(-1)^{2(I+J)}(-1)^{-2(M_J-M'_J)}(-1)^{2(M_J+M_I)}\cdot \\
&\quad\cdot\begin{pmatrix} J & 1 & J \\ -M_J & M_J-M'_J & M'_J \end{pmatrix}\begin{pmatrix} I & 1 & I \\ -M_I & M'_J-M_J & M'_I \end{pmatrix}+ \\
&+hb(J)(-1)^{M_J-M'_J}(-1)^{J+I-M_J-M_I}\frac{\sqrt{(2J+3)(J+1)(2J+1)J(2J-1)(2I+3)(I+1)(2I+1)I(2I-1)}}{4IJ(2I-1)(2J-1)}\cdot \\
&\quad\cdot(-1)^{2(I+J)}(-1)^{-2(M_J-M'_J)}(-1)^{2(M_J+M_I)}\cdot \\
&\quad\cdot\begin{pmatrix} J & 2 & J \\ -M_J & M_J-M'_J & M'_J \end{pmatrix}\begin{pmatrix} I & 2 & I \\ -M_I & M'_J-M_J & M'_I \end{pmatrix}= \\
&= (-1)^{2(I+J)}(-1)^{-2(M_J-M'_J)}(-1)^{2(M_J+M_I)}\langle\gamma_I\gamma_J IJM_IM_J|\hat{H}_{\text{hyp}}|\gamma_I\gamma_J IJM'_IM'_J\rangle = \\
&= \underbrace{(-1)^{2(I+M_I)}}_{=1}\cdot\underbrace{(-1)^{2(J+M'_J)}}_{=1}\langle\gamma_I\gamma_J IJM_IM_J|\hat{H}_{\text{hyp}}|\gamma_I\gamma_J IJM'_IM'_J\rangle
\end{aligned}
$$

The factors involving the powers of (-1) are both equal to $+1$ because $I+M_I$ and $J+M'_J$ are integers in any case. This proves

$$
\begin{aligned}
\langle\gamma_I\gamma_J IJ(-M_I)(-M_J)|\hat{H}_{\text{hyp}}|\gamma_I\gamma_J IJ(-M'_I)(-M'_J)\rangle &= \\
= \langle\gamma_I\gamma_J IJM_IM_J|\hat{H}_{\text{hyp}}|\gamma_I\gamma_J IJM'_IM'_J\rangle & \qquad \text{(A.4)}
\end{aligned}
$$

which is (6.2) of section 6.1.1.

A.2 Verification of Eq. (6.4)

In establishing relation (6.4), eq. (2.37) immediately leads to

$$
\begin{aligned}
&\langle\gamma_I\gamma_J IJ(-M_I)(-M_J)|\hat{H}_{\text{el,eff}}|\gamma_I\gamma_J IJ(-M'_I)(-M'_J)\rangle = \\
&= -\tfrac{1}{2}\alpha_0E^2\delta_{(-M_I)(-M'_I)}\delta_{(-M_J)(-M'_J)}-\tfrac{1}{2}\alpha_2E^2Q_{(-M_I)(-M_J),(-M'_I)(-M'_J)} = \\
&= -\tfrac{1}{2}\alpha_0E^2\delta_{M_IM'_I}\delta_{M_JM'_J}-\tfrac{1}{2}\alpha_2E^2Q_{(-M_I)(-M_J),(-M'_I)(-M'_J)}. \qquad \text{(A.5)}
\end{aligned}
$$

It is therefore sufficient to study the symmetry of the factor $Q_{M_IM_J,M'_IM'_J}$ given explicitly in eq. (2.38).

$$
\begin{aligned}
&Q_{(-M_I)(-M_J),(-M'_I)(-M'_J)} = \\
&\quad = \sqrt{\frac{15}{2}}\sqrt{\frac{(J+1)(2J+1)(2J+3)}{J(2J-1)}}\delta_{(-M_I)(-M'_I)}(-1)^{J+M_J}\,.
\end{aligned}
$$

$$
\begin{aligned}
&\cdot \sum_{q=-2}^{2} \begin{pmatrix} J & 2 & J \\ M_J & q & -M_J' \end{pmatrix} \sum_{\mu=-1}^{1} \sum_{\mu'=-1}^{1} \begin{pmatrix} 1 & 2 & 1 \\ \mu & q & \mu' \end{pmatrix} n_\mu n_{\mu'} = \\
= \;& \sqrt{\frac{15}{2}} \sqrt{\frac{(J+1)(2J+1)(2J+3)}{J(2J-1)}} \delta_{M_I M_I'} (-1)^{J-M_J} \cdot (-1)^{2M_J} \cdot \\
&\cdot \sum_{q=-2}^{2} (-1)^{2J+2} \begin{pmatrix} J & 2 & J \\ -M_J & -q & M_J' \end{pmatrix} \cdot \\
&\cdot \sum_{\mu=-1}^{1} \sum_{\mu'=-1}^{1} (-1)^{1+2+1} \begin{pmatrix} 1 & 2 & 1 \\ -\mu & -q & -\mu' \end{pmatrix} n_\mu n_{\mu'} \qquad \text{(A.6)}
\end{aligned}
$$

In the last line once more eq. (A.2) has been used. In order to find again the expression given in eq. (2.38) it is appropriate to substitute the summation indices q, μ and μ' by $-\tilde{q}$, $-\tilde{\mu}$ and $-\tilde{\mu'}$, respectively and simultaneously using the old names according to

$$
\begin{array}{rclcrcl}
\tilde{q} & := & -q & \qquad & \tilde{q} & \to & q \\
\tilde{\mu} & := & -\mu & & \tilde{\mu} & \to & \mu \\
\tilde{\mu'} & := & -\mu' & & \tilde{\mu'} & \to & \mu',
\end{array} \qquad \text{(A.7)}
$$

which gives

$$
\begin{aligned}
&Q_{(-M_I)(-M_J),(-M_I')(-M_J')} = \qquad \text{(A.8)} \\
= \;& (-1)^{2(J+M_J)} \sqrt{\frac{15}{2}} \sqrt{\frac{(J+1)(2J+1)(2J+3)}{J(2J-1)}} \delta_{M_I M_I'} (-1)^{J-M_J} \cdot \\
&\cdot \sum_{q=-2}^{2} \begin{pmatrix} J & 2 & J \\ -M_J & q & M_J' \end{pmatrix} \sum_{\mu=-1}^{1} \sum_{\mu'=-1}^{1} \begin{pmatrix} 1 & 2 & 1 \\ \mu & q & \mu' \end{pmatrix} n_{-\mu} n_{-\mu'}.
\end{aligned}
$$

Since in this particular case $E_y = E_z = 0$ one obtains by using the definition of n_μ (see eq. (2.36)) the following relations:

$$
\begin{aligned}
n_{-\mu} &= -n_\mu \\
n_{-\mu} n_{-\mu'} &= n_\mu n_{\mu'}.
\end{aligned} \qquad \text{(A.9)}
$$

Using eq. (2.38) now yields the desired symmetry relation for the factor $Q_{M_I M_J, M_I' M_J'}$:

$$
Q_{(-M_I)(-M_J),(-M_I')(-M_J')} = \underbrace{(-1)^{2(J+M_J)}}_{=1} Q_{M_I M_J, M_I' M_J'} = Q_{M_I M_J, M_I' M_J'}. \qquad \text{(A.10)}
$$

This, together with eq. (A.5) completes the proof of relation (6.4) of section 6.1.1:

$$
\begin{aligned}
&\langle \gamma_I \gamma_J I J (-M_I)(-M_J) | \hat{H}_{\text{el,eff}} | \gamma_I \gamma_J I J (-M_I')(-M_J') \rangle = \\
&= \langle \gamma_I \gamma_J I J M_I M_J | \hat{H}_{\text{el,eff}} | \gamma_I \gamma_J I J M_I' M_J' \rangle.
\end{aligned} \qquad \text{(A.11)}
$$

Appendix B

Listing of Atomic Constants

All the atomic constants given in the following two tables have been used in the numerical calculations. Even though some of the experimental values below show considerable errors, one is forced to work under the assumption that these values were exact so that one can display crossings and related phenomena, which occur in a very narrow range of the parameters. In reality, these phenomena may take place for somewhat different values of the field strengths, but anyway, they exist and their nature is such as found by these investigations, which in particular had to be done by numerical methods.

B.1 Atomic Constants of ^{6}Li

Symbol	*Name*	*Value*	*Ref.*
$A_{\frac{3}{2}}$, $a_{\frac{3}{2}}$ [MHz]	hyperfine structure constant	-1.155	[17]
$B_{\frac{3}{2}}$, b [MHz]	hyperfine structure constant	-0.1	[17]
$\alpha_0 \left[\frac{\text{MHz}}{\left(\text{kV/cm}\right)^2}\right]$	scalar polarizability	0.03163	[18]
$\alpha_2 \left[\frac{\text{MHz}}{\left(\text{kV/cm}\right)^2}\right]$	tensorial polarizability	$4.06 \cdot 10^{-4}$	[18]
g_J	Landé factor of the $2p\ ^2P_{\frac{3}{2}}$ fine structure level	1.335	[19]
$\hat{g}_I$	g-factor of nuclear spin (in Bohr magnetons)	$4.47654 \cdot 10^{-4}$	[19]

Table B.1: Numerical values of atomic constants in ^{6}Li

B.2 Atomic Constants of ^{7}Li

Symbol	*Name*	*Value*	*Ref.*
$A_{\frac{3}{2}}$, $a_{\frac{3}{2}}$ [MHz]	hyperfine structure constant	-3.055	[15]
$B_{\frac{3}{2}}$, b [MHz]	hyperfine structure constant	-0.2	[5]
a_{o} [MHz]	orbital hyperfine structure constant	8.628	[15]
a_{d} [MHz]	dipole hyperfine structure constant	-1.886	[15]
a_{c} [MHz]	contact hyperfine structure constant	-9.788	[15]
ζ_{2p} [MHz]	fine structure constant	6702.093	[5]
$\alpha_0 \left[\frac{\mathrm{MHz}}{\left(\mathrm{kV/cm}\right)^2}\right]$	scalar polarizability	0.03152	[18]
$\alpha_2 \left[\frac{\mathrm{MHz}}{\left(\mathrm{kV/cm}\right)^2}\right]$	tensorial polarizability	$4.09 \cdot 10^{-4}$	[18]
g_L	g-factor of orbital angular momentum	0.999922	[13]
g_S	g-factor of electron spin	2.0023193	[13]
g_J	Landé factor of the $2p\ ^2P_{\frac{3}{2}}$ fine structure level	1.335	[19]
$\hat{g}_I$	g-factor of nuclear spin (in Bohr magnetons)	$1.182213 \cdot 10^{-3}$	[19]

Table B.2: Numerical values of atomic constants in ^{7}Li

Bibliography

[1] Musso, M.E.: *Die Hyperfeinstruktur der Resonanzlinien des Natrium-Atoms in externen äußeren Feldern*; Dissertation, Technische Universität Graz (1990)

[2] Musso, M.E.,Windholz, L.: *The sodium D_2-line in electric and magnetic fields. Part III: adiabatic hyperfine level transfer in perpendicularly crossed fields*; Z. Phys. D **30**, 13-18 (1994)

[3] Windholz, L., Krenn, C., Gwehenberger, G., Musso, M., Schnizer, B.: *Adiabatic transfer between hyperfine levels in combined electric and magnetic fields*; Phys. Rev. Lett. **77**, 2190-2193 (1996)

[4] Heubrandtner, Th.: *Die Deutung des senkrechten Stark-Zeeman-Effektes des $3p\ ^2P_{\frac{3}{2}}$-Niveaus von Natrium*; Diplomarbeit, Technische Universität Graz (1996)

[5] Windholz, L.: *Laser-spectroscopic investigations of the lithium resonance lines*; Appl. Phys. B **60**, 573-582 (1995)

[6] Edmonds, A.R.: *Angular Momentum in Quantum Mechanics*; Princeton University Press (1960)

[7] Lindner, A.: *Drehimpulse in der Quantenmechanik*; Teubner Studienbücher Physik (1984)

[8] Schmieder, R.W.: *Matrix Elements of the Quadratic Stark Effect on Atoms with Hyperfine Structure*; Am. J. Phys. **40**, 297-310 (1972)

[9] Schmieder, R.W.: *A Level-Crossing Study of the $^2P_{\frac{3}{2}}$ States of the Stable Alkali Atoms*; IBM Research, 1969

[10] Brandl, R.: *Die Symmetrien des Hamiltonstöroperators für Hyperfeinstruktur und senkrechten Stark-Zeemaneffekt im Unterraum des* ^2P *Terms der Alkalien*; Diplomarbeit, Technische Universität Graz (1999)

[11] Heubrandtner, Th.,Schnizer, B.,Mussso, M.,Windholz, L.: *Theoretical interpretation of the adiabatic transfer between the* $Na\ ^2P_{3/2}$ *hyperfine levels in perpendicular electric and magnetic fields* in: Abstracts, 28-th EGAS Conference, Technical University Graz, 16 - 19 July 1996 (Windholz, L., Ed.), europhysics conference abstracts 20 D.

[12] VAN DER WAERDEN, B.L.: ALGEBRA I, *Die Grundlehren der mathematischen Wissenschaften in Einzeldarstellungen, Band 33*, Fünfte Auflage; Springer Verlag; Berlin, Göttingen, Heidelberg 1960

[13] Umfer, Ch.H.: *Untersuchungen der Hyperfeinstruktur der Resonanzlinien von Lithium-7 in starken Magnetfeldern*; Diplomarbeit, Technische Universität Graz (1992)

[14] Sobelman, I.I.: *Atomic Spectra and Radiative Transition*; 2$^{\text{nd}}$ edition, Springer Series on Atoms and Plasmas (1992)

[15] Orth, H.,Ackermann, H.,Otten, E.W.: *Fine and Hyperfine Structure of the 2* ^2P *term of* ^{7}*Li; Determination of the Nuclear Quadrupole Moment*; Z. Phys. A 273,221-232 (1975)

[16] Angel, J.R.P.,Sandars, P.G.H.: *The hyperfine structure Stark effect*; Proc. Roy. Soc. A **305**, 125-138 (1968)

[17] Orth, H.,Veit, R.,Ackermann, H.,Otten, E.W.: Abstracts of Contributed Papers,ed.by Kowalski, J.,Weber, H.G.,4$^{\text{th}}$ ICAP, Heidelberg (1981)

[18] Windholz, L.,Musso, M.E.,Zerza, G.,Jäger,H.: *Precise Stark-effect investigations of the lithium* D_1 *and* D_2 *lines*; Phys. Rev. A **46**, 5812 (1992)

[19] Arimondo, E.,Inguscio, M.,Violino, P.: *Experimental determinations of the hyperfine structure in the alkali atoms*; Rev. Mod. Phys. **49** (1), 31 (1977)

This work has been done mainly at the Institute of Theoretical Physics of the Technical University in Graz. I deeply wish to express my thankfulness above all to Prof. Dr. Bernhard Schnizer for his unlimited support in numerous discussions, for his understanding and not least for his willingness in putting his own computer at my disposal for hours and hours. I'd also like to thank all members of our small Stark-Zeeman group for the friendly admission and the pleasant working atmosphere.